Summer 8-19-2016

Voltage-gated K+ Channels and HIV-1-induced Neural Injury: Implications for Pathogenesis of HIV-1-associated Neurocognitive Disorders

Han Liu
University of Nebraska Medical Center

Voltage-gated K^+ Channels and HIV-1-induced Neural Injury: Implications for Pathogenesis of HIV-1-associated Neurocognitive Disorders

By

Han Liu

A DISSERTATION

Presented to the Faculty of
the University of Nebraska Graduate College
in Partial Fulfillment of the Requirements
for the Degree of Doctor of Philosophy

Medical Sciences Interdepartmental Area Graduate Program
(Pharmacology & Experimental Neuroscience)

Under the Supervision of Professor Huangui Xiong

University of Nebraska Medical Center
Omaha, Nebraska

August, 2016

Supervisory Committee:

Anna Dunaevsky, Ph.D. James Eudy, Ph.D.

Daniel T. Monaghan, Ph.D. George J. Rozanski, Ph.D.

Acknowledgments

I would like to acknowledge all the people whose support made the present work possible. My mentor, Dr. Huangui Xiong, provided me the great support and opportunities to complete this work in his electrophysiology lab.

I would like to thank my graduate supervisory committees who graciously donated their time to guide me with their expertise and constructive feedbacks.

I was also fortunate to work with many skillful individuals in the Xiong lab who were both great collaborators and friends. I wish to especially thank Dr. Jianuo Liu for showing me entrance to the scientific methodology, thank Enquan Xu and Guihua Tu for helping me with cell culture. I would like to thank my parents, my mother Tong Li and my father Chuanbao Liu, for their generous supports. Special thanks to my husband Zhengfeng Wang. He has managed to complete so many things to accompany me in U.S. I would like to thank my parents-in-law for their help to take care my daughter Aura Wang. Thank Aura for her arrival that lightens a new journey of my life.

Voltage-gated K^+ Channels and HIV-1-induced Neural Injury: Implications for Pathogenesis of HIV-1-associated Neurocognitive Disorders

Han Liu, Ph.D.

University of Nebraska Medical Center, 2016

Supervisor: Huangui Xiong, M.D., Ph.D.

Human immunodeficiency virus-1 (HIV-1)-associated neurocognitive disorder (HAND) is a subcortical disease involving neuronal loss and myelin damage. Myelin is deposited by oligodendrocytes through a complex process including oligodendrocyte progenitor cell (OPC) proliferation and maturation. Oligodendrocytes/OPCs are susceptible to viral proteins such as Tat and that myelin damage is associated with oligodendrocyte number decrease. It has been shown that activation of voltage-gated K^+ (K_V) channels mediates apoptosis in various cell types. K_V1.3 is the most predominant K_V channel expressed in OPCs/oligodendrocytes and potentially involved in OPC developmental regulation. We studied the involvement of K_V1.3 in Tat-induced OPC/oligodendrocyte injury and OPC maturation deficit. Tat increased K_V1.3 currents in cultured OPCs and oligodendrocytes may through direct interaction and interrupting channel phosphorylating regulation, leading to OPC maturation retardation and OPC/oligodendrocyte apoptosis. Tat-caused myelin injury was validated in corpus callosum and striatum of cultured rat brain slices. These effects were prevented by K_V1.3 antagonists or K_V1.3-siRNA knockdown.

Gelsolin (GSN), an actin-binding protein best-known for its modulation of cell motility and secretion. Neurons appear to be a major source of GSN in CNS and GSN-null neurons have enhanced cell death. The GSN level is decreased in CSF of HIV-1-infected individuals. Studies have demonstrated that enhancement of K_V currents results in neuronal apoptosis. To understand how the decreased level of GSN causes neuronal

injury in HAND, we studied the effects of GSN on HIV-1 glycoprotein 120 (gp120)-activated outward K^+ currents in primary rat cortical neuronal cultures. Gp120 enhanced outward K^+ and resulted in neuronal apoptosis. GSN suppressed the gp120-induced outward K^+ current increase and reduced vulnerability to gp120-induced neuronal apoptosis. The GSN-mediated suppression of gp120 enhancement of neuronal outward K^+ current was blocked by $K_V2.1$ inhibitor. In parallel, gp120 up-regulated $K_V2.1$ channel expression, which was also blocked by GSN.

Taken together, my thesis research demonstrates that Tat induces myelin damage by $K_V1.3$-mediated OPC/oligodendrocyte injury and maturation defects, which may have implications for the pathogenesis of HAND. GSN protects neurons from gp120-associated changes by suppression of gp120-induced enhancement of $K_V2.1$ K^+ currents, which may reflect a neuroprotective role of GSN in HIV-1-infected brain.

Table of Contents

Contents

List of figures and tables

List of abbreviations

4-AP:	4-aminopyridine
AIDS:	acquired immune deficiency syndrome
ANI:	asymptomatic neurocognitive impairment
BDNF:	brain-derived neurotrophic factor
cART:	combined antiretroviral therapy
cGSN:	cytoplasmic gelsolin
CNS:	Central nervous system
Co-IP:	Co-immunoprecipitation
Cp450:	cytochrome p450
CSF:	cerebrospinal fluid
DTI:	diffusion tensor magnetic resonance imaging
EAE:	experimental autoimmune encephalomyelitis
FBS:	Fetal bovine serum
FGF:	fibroblast growth factor
GalC:	galactocerebroside
Gp120:	glycoprotein 120
GSK-3β :	glycogen synthase kinase-3β
GSN:	gelsolin
GxTx:	Guangxitoxin-1E
HAD:	HIV-1-associated dementia
HAND:	HIV-1-associated neurocognitive disorder
HBSS	Hank`s buffered salt solution
HEK293:	Human embryonic kidney cell 293
HIV-1:	Human immunodeficiency virus 1
HIVE:	HIV encephalitis
I_A:	A-type outward K^+ current
I_K:	delayed rectified K^+ current
IL-1β	Interlukin-1 beta

IRIS:	immune reconstitution inflammatory syndrome
JCV:	human polyomavirus JC
JXP:	juxtaparanode
Kir:	inward rectified K^+ channel
K_V:	voltage-gated K^+ channel
LINGO-1:	Leucine-rich repeat and immunoglobulin domain-containing-1
MBP:	myelin basic protein
MgTx	Margatoxin
MND:	mild neurocognitive disorder
MOG:	myelin oligodendrocyte glycoprotein
MTT:	3-(4,5-dimethlthiazol-2-yl)-2,5-diphenyl tetrazolium bromide
NaV	Voltage-gated Na^+ channel
Nef:	negative regulatory factor
neuroHIV:	HIV neurology
NG2:	neuronal glial antigen 2
NGF:	nerve growth factor
NMDA:	N-methyl-D-aspartate
NPC:	neural stem/progenitor cell
NT-3	neurotrophin-3
OPC:	oligodendrocyte progenitor cell
PAP	5-(4-phenoxybutoxy) psoralen
PDGF:	platelet-derived growth factor
pGSN:	plasma gelsolin
PML:	progressive multifocal leukoencephalopathy
PNS:	Peripheral nervous system
Tat:	trans-activator of transcription
TBS:	Tris buffer solution
TEA:	tetraethylammonium
TGF-beta:	transforming growth factor beta

TIP30:	HIV-1 Tat interacting protein
TTX:	Tetrodotoxin
Tunel:	Terminal deoxynucleotidyl transferase dUTP nick end labeling
VDCC:	voltage-dependent $Ca2^{+}$ channel
WM	White matter

Chapter 1 Introduction

Review of HIV-1-associated Neurocognitive disorder, neurons, oligodendrocyte, and K^+ channels in HIV-1-associated neuropathogenesis

Abstract

Oligodendrocytes wrap neuronal axons to form myelin, which is an insulating sheath essential for the electrical saltatory conduction along axons. The process of myelination is highly regulated by neuronal and astrocytic signals and, maintenance of myelin sheaths is a very complex process. Oligodendrocyte injury results in demyelination and further neurological dysfunction. Demyelination in cerebrum may cause cognitive impairment in a broad array of diseases including human immunodeficiency virus type one (HIV-1)-associated neurocognitive disorder (HAND). Although the combined antiretroviral therapy has markedly reduced HIV-1 incidence of HIV-1-associated dementia, which is a severe form of HAND, milder forms of HAND remain prevalent even when viral load in blood is well controlled. HAND manifests as a subcortical dementia involving subcortical damage in white matter (e.g., corpus callosum), which mostly consists of myelinated axonal fibers. How HIV-1 brain infection causes myelin injury and resultant white matter damage is an interesting area of current HIV-1 neurology research. In this Chapter, we tentatively address recent progresses on oligodendrocyte dysregulation and HAND pathogenesis.

Key words: HIV-1, dementia, oligodendrocyte, myelin sheath

Although combination antiretroviral therapy (cART) has markedly reduced human immunodeficiency virus type one (HIV-1)-associated mortality, HIV-1-associated neurocognitive disorders (HAND) remains prevalent [1-3]. More than 50% of HIV-1 positive individuals have central nervous system (CNS) syndromes, involving subcortical damage in white matter (WM, e.g., corpus callosum) and/or deep grey matter [4-8]. HIV-1-related WM damage includes demyelination and axonal dysfunction and/or damage. Demyelination is when myelin sheath of neuronal axons, which enables rapid and efficient saltatory conduction, is impaired in the CNS or peripheral nervous system (PNS). Myelination, formation of myelin sheaths by oligodendrocytes wrapping neuronal axons in the CNS or Schwann cells in the PNS, is highly regulated by neuronal and astrocytic signals and, maintenance of myelin sheaths is a very complex process. Oligodendrocyte injury is the hallmarks of demyelination and WM damage. Oligodendrocyte injury can be induced by genetics, viral proteins, inflammation, autoimmune response and other unknown factors. HIV-1-related oligodendrocyte/myelin injury has been reported both in cell culture [9] and patients [10].

Earlier studies demonstrate that human polyomavirus JC (JCV) primarily causes demyelination in HIV-1-infected brain. Compared to HIV-1 infection of astrocytes and microglia in brain, JCV predominately infects oligodendrocytes and thus cause oligodendrocyte loss and demyelination. JCV is the main causative of progressive multifocal leukoencephalopathy (PML), a frequent opportunistic infection in the CNS and a common complication seen in AIDS patients [10, 11]. Recently, several research groups have reported that HIV-1 and viral proteins *per se* can target at oligodendrocytes and cause the detrimental effects, which are JCV-independent [9, 12, 13]. HIV-1 viral proteins, including the envelope glycoprotein gp120, trans-activator of transcription (Tat), and negative regulatory factor (Nef), have been implicated in oligodendrocyte toxicity [12,

14-17]. Among these proteins, Tat has been detected in both infected and uninfected oligodendrocytes in the brains of AIDS patients [10], and showed synergistic effect with JCV or addictive drug as morphine. The myelin injury-related milder neurocognitive disorders and the oligodendrocyte pathogenesis in HAND are attracting attention of neurovirologists worldwide.

1. Overview of HAND

HIV includes two types, HIV type 1 and 2 (HIV-1, 2). There is limited knowledge about HIV-2, which has not been commonly seen outside of Africa. Thus all of the diseases mentioned in this dissertation are HIV-1 associated. HIV-1 primarily infects CD4+ T cells and monocyte/macrophage lineage cells. HIV enters cells by interacting with CD4 receptor and two co-receptors, CXCR4 or CCR5.

Infected monocytes or macrophages traverse blood brain barrier (BBB) to invade brain. The invasion of HIV-1 happens in the early stage of primary infection. Invaded viruses replicate in brain, causing inflammatory and neurotoxic effects that contribute to cognitive, behavioral and motor function deficits. This progressive neurologic disease is clinically characterized by cognitive deficits in patients with HIV-1 infection [18].

1.1. HAND clinical diagnosis

HAND is divided to three categories depending on degree of severity: asymptomatic neurocognitive impairment (ANI), mild neurocognitive disorder (MND), and HIV-1-associated dementia (HAD). The detailed current diagnostic criteria for HAND are published on AIDS education and Training Centers National Coordinating Resource Center (http://aidsetc.org/guide/hiv-associated-neurocognitive-disorders). Patients accept standardized neuropsychological survey (*e.g.* learning function, construction, memory registration, attention, concentration) and are diagnosed by a combination of dementia scale, day-to-day functioning interference, and no pre-existing cause of

cognitive deficits [1, 19-21]. However, the impairments in ANI and MND may escape clinical diagnosis. HAD patients undergo marked neuron interference with daily functioning, acquire cognitive impairments particularly in the new information registration, information processing and attention/concentration deficits [20-22].

1.2. Overview of HAND neuropathogenesis

Obviously, HAND symptoms are closely attribute to neuronal dysfunction or/and loss. However, HIV-1 does not infect neurons directly. The mainly proposed mechanisms leading to HAND involve infected macrophages, microglia, or astrocytes secreting neurotoxins resultant in neuronal function alterations and death. Viral proteins (*e.g*. gp120, Tat, Nef, Vpr), arachidonic acid, free radicals ($NO^{\cdot}$ and $O_2^{\cdot-}$), glutamate, quinolinate, cysteine, cytokines (*e.g.*, CCL12, IL-1β, TNF-α), and amines have been reported that act as neurotoxins in HAND [23]. These toxic factors generally act through two proposed models: direct model and indirect model. The direct model offers hypothesis that viral proteins released from infected cells manifest direct cytotoxicity on neurons [24]. The indirect model proposes that the neuronal death or dysfunction is consequently mediated by inflammatory response designedly against HIV-1 infection or viral proteins [24, 25]. The HIV-1 infection-caused processes alter neuronal function and survivals have been extensively addressed. In the pre-cART era, inflammation and neurodegeneration were believed as the predominant pathogenesis drive HAND progression [26]. However, emerging evidences demonstrate the direct actions of viral proteins may take the major place particularly in these patients with good access of cART [27, 28].

2. Overview of oligodendrocytes

In the CNS, oligodendrocyte plasma membrane processes enclose axons leading to formation of myelin sheath, which is essential for fast axonal conduction. Myelinated

axons appear myelin-dependency during development, thus demyelination can lead to progressive decline in these axons [29]. Neuronal conduction deficits in HAND patients can be attribute to primary neuron injury or consequent injury caused by myelin dysfunction/loss, suggesting disruption of oligodendrocyte function my contribute to HAND progression [27]. Oligodendrocytes rise from oligodendrocyte progenitor cells (OPCs) or neural stem/progenitor cells (NPCs). These two populations are capable to generate new oligodendrocytes in response to myelin injury to maintain myelin function. [30]. As OPCs are the major proliferating cell population within the adult CNS, they have the most capacity to re-form myelin sheath. Thus, OPC proliferation, differentiation and maturation are critical processes for axonal remyelination. It has been shown that differentiation of OPCs into oligodendrocyte is greatly challenging during remyelination [31, 32]. OPC differentiation is controlled by a number of factors, many of which act to inhibit myelination, including Leucine-rich repeat and immunoglobulin domain-containing-1 (LINGO-1) [33, 34], Notch-1 [35, 36], Wnt [37] etc. Whereas, p38 MAPK [38, 39] and AKT [40] have been shown to be required for oligodendrocyte differentiation and myelination.

3. Myelin/oligodendrocyte injury in HIV-1 patients

The oligodendrocyte and myelin injury have been observed clinically from neurological imaging studies, serum biochemistry and brain biopsies [6, 8, 41, 42]. The diffusion tensor magnetic resonance imaging (DTI) promotes the investigations of WM damage in early HAND and, allows revealing the microstructures of myelin and oligodendrocytes. The changes of water molecules diffusive parameters in brain WM of HIV-1 patient, which indicate demyelination, have been detected in several DTI studies [6, 43, 44]. These findings were supported by a recent study in HIV-1-infected humanized mice that the decreased expression myelin structural proteins were observed

in whisker barrels, corpus callosum, and hippocampus, suggesting the loss of myelin elements [45]. In the serum and CSF of patients with HAND, antibody titers of myelin oligodendrocyte glycoprotein (MOG), an important myelin structural protein indicating CNS-specific autoimmune reaction for primary demyelination, are significantly higher compared with asymptomatic HAND patients and HIV-1-negative patients with other neurological disease. In particular, CSF anti-MOG antibodies exhibit a high sensitivity and specificity (85.7% and 76.2%) in those patients with active HAND. The performances on HIV dementia scale test are significantly worse and the viral loads in CSF are higher in MOG immunopositive HAND patients than those in asymptomatic HAND patients [46], suggesting the dysfunction of oligodendrocyte is closely related with HIV-1 infection and HAND.

Compared to astrocytes that tend to promote recovery in response to injury, oligodendrocytes are more susceptible and appear to be damaged as a general response to insults [47]. In biopsy studies, the significant loss of nerve fibers and axons are observed in HIV-1-infected brain, in particular in the frontal and occipital parts of the corpus callosum. The myelin sheath thickness diminishes in corpus callosum as well [8]. Weighted gene co-expression network analysis showed an increase of oligodendrocyte-related genes particularly in the HIV encephalitis (HIVE) group, suggesting specific dysfunction of oligodendrocyte in HIVE [48].

In those HIV-1 positive patients with PML, the myelin loss is apparent both macroscopically and microscopically [49]. Neuroimaging studies show the myelin lesions are more frequently seen in the sub-cortical WM areas [50]. PML is believed to be developed exclusively in immunosuppressive patients with significantly higher incidence in patients with AIDS, particularly in AIDS patients without cART and with a low lymphocyte CD4+ count, than in patients with any other immunosuppressive conditions.

Although cART has decreased the incidence of PML and improved the patient survival [51], PML was recently reported that occurred in HIV-1-positive patients with good access of cART and even with normal $CD4^+$ lymphocyte level [52, 53]. These findings suggest PML-related oligodendrocyte/myelin damage is often, but not necessarily, associated with severe immunosuppression or an immune reconstitution inflammatory syndrome (IRIS) in pathogenesis of cART era HIV neurology (neuroHIV) [54].

4. Fate of oligodendrocytes in HIV-1-infected brain

Early publications reported that HIV-1 cannot be detected in oligodendrocytes [55, 56], may due to the limitations of methodology to identify oligodendrocytes. Dissenting result was found in purified human oligodendrocytes from temporal lobe resections, HIV-1 (IIIB and BaL) infectivity was confirmed by detection of p24gag antigen and PCR amplification [57]. It is well-known that HIV-1 attaches and infects human host cells through CD4 receptor, along with CXCR4 and CCR5 as co-receptors. Oligodendrocytes are CD4 and CCR5 negative but do express CXCR4 [28, 55, 58], which designedly promote the OPC migration and remyelination [59], may provide the anchor for HIV-1-induced oligodendrocyte toxicity. However, most investigators agree that HIV-1 primarily infects microglial cells of the brain but oligodendrocyte is not the main target. HIV-1-associated oligodendrocyte injury is believed to be mediated through viral proteins shed from viruses released from infected other cells [12, 14, 15].

In HIV-1 patients with PML complication, Tat and JCV are both present in oligodendrocytes. Tat has been shown to synergize with JCV, and facilitate of JCV gene transcription and replication, leading to robust JCV infection [60, 61]. Tat stimulates JCV gene transcription by cooperating with SMAD proteins, the intracellular effectors of TGF-beta, at the JCV DNA control region (Fig. 1A) [60]. The effectiveness of Tat on facilitating JCV transcription and replication varies from different HIV clades [61].

Because Tat can continuously exist in brain while the viral load is controlled in blood, this may partially explain the cases that HIV-1 patients develop PML even with good access of cART [62]. Besides the synergistic effect of Tat and JCV in oligodendrocytes, cytotoxic $CD8^+$ T cells aggregate at demyelinated lesions in brain to engage JCV-infected oligodendrocytes, which tends to control JCV dissemination but at the cost of oligodendrocyte death and further demyelination in PML [63].

In addition to Tat, gp120 seems to involve in HIV-1-associated oligodendrocytes/myelin injury as well. It has been shown that gp120 inhibits myelination in rat cerebral cortex culture [14] and to induce functional dysregulation and apoptosis in cultured oligodendrocytes [15, 64], which is discussed in subsequent section. The primary oligodendrocyte injury, which leads to secondary axonal injury (outside-in) to further exacerbate neurocognitive impairments, oligodendrocyte injury can be caused by primary axonopathy as well (inside-out) [65]. The recent study has shown that gp120-induced β-APP accumulation and axon injury in corpus callosum was attenuated by a CXCR4 antagonist, exampling HIV-1 injury of oligodendrocyte/myelin injury via CXCR4 receptors [28]. Although it is not clear whether gp120 cause such a detrimental effect through “outside-in” or “inside-out” mechanism or both, CXCR4 expressed on oligodendrocytes can be a potential target [65].

5. Association between BBB disruption and myelin deficits

Increasing evidences indicate that myelin injury may be associated with dysregulated BBB since WM pallor is often observed in perivascular sectors [66] [67]. BBB is a critically protective barrier for the brain. It serves as a highly selective layer that separate CNS from the rest of the body. HIV-1-related BBB alteration is attributed to proinflammatory cytokine secretion, released viral proteins from infected cells, and HIV-1 infection of endothelial cells [68, 69]. The reported direct mechanisms are often related

to alterations of vascular tight junctions, direct toxicity of brain endothelial cells, production of matrix metalloproteinase, and NMDA receptor activation [70, 71]. The disruption of BBB is believed essential for HIV-1 to access to brain. In another hand, BBB alteration *per se* may also underlie neurologic deficits in neuroHIV patients. This is supported by an observation that HIV-1 patients with impaired BBB showed poorer neurologic status than those with intact BBB [72]. However, myelin damage may be related to BBB disruption without HIV-1 brain invasion. In a case report, diffuse myelin pallor in WM and massive perivascular dilatation were observed in an AIDS patient without evidence of brain HIV infection, significant inflammation, or microglial activation [73]. Postmortem studies on AIDS patients brains showed that the discrete myelin pallor areas are always associated with capillaries or venules [67]. These findings suggest that BBB breakdown caused diffuse leak and other circulating factors may contribute to the observed myelin pathogenesis.

Under physiological conditions, the BBB endothelial cells and components of the extracellular matrix support OPC survival, and promote NPC differentiate to neurons, astrocytes and oligodendrocytes [74-76]. The critical function of BBB and the consequences of BBB alteration imply the contributions of BBB disruption in HIV-1-associtated oligodendrocyte/myelin injury. It is not surprising the BBB disruption will result in enhanced entrance of free virus, infected T cells, and toxic components from blood. It has been reported that OPC proliferation can be reduced by plasma, serum, thrombin and plasmin in primary culture. Thrombin also suppresses the differentiation of OPCs into mature oligodendrocytes [77]. In addition, the expression level of TNF-α is elevated in blood mononuclear cells of HIV-infected patients [78], of which TNF-α is demonstrated that promoting oligodendrocyte death [79]. HIV-1 infection also induces interleukin (IL)-1β production in human monocytes [80], of which IL-1β can promote

oligodendrocyte death through glutamate excitotoxicity [81]. These findings provide potential mechanisms of BBB disruption contribution to HIV-1-associated myelin/oligodendrocyte damage.

6. Cellular mechanisms of oligodendrocyte loss in HIV-1-infected brain

Apoptosis of oligodendrocytes has been demonstrated in HAND patients. Accumulating evidences indicate that HIV-1 viral proteins can injure oligodendrocytes directly or through a comorbid effect with addictive drugs.

It is well-known that tumor suppressor p53 induce apoptosis by activating transcription of various pro-apoptotic genes [82]. Activation of p53 is detected in the oligodendrocyte lineage cells in the brain of HAND patients, which cannot be detected in control brains [83]. Because of difficulties to distinguish differentiating stages of oligodendrocyte lineage on autopsy samples, the detected p53 reactivity reflects apoptosis of mature oligodendrocytes (Fig. 1B) and OPCs. This suggests that in addition to oligodendrocyte injury, proliferation of OPCs may be also impaired in HAND.

Gp120 causes slow but progressive oligodendrocyte cytosolic Ca^{2+} rise in a mixed culture of cerebellar cortex cells [64], which is a potential apoptotic cause. Exposure of oligodendrocytes to Tat also triggers rapid increase in intracellular Ca^{2+} level through targeting at NMDA and AMPA receptors thus cause consequent oligodendrocyte injury. It is worth to mention that the roles of NMDA and AMPA receptors appear to be different and dependent on the stage of OPC differentiation [9]. Our data suggest that Tat can cause oligodendrocyte apoptosis *in vitro* and myelin loss *ex vivo* by enhancing voltage-dependent K^+ channel (K_V) 1.3 activity (Chapter 2). The efflux of K^+ ions causes the cell shrinkage leading to apoptotic cell volume decrease and eventual apoptosis (Fig. 1B) [84]. Oligodendrocytes within the striatum are highly sensitive to the effects of morphine in HIV-1 Tat transgenic mice [12]. Striatal oligodendrocytes are the only apoptotic cell

type in response to combined morphine exposure and Tat induction in the Tat transgenic mice [12]. Tat also interacts with morphine to decrease the proliferation of OPCs [85]. Opioid abuse causes synergistic toxicity in HIV-1-associated pathogenesis by direct actions on immature astrocytes and oligodendrocytes which express μ-opioid or κ-opioid receptors [86].

In other virus-induced demyelination, there is clear evidence that mouse hepatitis virus can directly infect and activate microglia during acute inflammation which eventually causes phagocytosis of myelin sheath and thus leading to demyelination during chronic inflammation stage [87]. Similar theory has been well established in multiple sclerosis, which is the most prevalent demyelinating disease, that immune-activated microglia strip the myelin. Recent evidences show that microglia appear to be more phagocytotic in response to HIV-1 Tat and result in neuronal loss [88, 89]. Although there is no direct evidence indicating microglia phagocytosis of oligodendrocyte in neuroHIV [54], it is likely that the infected and activated microglia can also phagocyte oligodendrocytes and myelin sheath, leading to the myelin damage and consequent HAND pathogenesis.

7. Myelin maintenance and remyelination in HIV-1-infected brain

Repair of the damaged myelin sheath, which is called remyelination, is physiologically required to maintain the myelin homeostasis. The myelin injury in neuroHIV may also be induced by abnormalities of remyelination, in addition to loss of existing myelin sheath. Remyelination requires proliferation and survival of OPCs, migration of OPCs to the local lesion site, development from immature oligodendrocytes to myelinating mature oligodendrocytes. The alterations of OPC regulating signals related to remyelination process are found in HIV-1.

7.1. Altered OPC proliferation and differentiation in HIV-1-infected brain

In HIV-1-infected brain, mild myelin damage is associated with an increase in oligodendrocyte number, but the number decrease in severe myelin damage [90]. In an agreement with the aforementioned results, mRNA levels of transcription factor Olig2, a marker expressed with higher levels in OPC and lower levels in mature oligodendrocytes [91], are elevated in the front cortex of patient with HIVE [48], indicating an increase of OPC proliferation is needed for repairing damaged myelin sheath. Mature oligodendrocytes defect is also observed in animal model of secondary degeneration, which represents additional loss of neurons, myelin, and glial cells through toxic events. Early onset of secondary degeneration triggers OPC proliferation, but the cell numbers decrease in a long-term [31]. However, Tat exposure reduces the population of undifferentiated $Sox2^+$ NPC (ancestor of OPC) and $Olig2^+$ OPCs, but progenitor survival is unaffected [85], suggesting the proliferation was interrupted. Tat may inhibit NPC proliferation by down-regulating cyclin D1, which is an important cell cycle component interacts with cyclin dependent kinase 4 and 6 [92] (Fig. 1C). Over all, HIV-1 infection or viral protein exposure tends to incline NPC fate toward generation of astroglia cells at the expense of neurons and/or oligodendrocytes [85, 93, 94]. Thus we consider OPC differentiation and maturation are likely to be the key point for remyelination in neuroHIV.

7.2. Imbalance of OPC differentiation and remyelination in HIV-1-infected brain

It has been shown that differentiation of OPCs into post-mitotic oligodendrocytes is a major check-point in the myelination process. As mentioned in Section 2, oligodendrocyte differentiation is controlled by various factors, which are most negative mediators. While molecular mechanisms in the regulation of developmental myelination are discussed in excellent review papers published elsewhere [95, 96], the direct interaction between HIV-1 and these molecules remains largely unknown. It is, however, believed that HIV-1 may disturb the complex regulating network leading to the

remyelination imbalance based on the following findings: 1) HIV-1 alters cell cycle by Wnt signaling pathways and further impact the cell proliferation and differentiation in different cell types, including peripheral blood mononuclear cells [97], HEK293 cells [98], and astrocytes [99]. 2) HIV-1 infection of primary-derived astrocytes altered astrocyte Wnt profile by elevating Wnt family members 2b and 10b [99]. 3) Elevation of secreted Wnt signal from astrocytes may negatively regulate oligodendrocyte differentiation in neuroHIV (Fig. 1C). 4) Notch-1 signaling is permissive for OPC expansion but inhibit differentiation and myelin formation [100]. 5) In Kaposi`s sarcoma cells, which is a neoplasm in HIV-1-infected individuals, overexpression of activated Notch-1 signaling is detected [101]. However, to our knowledge, there is no yet report on how OPC/oligodendrocyte Notch-1 signaling in responding to HIV-1. Moreover, overexpression of CD44, a predominant hyaluronan receptor widely expressed in nervous system, on precursor cells inhibits differentiation toward oligodendrocytes and promotes differentiation into astrocytes, thus plays a negative role in OPC differentiation and myelination [102, 103]. In lymphocyte cell lines of Jurkat and U937 cells, HIV-1 infection-caused particle production is accompanied by CD44 up-regulation [104]. In HIV-1-related diffuse large B-cell lymphoma patients, the CD44 levels significantly increased compared with HIV-1-unrelated diffuse large B-cell lymphoma patients (87% vs. 56%) [105]. These findings suggest CD44 may play a role in HIV-1-related remyelination failure.

Neurotrophins are important factors in the regulation of oligodendrocyte myelination and remyelination. The main cellular sources for neurotrophins in brain are astrocytes, microglial cells, and neurons, in addition to contribution of lymphocytes through the blood circulation. Being aware of excellent reviews on the alteration of neurotrophins in HAND [106] and immunological communications between oligodendrocytes and

microglia [107], we here focus on the HIV-1-induced alterations of neurotrophins that potentially associate with oligodendrocyte abnormalities.

The platelet-derived growth factor (PDGF) is the most predominant mitogen for oligodendrocyte lineage cells. PDGF A and B chain both promote proliferation through activating PDGF receptor alpha (PDGFRα) expressed on OPCs, whereas the PDGF B chain appears to be more important for early NPC expansion [108, 109]. It has been shown that PDGF regulates OPC development via glycogen synthase kinase-3β (GSK-3β) signaling pathway, which is a negative regulator of OPC differentiation and remyelination [110, 111]. PDGF-BB prevents NPC from Tat-mediated proliferating impairment by inactivating GSK-3β/β-catenin pathways and, this effect is significantly inhibited by the p38 and JNK inhibitors [112]. The levels of fibroblast growth factor (FGF), which is an important pro-survival signal to stimulate OPC proliferation [113], increased in the sera of HIV-1-infected patients [114, 115], but decreased in CSF [115]. FGF signaling complex is interrupted in HIV-1-infected brain, results in the abnormal activation of downstream signals including GSK-3β [116, 117], p38, ERK, and JNK cascades [118] in neurons through the surface receptors such as NMDA receptor and CXCR4, which are also expressed on oligodendrocytes [59, 119, 120]. In addition, HIV-1 Tat and FGF-2 share a common core mechanism of unconventional secretion [121], although it is not clear whether they compete for the secretory routine. The brain-derived neurotrophic factor (BDNF), predominantly derived from astrocytes, has also been found to be essential for oligodendrocyte lineage development [122-125]. In rat primary neurons, gp120 promotes a time-dependent proBDNF accumulation at both intracellular and extracellular spaces by decreasing the expression level of intracellular furin, an enzyme required for cleavage and release mature BDNF, leading to a reduction in mature BDNF (Fig. 1C). A similar imbalance in the ratio of proBDNF/mature BDNF was

confirmed in postmortem brains of HAND patients [126]. These findings suggest that HIV-1 decreases the brain BDNF level by infecting astrocytes and gp120-associated neurotoxicity, resulting in down-regulated remyelination. As BDNF is believed to protect neurons from HIV-1-induced apoptosis, thus the reduction of BDNF may also make the oligodendrocyte losing the support from neuronal axons that consequently cause myelin damage through “inside-out” mechanism as proposed [65].

Besides these signaling molecules, HIV-1 Tat interacting protein (TIP30), a co-factor that specifically enhances HIV-1 Tat-activated transcription [127], negatively regulates oligodendrocyte development. Overexpression of TIP30 dramatically inhibits the OPC differentiating progression, while knockdown of TIP30 enhances the differentiation of OPC remarkably [128]. Blockade of TIP30 may have dual benefits on inhibiting Tat-dependent genes transcription and promoting OPC differentiation, which is a potential therapeutic strategy on HIV-associated demyelination. Ion channels are also involved in regulation of OPC development. Kv1.3 [129, 130], Kv1.6 [129], inward rectified K^+ channel 4.1 [131, 132] play crucial roles in regulation of OPC/oligodendrocyte proliferation and differentiation. Generally, channels expressions on oligodendrocyte lineage cells correlate with differentiating stages and the correlations are more complex in OPCs than in oligodendrocytes. Particularly, Kv1.3 channel plays a crucial role in G1/S transition in proliferating OPCs through regulating AKT signaling [130, 133]. Moreover, L-type voltage-operated Ca^{2+} channel 1.2 knockdown induces a decrease in the proportion of oligodendrocytes expressing myelin proteins, and an increase in the population of immature oligodendrocyte [134].

Very recent study proposed that myelin injury in HAND is partially due to effects of antiretroviral drugs on oligodendrocyte survival and differentiation. The common

prescribed antiretroviral drugs, ritonavir and lopinavir, impair both the differentiation of OPCs into myelin-producing oligodendrocytes and the maintenance of myelin proteins *in vivo*. Ritonavir induces accumulation of reactive oxygen species, which arrest oligodendrocyte differentiation process [135, 136]. Controversial results were reported in HIV-1-infected children in Africa that significant myelin loss in cART-naïve children was observed in comparison with cART-treated children. However, cART-treated children also exhibited a significant myelin loss in the corpus callosum [137]. Interestingly, myelin-related genes encoding myelin-associated oligodendrocyte basic protein, myelin transcription factor 1 and myelin basic protein are down-regulated in both cART-treated and untreated HAND patients [138]. Apparently, the impact of antiretroviral drugs on oligodendrocyte pathophysiology requires further investigation.

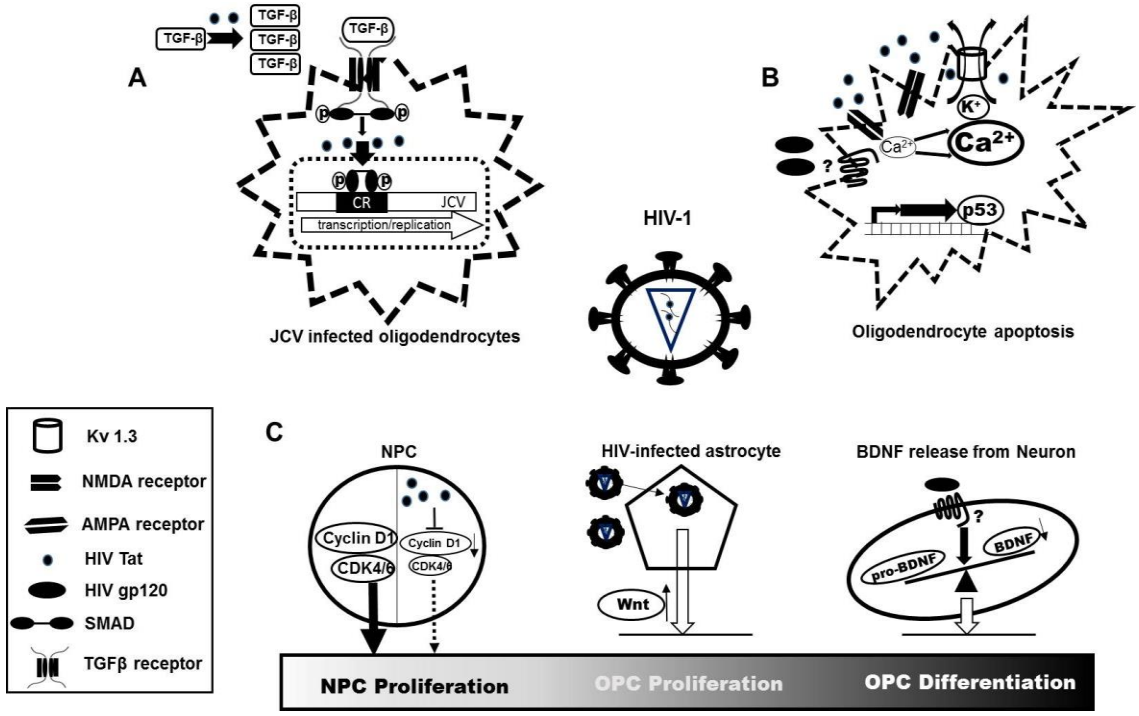

Figure 1. Potential mechanisms for HIV-induced oligodendrocyte/myelin injury. A, HIV-1 Tat enhances JCV transcription and replication. B, HIV-1 proteins induce oligodendrocyte apoptosis. C, The progenitor cell proliferation and differentiation are interrupted in neuroHIV.

Sections 3-7 are from review “Oligodendrocyte Injury and Pathogenesis of HIV-1-Associated Neurocognitive Disorders” published on Brain Science. 2016, 6(3), 23.

8. K^+ channels in brain: implications for channelopathy in HAND

K^+ channels are highly diverse and expressed on almost all cell types. Normal function of K^+ channels is required for basic cell survival and normal activity. In contrast, K^+ channel hyperactivation, especially outward K^+ currents conducted by K_V channels, may cause cell apoptosis in a variety of cell types via apoptotic volume shrinkage. Enhanced K^+ efflux can resultant in apoptotic cell shrinkage, downstream caspase activation, and further DNA fragmentation [84, 139]. Hyperactivation of K^+ channel can also cause immune cells activation like macrophages, microglia, and T lymphocytes [140, 141]. The non-specific K_V blocker 4-AP has been approved by the Food and Drug Administration to proceed to clinical trial for neurodegenerative disease [142]. Previous studies from our laboratory describe apoptosis of rat cortical neurons associated with enhancements of K^+ efflux conducted by voltage-gated K^+ (K_V) channels in HAND. $K_V1.3$ and $K_V1.5$ in microglia are highly involved in pathogenesis of experimental autoimmune encephalomyelitis animal models and HAND [143-145]. Microglia $K_V1.3$ is involved in microglial activation-induced neuronal injury [141]. These data suggest K_V channels are closely associated with HIV pathogenesis.

8.1. K^+ channels in neurons

Action potential propagation is the most essential character for neural function. The two most important properties of axonal action potentials are high conduction velocity with quick recovery. High velocity requires rapid inactivation of Na^+ channels and a high K^+ permeability [146]. It is believed that Na^+ channels are enriched in the node of Ranvier, meanwhile, K_V channels are enriched at the juxtaparanodes (JXP) (Fig. 2). The cluster of K_V1 family members on neuronal axon JXP indicates myelination [147] [148]. In coculture model of hippocampal neurons and oligodendrocytes, endogenous $K_V1.2$ channels enriched in JXP of myelinated hippocampal axons after two weeks of

coculturing neurons and oligodendrocytes [149]. In contrast, K_V1.2 distribution on myelinated axons is disrupted within demyelinated lesions in the WM of spinal cord in experimental autoimmune encephalomyelitis [150]. These data suggest that K_V channels, particularly K_V1.2, are essential for axon cable properties.

It has been reported that depolarization-activated K^+ currents limit the peak amplitude of the depolarizing after-potential in both lizard and rat axons [151]. However, overexcited K_V channels hyperpolarize the neuronal membrane increasing the threshold to trigger action potential, even leading to neuronal death. As mentioned above, research on programmed cell death has demonstrated the necessary contribution of K^+ channels in the process of apoptosis. In previous experiments, our laboratory confirmed the association of rat cortical neuron apoptosis and increased K^+ channel currents in HIV-1 proteins treated cells [143-145]. While several K_V channel subtypes have been implicated in cortical neuron apoptosis, including K_V2.1 [152], K_V1.1 [144], K_V3.4 [153], K_V4.2, and K_V4.4 [154], the specific subtypes involved in HAND pathology and the mechanism underlying its dysfunction remains to be extensively characterized. Collectively, these observations suggest that specific K_V channel subunits may perform neurotoxic activity under particular pathological conditions.

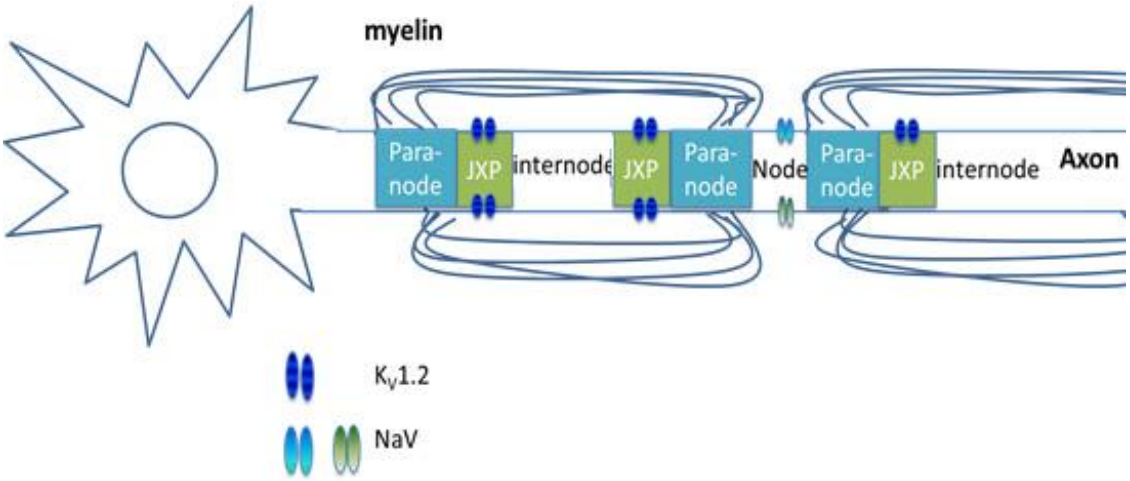

Figure 2. The distribution of voltage-gated ion channels on neural axon. K_V1 family members $K_V1.2$ express at the JXP region of axon. Voltage-gated Na^+ channels (NaV) express on the node area.

8.2. K^+ channels in oligodendrocytes

As early in 1988, Betty et al. performed whole cell clamp patch on cultured ovine oligodendrocytes. They found oligodendrocytes express outward currents considered as K^+ currents, because that represent an transient-inactivating component and non-inactivating component, which showed reversal potential at -66 mV and were sensitive to K_V blockers [155]. The transient component decreased within the oligodendrocyte lineage cell development, while accompanied by an up-regulation of steady-state outward and inward rectifier current [129, 155, 156]. Generally, K_V channel expression on oligodendrocyte lineage cells correlate with differentiation stage and are more complex in OPCs than in oligodendrocytes. To date, K_V1 subfamily is relatively well studied in oligodendrocytes [129, 130, 157]. In addition to what has been addressed in section 7.2., in cultured oligodendrocytes from basal forebrain, high concentration of KCl (25 mM), which can depolarize cell membrane via inhibiting K^+ efflux, approximately doubles BDNF mRNA expression, while nerve growth factor (NGF) and neurotrophin-3 (NT-3) expression is not altered. The number of cells expressing mature myelin basic protein positive (MBP^+), which is a structural protein of myelin sheath, increased [158]. These data suggest that K_V channels activity affect the trophic function of oligodendrocytes that further affect neuronal function and survival.

Since oligodendrocytes are the most important cell type for myelin sheath production and maintenance in CNS, K^+ channels may act as a mediator in myelin injury and remyelination by regulating OPC/oligodendrocyte biogenesis. It is not surprising that apoptosis of oligodendrocytes is an important component of lesion formation. The crucial role of oligodendrocyte indicates any damage or/and loss of oligodendrocytes may relate to the observed myelin damage and cognitive deficits in HAND patients.

8.3. K^+ channels in astrocytes

Astrocytes are indispensable for neuronal survival and function, including an additional beneficial effect on oligodendrocyte regeneration during remyelination. Astrocytes pivotally regulate extracellular concentration of glutamate and K^+ to support neuron function [159]. During normal neuron firing, K^+ ions flow to the extracellular space from neurons. Increased extracellular K^+ concentration can potentially cause membrane depolarization. Kir4.1 channels in astrocytes may play a critical role in K^+ buffering to avoid neuronal membrane depolarization, which may result in interruption of axonal conduction and synaptic transmission [160, 161] [162-164]. So far, there is no clear evidence indicates close association of astrocyte K^+ channels and HAND pathogenesis. Astrocyte Kir channels may serve to provide the network of regulation in K^+ and glutamate concentration in brain [161].

8.4. K^+ channels in microglia

Microglia are the residual immune cells in the brain [165]. The protective effect of microglial immune activation in HAND is mostly temporary. Hyperactivation of microglia and macrophages are often accompanied with disease progression. In addition, depletion of these cells significantly decrease the severity of HIV-1-related CNS neuropathology [166].

Microglia express several K^+ channel families including K_V1, K_V3, Kir [167-169]. Kir channels are often considered to be functional on resting microglia. $K_V1.3$ and $K_V1.5$ are highly involved in pathogenesis of HAND [140, 141, 170]. Activation of microglia leads to neuronal injury through a mechanism requiring microglial $K_V1.3$ activity. Data published from our lab found that collected culture medium from K_V blocker-treated microglia attenuate HIV-1 Tat-induced neuronal apoptosis that corresponds with Erk1/2 MAPK

kinase activation. Moreover, enhancement of outward K^+ currents on microglia increases the cell motility [141]. Blockade of $K_V1.3$ significantly reduce microglia migration to cellular debris [171]. In addition, Ca^{2+} activated K^+ channels 3.1 (KCa3.1) promote rat microglia migration [172]. KCa3.1 blocker reduced the microglial activities of phagocytosis and chemotactic in primary culture [173].

Summary and Discussion

There are increasing interests in myelin sheath loss and WM damage in HIV-1 brain. The clinical and postmortem manifestations of myelin damage of HAND patients, contributions of BBB integrity disruption, oligodendrocyte apoptotic molecular mechanisms, and OPC regulation imbalance in oligodendrocyte/myelin abnormalities have been addressed in this chapter. All of these factors potentially involve in generation of HAND pathology. Given that milder forms of HAND remain prevalent and HIV-1 proteins and toxic factors released from infected cells persist in brain even in the era of cART, the studies on direct toxicity of HIV-1 viral proteins on oligodendrocytes and OPCs, as well as neurons, are emerging. Because the transcription of HIV-1 viral protein continues in the CNS even the viral detection is minimal [174], this concept orchestrates with the context of changed HAND pathogenesis in cART era, of which inflammation, encephalitis, and neurodegeneration has been significantly decreased by the advent of cART. The ways on the regulation of oligodendrocyte lineage cell development are well-established including the extracellular pathways, cell to cell contact, and intracellular pathways. Since $NG2^+$ cell is the biggest population of progenitor cells in human adult brain, the decreased absolute cell number and proliferation of NPC and OPC may be less contributive to myelin deficits in HAND. However, the evidences of HIV-1-related OPC differentiation and remyelination imbalance serve to better understand the impact

of remyelination for CNS repair in HAND patients, providing a new therapeutic strategy [175].

Chapter 2

Human immunodeficiency virus protein Tat induces oligodendrocyte injury by enhancing outward K^+ current conducted by $K_V1.3$

Abstract

Brain white matter damage is frequently detected in patients infected with human immunodeficiency virus type 1 (HIV-1). White matter is composed of neuronal axons sheathed by oligodendrocytes, the myelin-forming cells in central nervous system. Oligodendrocytes are susceptible to HIV-1 viral trans-activator of transcription (Tat) and injury of oligodendrocytes results in myelin sheath damage. It has been demonstrated that activation of voltage-gated K^+ (K_V) channels induces cell apoptosis and oligodendrocytes predominantly express K^+ channel $K_V1.3$. It is our hypothesis that Tat injures oligodendrocytes via activation of $K_V1.3$. To test this hypothesis, we studied the involvement of $K_V1.3$ in Tat-induced oligodendrocyte/myelin injury both *in vitro* and *ex vivo*. Application of Tat to primary rat oligodendrocyte cultures enhanced whole-cell $K_V1.3$ current recorded under voltage clamp configuration and confirmed by specific $K_V1.3$ antagonists Margatoxin (MgTx) and 5-(4-phenoxybutoxy) psoralen (PAP). The Tat enhancement of $K_V1.3$ current was associated with Tat-induced oligodendrocyte apoptosis, which was blocked by MgTx and PAP or by siRNA knockdown of $K_V1.3$ gene. The Tat-induced oligodendrocyte injury was validated in cultured rat brain slices, particularly in corpus callosum and striatum, that incubation of the slices with Tat resulted in myelin damage and reduction of myelin basic protein which were also blocked by aforementioned $K_V1.3$ antagonists. Further studies revealed that Tat interacts with $K_V1.3$ as determined by protein pull-down of recombinant GST-Tat with $K_V1.3$ expressed in rat brains and HEK293 cells. Such protein-protein interaction may alter channel protein phosphorylation, resultant channel activity and consequent oligodendrocyte/myelin injury. Taken together, these results demonstrate an involvement of $K_V1.3$ in Tat- induced oligodendrocyte/myelin injury, a potential mechanism for the pathogenesis of HIV-1-associated white matter damage.

Keywords: HIV-1, Tat, brain white matter, myelin, oligodendrocyte, $K_V1.3$, neurodegeneration

1. Introduction

Neurologic complications of human immunodeficiency virus type 1 (HIV-1) infection remain common in the era of effective combination antiretroviral therapy (cART). Up to half of infected individuals develop HIV-1-associated neurocognitive disorders (HAND), the cause(s) remain obscure. Many studies have revealed a preferential damage to cerebral white matter in HIV-1-infected brain [8, 41, 82, 91], and such damage is prevalent even in the era of cART and more severe in patients with HAND [111, 127]. Structure magnetic resonance imaging and diffusion tensor imaging studies in HIV-1-infected individuals have revealed a subcortical white matter damage mainly in the regions of the corpus callosum, internal capsule and other brain regions [41, 54, 91, 92, 111, 176]. Moreover, cognitive impairment in HIV-1-infected individuals with AIDS was found to be associated with white matter injury in the corpus callosum, internal capsule, and superior longitudinal fasciculus [41, 176]. It appears that subcortical damage in white matter plays a more important role than cortical damage in the mediation of HAND symptoms which are predominantly of the subcortical type [22, 24, 177, 178].

Cerebral white matter consists mostly of myelinated axons and axonal myelination is formed by oligodendrocytes. The integrity of the myelin sheaths is essential for the propagation of nerve impulses along axons. It has been demonstrated that myelin pallor, an abnormality that could reflect a decrease in myelin components [29, 179], is frequently seen in patients with HIV-1 encephalitis and in cART naïve subjects. Myelin sheath damage and changes in numbers of oligodendrocytes have also been observed in HIV-1-infected individuals [90, 180]. *In vitro* studies have shown that exposure to recombinant viral envelope protein gp120 resulted in alterations of oligodendrocyte functional activity and myelin formation in rat oligodendrocytes maintained in a cell culture system [14, 15], exampling HIV-1 protein impairment of oligodendrocyte/myelin, which may lead to axonal injury, demyelination and ultimately white matter damage.

Nevertheless, how HIV-1 proteins induce oligodendrocyte/myelin injury is not fully understood.

Increasing evidence indicates that activation of voltage-gated K^+ channels (K_V) is an essential pathway in programmed cell death [26, 84] and enhancement of outward K^+ current results in neural cell apoptosis [181, 182]. Oligodendrocytes express several subtypes of K_V channels including a predominant $K_V1.3$ [129, 183]. A decrease of $K_V1.3$ expression or outward K^+ current in oligodendrocytes is essential for synthesis of myelin structural proteins and suppression of outward K^+ current promotes oligodendrocyte maturation and survival. These results suggest a role of $K_V1.3$ in the regulation of oligodendrocyte functionality [130, 133]. Moreover, activation of p53 has been detected in the oligodendrocyte lineage cells in the postmortem brains of HAND patients, but not in control brains [83], suggesting oligodendrocytes undergo apoptosis in HIV-1-infected brains. Thus, it is our hypothesis that continued viral replication and viral proteins induce oligodendrocyte/myelin injury by activation of oligodendrocyte $K_V1.3$ channels, leading to myelin/white matter damage and HAND pathogenesis. To test this hypothesis, we studied how HIV-1 protein Tat induces oligodendrocyte/myelin injury, as infected brain cells continuously express and release Tat protein despite the controlled viral replication [184, 185]. Our results showed that HIV-1 Tat enhances outward K^+ current conducted by $K_V1.3$ leading to oligodendrocyte/myelin injury.

2. Materials and Methods

2.1. Materials. HIV-1 Tat IIIB was purchased from Immunodiagnostic, Inc. (Woburn, MA). Tat was dissolved in sterile distilled water and, aliquots of Tat were kept as 50 µg/ml stock solution at -80 °C.

2.2. Animals. Pregnant Sprague-Dawley rats were purchased from Charles River (Wilmington, MA) and maintained under the ethical guidelines for the care of laboratory animals, and all animal procedures were reviewed and approved by the Institutional Animal Care and Use Committee (IACUC) of the University of Nebraska Medical Center.

2.3. Oligodendrocyte preparation and culture. Oligodendrocyte cell cultures were prepared as described previously [186] and all culture materials were purchased from Sigma-Aldrich (St. Louis, MO) unless otherwise stated. Briefly, P1-2 neonatal rat pups were decapitated with large scissors and place the heads in 10 cm-petri dish filled with cold Hank`s buffered salt solution (HBSS). Microdissecting scissors was used to carefully cut skin and skull along the midline from neck toward the nose. Brains were taken out with a spatula and placed to another petri dish contained cold HBSS. The meninges were removed with forceps under a dissection microscope. Cortex tissue was dissociated by cutting the brain to two hemispheres and removing hippocampus and olfactory bulbs.

Dissociated cortex tissue was incubated in 0.25% trypsin and 200 U DNase contained in HBSS at 37 °C for 15 min. Then 1 ml FBS was added to stop trypsinization. Homogenate was collected into a 50-ml tube and the contents were triturating by pipetting several times to separate any tissue block. The tissue suspension was next collected into a clean 50-ml tube and followed by centrifugation at 1500 r.p.m. for 10 min. The supernatant was removed and 20 ml HBSS was added to re-suspend the remained cells/tissues by triturating cells/tissue for about 20 times. The remaining tissue

suspension was passed through nylon mesh with pore diameter size of 100 μm and 40 μm sequentially. Cells were collected by centrifugation at 1500 r.p.m. for 10 min. Collected cells were re-suspended in DMEM (with L-glutamine and sodium pyruvate, Cellgro, Manassas, VA) supplemented with 20% FBS (Gibco, Grand Island, NY) and 1% penicillin/streptomycin (Gibco). Mixed glia cultures were grown on poly-D-lysine-coated T75 flasks (Thermo, Nazareth, PA) for 10 d and refreshed medium every 3 d.

To isolate OPCs, the flask was pre-shaken for 1 h on an orbital shaker at a speed of 200 r.p.m. in order to remove microglia. OPCs were isolated by shaking overnight at 200 r.p.m. at 37 °C. Cell suspensions were transferred into non-treated 10 cm petri dishes for 30 min to further separate OPCs by differential adhesion (astrocytes and microglia can attach to bottom faster than OPCs/oligodendrocytes). OPC-contained supernatant was collected by slightly swirling petri dish and transferring the supernatant in a sterile 50-ml tube, then the supernatant was passed through 40 μm nylon cell strainers. OPCs were collected by centrifugation at 800 r.p.m. for 5 min and suspended in OPC medium (described below). OPCs were plated onto poly-D-lysine-coated coverslips, culture dishes, or plates in OPC culture media in a density of $1 \times 10^4/cm^2$.

Different stages of oligodendrocytes are characterized by unique combinations of genes [187], and three major markers were chosen to specify the following stages in the present study: $NG2^+$ OPCs, galactocerebroside $(GalC)^+$ immature oligodendrocytes, and MBP^+ mature oligodendrocytes. Basal chemically defined medium (BDM) was made of DMEM containing 0.1% BSA, 1% Insulin-Transferrin-Selenium (Gibco), 10 nM D-biotin, and 10 nM hydrocortisone. $NG2^+$ OPCs were maintained in BDM supplemented with 10 ng/ml PDGF-AA (homodimer PDGF consists of 2 A domains) and 10 ng/ml bFGF (both from Peprotech, Rocky Hill, NJ) for 0-7 d. $GalC^+$ immature oligodendrocytes were cultured in the same medium as $NG2^+$ OPCs for additional 3 d. MBP^+ mature

oligodendrocytes were obtained by transferring cells to differentiating medium (BDM, 15 nM triiodothyronine, 10 ng/ml CNTF (Peprotech) and 5 µg/ml N-acetyl-L-cysteine) for 2-3 d (Fig. 3).

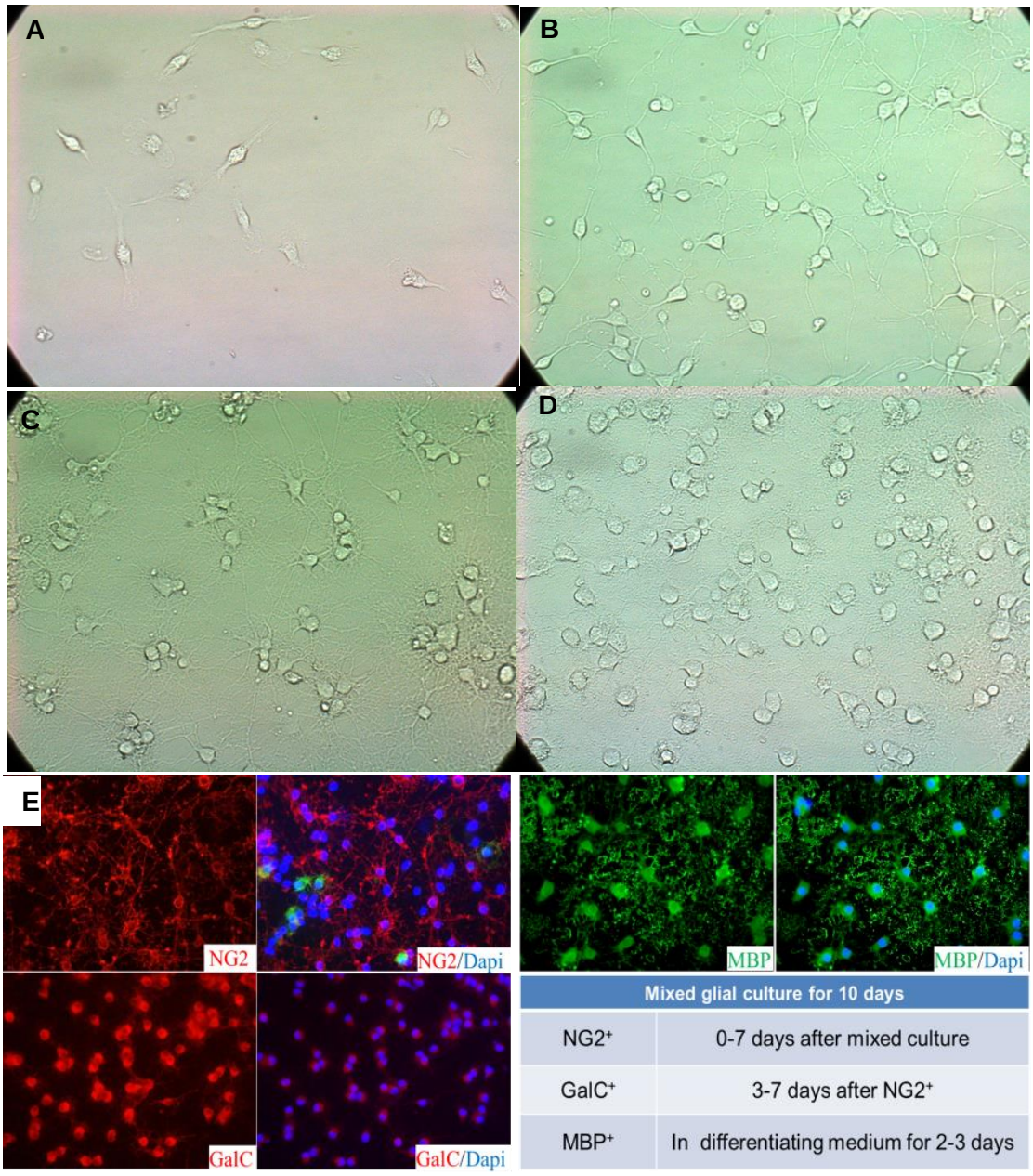

Mixed glial culture for 10 days	
NG2$^+$	0-7 days after mixed culture
GalC$^+$	3-7 days after NG2$^+$
MBP$^+$	In differentiating medium for 2-3 days

Figure 3. Primary culture of oligodendrocyte lineage cells. Panel A, B, C, representative fields of OPC culture of 1, 4, and 7 d representatively after isolation from mixed glial culture. Panel D, a representative field of oligodendrocyte cultured in differentiating medium for 2 d. A, B, C, D images were taken under white field (×200). E, Portrayed cell purity revealed by staining with NG2, MBP and GalC respectively depends on different stages of cells. The nuclei were visualized by Dapi staining. All Images were visualized by fluorescent microscopy (×400). Cell counting is normalized by Dapi staining. The table shows corresponding conditions in culture along with the OPC/oligodendrocyte development.

2.4. Electrophysiology. Cells were seeded onto 3.5-cm culture dishes for whole-cell recording of ionic currents. Recording electrodes were pulled from borosilicate glass micropipettes (WPI Inc., Sarasota, FL) with a P-97 horizontal micropipette puller (Sutter Instruments, Novato, CA) to a resistance of 5-8 MΩ. The electrode solution contained (in mM): 140 KCl, 2 $CaCl_2$, 2 $MgCl_2$, 11 EGTA, 10 HEPES/KOH, pH7.3, and had an osmolarity of 300 mOsm, as measured by a vapor pressure osmometor (WESCOR, Logan, UT). The standard bath solution contained (in mM): 140 NaCl, 5.4 KCl, 2 $CaCl_2$, 1 $MgCl_2$, 10 HEPES/NaOH, pH7.3. D-sucrose was used to adjust the osmolarity of this solution to 305 mOsm prior to recording. Stock solutions of K_V1.3 specific inhibitors, 5-(4-phenoxybutoxy) psoralen (PAP, Sigma) and Margatoxin (MgTx, Sigma), were prepared in deionized water before being diluted to a working concentration with bath solution, and applied by super-fusion. External super-fusion of the cells was performed by exchanging the bath at a rate of 1 ml/min. A Burleigh micromanipulator (PC-5000, EXFO, Canada) was used to position the recording electrode.

Under 40 × objective lens, cells appeared bright and dimensional were chosen to patch at. The electrode solution was filled into electrodes by a syringe linked with a micro-loader tip. Air bubbles were eliminated by tapping pipette several times. Then the glass electrode was placed onto the pipette holder connected with head stage. A positive pressure was provided to electrode by giving 0.2 ml air through syringe. Following this, the electrode was placed into the bath solution and off-set was adjusted to zero. The oscilloscope showed square current response to the seal test. Under voltage-clamp mode, the electrode resistant was checked in membrane test function in Clampex software.

Under the 10 × objective lens, adjusted the focus onto the tip of electrode and then switched the objective lens to 40 ×. The electrode was slowly approached to the chosen

cell by the micromanipulator. During approaching, it was important to keep the focus on the tip of electrode but not the cells. When the cells were becoming clearer, the electrode tip was being closer to the cell. The electrode tip was positioned to touch the cell surface at the middle right where close to the center of cell body. Once get touched, the positive pressure was released and instead, a negative pressure was applied to gain a GΩ seal. The oscilloscope showed flat while GΩ seal was achieved. Followed seal, the fast capacitance was corrected.

To rapture the cell membrane, further suction was applied by the syringe. Once the membrane was broken through, the current response showed exponential decay. The membrane capacitance of each cell was read and recorded under cell mode in membrane test function. The membrane capacitance was adjusted by at least 70%. The currents were recorded in Clampex.

Whole-cell K^+ currents were induced by applying voltage steps from -150 mV to +60 mV in increments of 15 mV, and current amplitudes were measured at the peak for each test potential. Current density (pA/pF) was calculated by dividing the digitized current values by whole-cell capacitance, which represents cell membrane surface area. All experiments were done at room temperature (22-23 °C). Recordings were obtained with an Axopatch-200B amplifier (Molecular Devices, Sunnyvale, CA). Current signals were filtered at 1 kHz and digitized at 5 kHz using a Digidata 1440A interface (Molecular Devices). The current and voltage traces were displayed and recorded on a computer using Clampex 9.0 data acquisition and analysis software (Molecular Devices). Data were analyzed by Clampfit 10.0 (Molecular Devices). All final graphics in the present work were constructed by Origin 8.0 (OriginLab, Northampton, MA).

2.5. MTT Assay. MTT assay was used to assess cell viability. Cells were cultured in 48-well plates for MTT assay to minimize diversity between replicates. The 3-(4,5-

Dimethylthiazol-2-yl)-2,5-Diphenyltetrazolium Bromide (MTT) was prepared in sterile PBS at concentration of 5 mg/ml (10 ×) and stored at -20 °C. The working solution was made by diluting the stock MTT solution 10 times with DMEM. The pre-treated cells were exposed to working solution and incubated in 37 °C for 2 h. The MTT solution was discarded and replaced with 150 µl dimethyl sphingosine (DMSO). Cells were then shaken for 15 min at 200 r.p.m. for completed lysis. The dissolved solution was transferred of 100 µl from each well to a 96-well plate and, 96-well plate was eventually placed to a plate reader and tested the optical density at 560 nm.

2.6. Apoptosis Assay.

A) Terminal deoxynucleotidyl transferase dUTP nick end labeling (Tunel) staining was performed with the *in situ* cell death detection kit (Fluorescein, Roche Applied Science, Indianapolis, IN). Cultures plated on coverslips were fixed in 4% paraformaldehyde for 1 h at room temperature and permeabilized with 0.1% Triton X-100 for 30 min. Cover slips were washed 5 min × 3 times with PBS. Tunel reaction mixture was made by adding label solution to enzyme solution (terminal deoxynucleotidyl transferase and fluorescein-labeled nucleotides) at a ratio of 1:50. Each cover slip was prepared 30 µl of reaction mixture. The reaction mixture was applied onto clean Para film and, cover slips were flipped onto reaction mixture solution drops and incubated for 90 min at 37 °C. After washing, coverslips were mounted in vectashield mounting medium with Dapi stain (Vector Laboratories, Burlingame, CA) and cells were visualized by a fluorescent microscope. Apoptosis was assessed in each of three experimental preparations by examining 10 microscopic fields per experimental group.

B) Propidium iodide (PI) staining. Fixation of cultures was performed same as mentioned above in Tunel staining. Cells were briefly equilibrated in 2 × SSC (0.3 M

NaCl, 0.03 M sodium citrate, pH 7.0), and then incubated the in 100 µg/ml DNase-free RNase in 2 × SSC for 20 minutes at 37°C to remove RNase. Coverslips were rinsed 1 minute × 3 times with 2 × SSC. PI solution was made at a concentration of 500 nM by diluting the 1 mg/ml (1.5 mM) stock solution 1:5000 in 2 × SSC. Cells were incubated with the diluted working staining solution for 1 m. Cells were washed 4 times with shaking in 2 × SSC. Excessed buffer was drained from the coverslips and, coverslips were mounted in vectashield mounting medium with Dapi stain. The analysis procedures were performed same as Tunel assay.

2.7. Brain slices culture. Coronal brain slices were prepared from 21-d-old neonatal Sprague-Dawley rats. The culture procedures were performed as described by Stoppini, etc [188]. All surgical instruments were autoclaved. Vibrotome (Campden instruments, MA752 Motorised advance vibroslice) was sterilized by exposure to ultraviolet light for 1 h. The 2% of agarose gel was prepared in sterilized water to help positioning rat brains. Artificial cerebrospinal fluid (ACSF) contained (in mM) NaCl 124.0, KCl 3.0, $CaCl_2$ 2.0, $MgCl_2$ 2.0, NaH_2PO_4 1.25, $NaHCO_3$ 26.0, and glucose 10.0, pH 7.2. The culture medium consisted of 50% MEM with HEPES (Gibco), 25% horse serum (Atlanta biological, Flowery Branch, GA), 25% Hank`s solution (Invitrogen), and 6.5 mg/ml glucose. Inserts with 30 mm diameter, sterile, porous (0.8 µm), transparent and low-protein-binding membrane were placed into 6-well plates as scaffold for the brain slices.

Agarose gel was cut to a small cube and fixed onto stage of vibrotome by super glue (Fig. 4 Top). Rats were anesthetized with isoflurane, and then quickly decapitated by small animal decapitator (Stoelting, 51330). The whole brain was dissected and fixed onto the stage of vibrotome next to agarose gel cube (Fig. 4 Top). The stage was placed into cutting chamber filled with pre-cooled and oxygenated ACSF. Oxygen was provided

to ACSF during the whole cutting procedure. Slices of 400 µm were cut and separated in ACSF. The slices were then transferred on to culture insert plated in 6-well plate with 1 ml/well pre-warmed (37 °C) culture medium. The 6-well plates were then kept in incubator at 37 °C with 5% CO_2. It was important to keep the slices placed on the interface between air and medium (Fig. 4 Bottom).

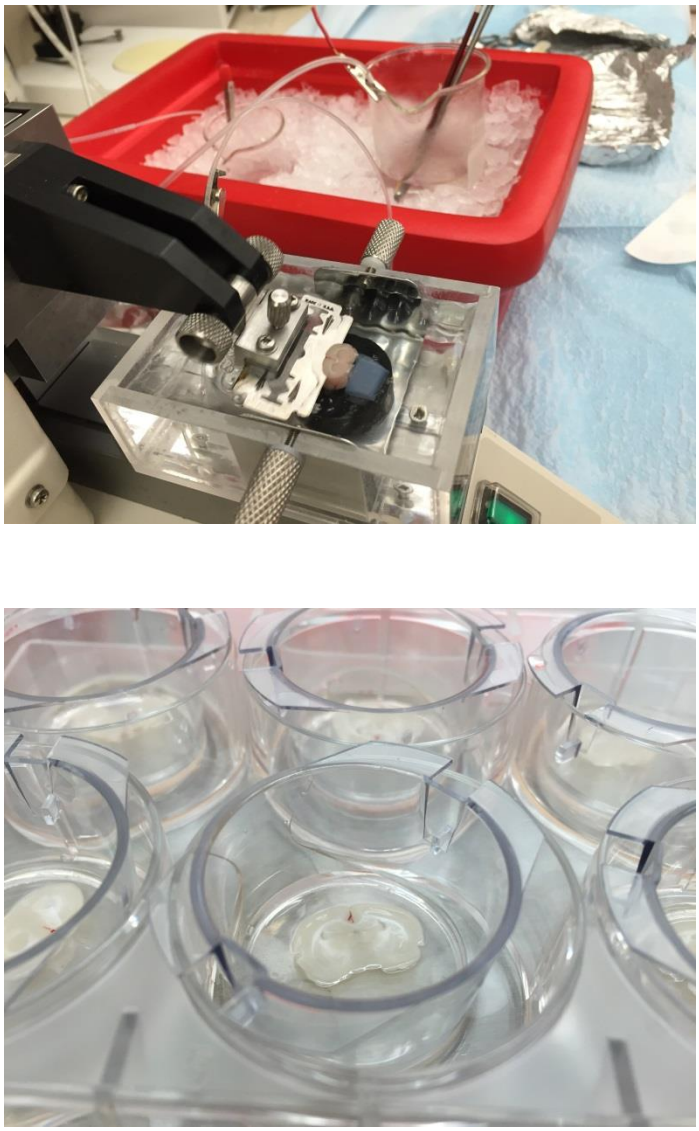

Figure 4. Illustration of the cutting and culturing technique. Top: photograph of cutting brain slices. Bottom: photograph of a culture plate containing brain slices. Medium should not cover the insert membrane.

2.8. Cryostat section. The brain slices were washed with PBS for 3 times after treatments, then fixed with 4% paraformaldehyde for 24 h. The tissue was then progressively changed into graded 10%, 20%, and 30% sucrose/PBS solution each for 24 h for cryoprotection. The tissues were orientated and embedded within OCT and quickly frozen in -80 °C. The tissue blocks were cut into 10 µm sections by Leica cryostat (LEICA CM1850 UV).

2.9. Immunofluorescences. The prepared brain sections were blocked and permeabilized in 10% goat serum/0.1 % Triton/PBS solution for 30 min in room temperature. The slides were dried carefully, and the tissue sections were circled by hydrophobic pen, followed by applying 50 µl of the primary anti-rat MBP antibody (1:200, Chemicon) for each section. Slides were placed in a humidified chamber and incubated at 4 °C overnight. Next day, after washing the sections with PBS 5 min × 3 times, sections were incubated in goat anti-rat fluorescent secondary antibody (1:1000, Invitrogen) for 2 h in room temperature by using the same technique as described for primary antibody incubation. Sections were washed 5 min × 3 times and mounted with coverslips in vectashield mounting medium with Dapi (Vector Laboratories, Inc. Burlingame). The myelin sheath was visualized under fluorescent microscope.

2.10. Total protein extraction. The whole cell lysates were prepared in RIPA buffer (BioRad, Hercules, CA) while tissue was lysed in tissue extraction reagent (Invitrogen). In details, following experimental treatments, cells or brain tissue were washed twice with ice-cold PBS and then PBS was aspirated. For cultured cells, 150 µl RIPA buffer supplemented with protease inhibitor was added to each well of 6-well plate. Cells were detached by scraping the well bottom and gently transferred into a microcentrifuge tube. For brain tissue, dissected corpus callosum and striatum from cultured brain slices were put into separate tubes, followed by addition of 200 µl tissue homogenate reagent to each tube. Sonication was performed 3 times for 15 seconds to

lyse brain tissues. Homogenate was then projected to a freeze-thaw cycle for complete lysis. Cell lysate or tissue homogenate were centrifuged at 10,000 r.p.m. for 10 min and supernatant was collected to a fresh tube. Next, 20 µl of each sample was taken out for protein concentration determination. A quarter of the sample volume of 5 × loading buffer was added to protein samples. Protein samples were denatured by boiling water for 7 min, and stored in -20 °C for western blotting.

5 × loading buffer consisted of 0.25% Bromophenol blue, 0.5 M dithiothreitol, 50% glycerol, 10% sodium dodecyl sulfate, and 0.25 M Tris-Cl (pH 6.8).

2.11. Extraction of total membrane proteins. Membrane protein enriched fraction was extracted by Membrane Protein Extraction Kit (BioVision Inc, CA). Cells were cultured in 6-cm culture dishes for membrane protein extraction. After experimental treatments, cells were washed twice with ice-cold PBS. Firstly, 1 ml homogenization buffer was applied to each culture dish. Cells were scraped and then homogenized by vortex for about 10 times. Homogenate was then collected to a 1.5-ml tube and, centrifuged at 700 g for 10 min at 4 °C. The supernatant was transferred to a fresh tube and the pallet was discarded. Collected supernatant was centrifuged from at 10,000 g for 30 min at 4 °C.

Following the centrifugation, protein would be separated to the cytosol protein fraction (supernatant) and the total cellular membrane protein fraction (pallet). Dissolve the pellet in 60 µl 0.5% Triton X-100 in PBS buffer. Then 20 µl from each sample was taken for concentration determination.

2.12. Protein concentration determination. The BCA protein assay kit (ThermoFisher Scientific, Waltham, MA) was employed to quantify protein concentration. BCA working reagent was prepared by mixing 50 parts of BCA Reagent A with 1 part of BCA reagent B. The needed total volume of working reagent was determined by the

following equation: (number of standards + number of unknowns) × (number of replicates) × 100 µl = total volume of working reagent required.

Standards were prepared by diluting 2 mg/ml albumin ampules in working reagent to 200, 100, 50, 25, 12.5 µg/ml. Then 100 µl of each standard was put into a 96-well plate. At separate wells, 100 µl of working reagent only was placed as zero. Next, 10 µl of each unknown samples was diluted to 90 µl working reagent. Every standard and sample was duplicated. After all samples were prepared, the plate was incubated in 37 °C for 30 min. The plate was then placed in a plate reader and the absorbance of all the samples were measured with the testing wavelength at 560 nm.

Standard curve was made by plotting the average blank-corrected measurement for each albumin standard versus its concentration in µg/ml. The standard curve was used to determine the protein concentration of each unknown sample. The volume for 15 µg protein of each sample was calculated and then the denatured samples were projected to Western blotting.

2.13. Western blotting. 10 × Tris/glycine buffer, 10 × Tris/glycine/SDS buffer, 10% SDS, and 30% Acrylamide/bis solution were all purchased from Bio-Rad. The 10 × TBS (Tris-buffered saline, 1 liter) was prepared by dissolving 24.2 g Tris base, 80 g NaCl in distilled water, and adjust pH to 7.6 with HCl. Washing buffer was prepared by diluting 1 ml 100% Tween-20 to 1 liter 1× TBS (TBST). Separating gel (10%)consisted of 1.5 mM Tris-HCl (pH 8.8) 2.5 ml, ddH_2O 4.0 ml, 30% acrylamide/bis solution 3.3 ml, 10% SDS 100 µl, 10% ammonium persulfate 100 µl, and TEMED 5 µl. Stacking gel (5%) consisted of 1mM Tris-HCl (pH 6.8) 0.63 ml, ddH_2O 3.4 ml, 30% acrylamide/bis solution 0.83ml，10% SDS 100 µl，10% ammonium persulfate 100 µl，TEMED 5 µl.

Proteins were firstly separated by electrophoresis depending on the molecular weight. In details, 15 μg protein of each sample was loaded onto SDS-polyacrylamide gels. Electrophoresis was run under 70 mV constant voltage and switched to 110 mV when samples enter lower separating gel. Electrophoresis was stopped when the Bromophenol blue reached the bottom edge of SDS-polyacrylamide gel.

After electrophoresis, proteins were transferred from gel to a polyvinylidene difuoride (PVDF) membrane by 100 mV constant voltage in 1 × Tris/glycine/SDS buffer containing 20% methanol for 70 min at 4 °C. The PVDF membrane was then blocked in 5% dry milk (3% BSA for phosphorylated-protein examination) in TBS for 1 h in room temperature. Following blocking, membranes were incubated in primary antibodies diluted in blocking buffer at 4 °C overnight. Primary antibodies were rabbit polyclonal anti-K_V1.3 (1:100, Alomone Lab, Israel), rat monoclonal anti-MBP (1:500, MAB386, Chemicon/Millipore, Billerica, MA) and mouse monoclonal anti-β-actin (1:5000, Sigma). Afterwards, membranes were washed in TBST 10 min × 3 times and then incubated in HRP-conjugated anti-rabbit, anti-rat or anti-mouse secondary antibodies (1:10,000, all from Jackson ImmunoResearch Laboratories, West Grove, PA) for 1.5 h at room temperature. Finally, membranes were washed in TBST 10 min × 3 times and incubated with Pierce ECL Western blotting substrate (Thermo Scientific, Rockford, IL), imaged by the FluorChem M system (ProteinSimple, Santa Clara, CA), and band densities were measured by Alphaview software (ProteinSimple).

2.14. siRNA silencing. Pre-designed ON-target plus SMARTpool siRNA against rat KCNA3 (K_V1.3, NM-019270) mRNA was purchased from Dharmacon, Inc. (Chicago, IL). Non-targeting (NT) siRNA (rat) (Dharmacon, Inc) was transfected at the same concentration as control. K_V1.3-siRNA and NT-siRNA were transfected 72 h in prior to gaining the protein level knockdown.

OPCs were plated into 6-well plates at a density of 0.35×10^6 cells/well. Stock siRNA was diluted to 5 µM siRNA solution in RNase-free siRNA buffer solution from stock solution in a sterile tube. For each well, 10 µl of the prepared siRNA was diluted to 190 µl DMEM, labeled as Tube A. In separate tubes, 2 µl DharmaFECT transfection reagent was diluted with 198 µl DMEM labeled as Tube B. Each tube was shaken to mix solution and incubated at room temperature for 5 min. The content was gently mixed from Tube A to Tube B by pipetting carefully up and down several times. Mixed solution was incubated for 20 minutes at room temperature. Then 1.8 ml of BDM was added to the mixed contents for a final volume of 2 ml transfection medium and a final siRNA concentration of 25 nM. The culture medium was refreshed with transfection medium and incubated cells at 37 °C in 5% CO_2 for 72 h.

2.15. HEK293 cell line culture. HEK293 cells were kindly provided by Dr. Buch. The frozen cells-contained vial was thaw in 37 °C water bath by gentle agitation. The vial was removed from the water bath as soon as the contents were thawed. The contents were transferred in to a fresh 10-ml tube containing 9 ml culture medium (DMEM supplemented with 10% FBS and 1% penicillin/streptomycin). Cells were pelleted by centrifugation at 800 r.p.m. for 5 min. The supernatant was discarded and cells were re-suspended in 20 ml culture medium and seeded in T75 culture flask. Cells were kept in 37 °C, 5% CO_2 atmosphere and replaced with 10 ml fresh medium every the other day until the cells were ready for experiments or to be subcultured. For subculture, the culture medium was removed and cells were washed with sterile PBS twice, 3 ml of 0.25% Trypsin-EDTA solution was added to culture flask for 5 min to detach the HEK293 cells. After achieving complete detachment, 6 ml of culture medium was added to stop trypsinization. Cells were collected by centrifugation at 800 r.p.m. for 5 min and then re-suspended in 15 ml culture medium. Aspirations were performed for about 50 times to

dissociate cells. Aliquots of the cell suspension were placed into new flasks or culture plates at a density of $6 \times 10^3/cm^2$ for continue culture or $6 \times 10^4/cm^2$ for overexpression.

2.16. K_V1.3 overexpression. The pJK and pJK/K_V1.3 plasmids are kind gifts from Dr. Erich Gulbins [189]. The HEK293 cells were seeded in 6-well plates at a density of 0.6×10^6/well and, grow overnight to reach 70-90% confluent. Lipofectamine 2000 reagent was diluted in Opi-MEM (Invitrogen) at a ratio 5 µl: 95 µl. The pJK or pJK/K_V1.3 plasmid at amount of 2.5 µg was diluted in Opi-MEM to make the final volume at 100 µl. Diluted plasmids were added to each tube of diluted lipofectamine 2000 and, incubated at room temperature for 15 min. DNA-lipofectamine complex were applied to cells. Transfected-cells were collected and lysed after 48 h.

2.17. Pull-down assay. The HEK293 whole cell lysate was prepared same as described above in section 2.10.. Rat brain tissue sample was homogenized in the isotonic sucrose homogenization buffer (2 ml) containing 0.32 M sucrose, 10 mM HEPES, pH 7.4, 2 mM EDTA, and a protease inhibitor cocktail (Thermo Scientific, Rochester, NY) in a glass grinding vessel with a motor driven Teflon pestle at 700 r.p.m.. The homogenate was then centrifuged at 800 g for 10 min at 4 °C. The supernatant was aspirated into a new tube and centrifuged at 12,000 g for 15 min at 4 °C. Pellets were dissolved in buffer containing 10 mM HEPEs, 1% Triton X-100 (pH 7.4) and proteinase inhibitor cocktail for 60 min at 4 °C with rotation. Then the tube was centrifuged at 12,000 g for 15 min at 4 °C. The supernatant (membrane enriched part) was collected for pull down assay. GST-HIV-Tat recombinant protein (1 µg for transfected-HEK293 and 10 µg for rat brain tissue protein) were put into protein lysate with rotation overnight at 4 °C. The next day, 50 µl sepharose beads (GE health) were put into the rotating tube for another 3 h rotation. The beads were collected by centrifugation of 5,000 g for 2 min and followed with three times wash by PBS. Then the beads were added with 30 µl 2 × loading buffer boiled 95 °C for 10 min to elute the binding protein complex. The

eluted samples were subjected to Western Blot for analysis of $K_V1.3$ presence with specific $K_V1.3$ antibody (1:1000, NeuroMab).

2.18. Co-immunoprecipatation (Co-IP). For native protein Co-IP, rat brain was taken from 30-d-old Sprague Dawley rat and homogenized in the tissue extraction buffer (Invitrogen) with addition of proteinase inhibitor cocktail (Sigma). Sonication was performed 3 times for 15 seconds to lyse tissues. Homogenate was then projected to a freeze-thaw cycle for complete lysis. Then homogenate was centrifuged at 10,000 r.p.m. for 10 min and supernatant was collected to a fresh tube. BCA assay was then performed as described to quantify protein. The amount of 1 mg protein was taken for co-IP. To pre-clear protein lysate, 20 µl of 50% Protein A magnetic beads (GE Healthcare, Sweden) were added to lysate and then incubated with rotation at 4 °C for 1 h. Beads were pelleted by centrifugation at 1000 g for 30 s. The supernatant was collected to a fresh tube for immunoprecipitation. $K_V1.3$ mouse primary antibody (Neuromab, 10 µl) was added to pre-cleared lysate and incubated with rotation overnight at 4 °C. Next day, 20 µl of Protein A magnetic beads was added and incubated with rotation for 30 min at 4 °C. Bead was pelleted by centrifugation at 1000 g for 30 s. The supernatant was discarded and pellet was washed with 500 µl tissue extraction buffer for 5 times. Pellet was re-suspended in 1 × protein loading buffer and proceeded to Western Blotting for analysis of p-Src (Cellsignaling, 1:1000) presence.

2.19. Statistics. All data are expressed as mean ± S.D. unless otherwise indicated. Statistical analyses were performed by student`s *t* test or one-way ANOVA followed by a Fisher`s least-significant difference test for multiple comparisons. The difference between groups was considered significant at $p < .05$.

3. Results

3.1. HIV-1 protein Tat enhancement of $K_V1.3$ current in oligodendrocyte lineage cells

To determine if HIV-1 protein Tat induces oligodendrocyte/myelin injury via activation of $K_V1.3$ channels, we first examined the expression of $K_V1.3$ current in oligodendrocyte cells. Two specific $K_V1.3$ channel antagonists, MgTx and PAP, were utilized to isolate $K_V1.3$-conducted K^+ currents. Whole-cell outward K^+ currents, induced by voltage-steps, were recorded in oligodendrocytes at the age of 14 DIV in the absence (total) and presence of specific $K_V1.3$ antagonist 5 nM MgTx (IC_{50} ~1 nM) or 10 nM PAP (IC_{50} = 2 nM [190]) in the perfusate. $K_V1.3$ currents were calculated by subtraction of the outward K^+ currents recorded 20 minutes after the entrance of MgTx (MgTx) or PAP (PAP) into the bath chamber from the outward K^+ currents recorded in the absence of MgTx or PAP in the perfusate (Total). These MgTx-sensitive and PAP-sensitive currents are $K_V1.3$ currents as illustrated at the right column (Fig. 5). These results clearly demonstrated the expression of $K_V1.3$ currents in oligodendrocyte lineage cells.

After demonstration of $K_V1.3$ expression in the oligodendrocytes, we next tested effects of Tat on $K_V1.3$ current recorded in the oligodendrocytes. Experiments were carried out on two groups of oligodendrocytes, one was untreated controls (Ctrl, n = 6) and the other was incubated with Tat (Tat, 50 ng/ml, n = 6) for 2 h before conducting electrophysiology recording. Whole-cell outward K^+ currents were recorded in the absence (Total) and presence of MgTx (MgTx). The $K_V1.3$ ($K_V1.3$) currents were calculated as described above. Incubation of the oligodendrocytes with Tat produced an increase of $K_V1.3$ currents (Fig. 6A). The average peak current densities, when measured at +60 mV, were 61.17 ± 5.66 pA/pF in control oligodendrocytes and 94.60 ±

3.59 pA/pF in Tat-treated cells (Fig. 6B). The difference is statistically significant, indicating Tat enhancement of $K_V1.3$ current in oligodendrocytes.

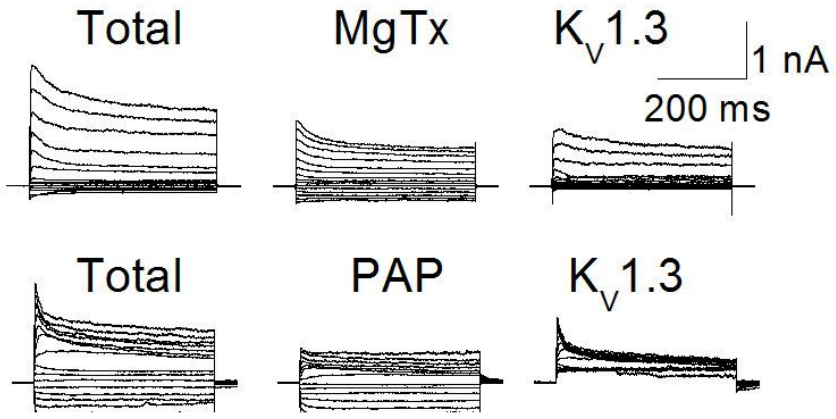

Figure 5. Expression of $K_V1.3$ current in oligodendrocytes. Representative traces are whole-cell outward K^+ currents recorded in oligodendrocytes before (total) and after super-fusion of oligodendrocytes with PAP (10 nM) or MgTx (5 nM). $K_V1.3$-excluded currents showed in the middle column were recorded 20 min after super-fusion of oligodendrocytes with each specific $K_V1.3$ antagonist as indicated. The $K_V1.3$ antagonist-sensitive currents, which represent the $K_V1.3$ current, are calculated by subtraction of individual $K_V1.3$-excluded current from corresponding total current and shown in the right column. $K_V1.3$ current contributes to approximately 50% of the total outward K^+ currents in oligodendrocytes.

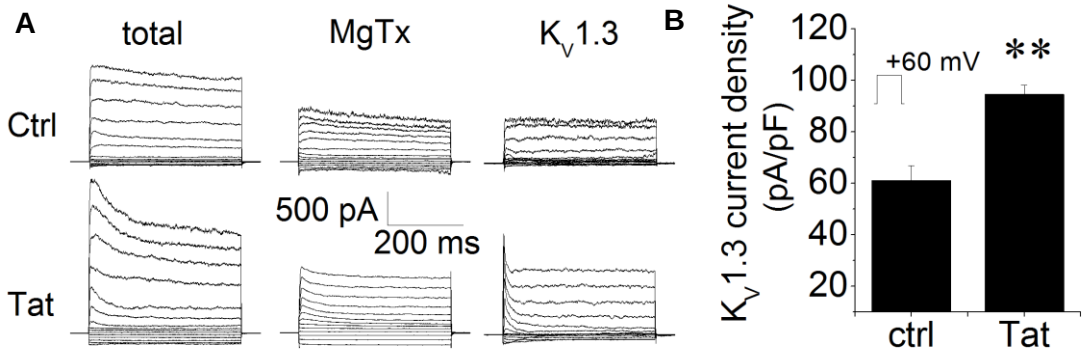

Figure 6. Tat increased $K_V1.3$ current on oligodendrocytes. Data were obtained from oligodendrocytes with (Tat) or without (Ctrl) incubation of 50 ng/ml Tat for 2 h. Panel A shows representative whole cell outward K^+ currents recorded before (total, left column) and 15 min after addition of 5 nM MgTx (MgTx, middle column) to the bath. The $K_V1.3$ currents were then isolated by subtraction of outward K^+ currents recorded in the presence of MgTx from the total currents ($K_V1.3$, right column). Panel B is a summary bar graph illustrating average $K_V1.3$ current density (pA/pF) obtained from oligodendrocytes without (Ctrl) and with Tat treatment (Tat). Note that Tat significantly increased $K_V1.3$ current density measured at +60 mV. ** $p < .01$ vs. control Ctrl. n = 6 in each group.

3.2. Involvement of $K_V1.3$ in Tat-induced oligodendrocyte injury

It has been reported that enhancement of outward K^+ current causes neural cell apoptosis [181, 182]. To explore whether the Tat enhancement of $K_V1.3$ current is associated with Tat-mediated neurotoxic activity, we examined involvement of $K_V1.3$ channel in Tat-induced oligodendrocyte injury by MTT assay in the absence and presence of pre-added (1 h earlier) PAP (10 nM), a specific $K_V1.3$ antagonist. Our results showed that addition of Tat to the culture media for 48 h significantly decreased oligodendrocyte viability in a concentration-dependent manner. At the concentrations of 50 ng/ml and 100 ng/ml, Tat reduced oligodendrocyte viability to 80.50% ± 6.81% of control level ($p < .05$) and 64.76% ± 5.83% of control level ($p < .01$), respectively, indicating that Tat induces oligodendrocyte injury *in vitro* (Fig. 7). Increase of Tat concentrations to 200 ng/ml and 400 ng/ml did not produce further decrease of oligodendrocyte viability (Fig. 7). The Tat-induced decrease of oligodendrocyte cell viability was blocked by pre-treatment of the oligodendrocytes with PAP, demonstrating an involvement of $K_V1.3$ in Tat-induced oligodendrocyte injury (Fig. 7). It has been shown that Tat concentration can reach as high as ~40 ng/ml in the serum of HIV-1-positive patients, with potential higher concentrations at local tissue sites because Tat *in vivo* might be sequestered by endogenous anti-Tat and/or by glycosaminoglycans [32, 191]. Thus, Tat at a concentration of 50 ng/ml was considered as being physiological relevant and adopted for the subsequent studies reported hereinafter.

Increasing evidence indicates that activation of K_V channels is an essential pathway in programmed cell death [26, 84] and activation of apoptotic pathway has been observed in both HAND patients and Tat transgenic mice [12, 83]. Whether Tat enhancement of $K_V1.3$ current contributes to Tat-induced oligodendrocyte apoptosis was further investigated using pharmacological and molecular genetic approaches. As

anticipated, addition of Tat to the oligodendrocyte culture for 48 h resulted in oligodendrocyte apoptosis as detected by Tunel assay. Heated Tat (boiled for 15 minutes) had no significant effect on inducing oligodendrocyte apoptosis (Fig. 8). The Tat-induced apoptosis was significantly attenuated by pre-addition (1 h earlier) of specific $K_V1.3$ antagonists PAP (10 nM) or MgTx (5 nM) to the culture media. In contrast, pre-addition of Guangxi Toxin (GxTx), a specific antagonist for K^+ channel K_V 2.1 which is also expressed in oligodendrocytes [162], failed to block Tat-induced oligodendrocyte apoptosis. Addition of PAP, MgTx or GxTx each alone had no apparent effects on oligodendrocyte apoptosis. These results showed a clear involvement of $K_V1.3$ in Tat-induced oligodendrocyte apoptosis (Fig. 8). The Tat-induced oligodendrocyte apoptosis was also blocked through genetic knockdown of $K_V1.3$ gene. As shown in Fig. 9, transfection of oligodendrocytes with $K_V1.3$-siRNA for 72 h prevented Tat-induced oligodendrocyte apoptosis. In contrast, oligodendrocytes transfected with Non-targeting (NT) siRNA (controls) did not block Tat-induced oligodendrocyte apoptosis. $K_V1.3$-siRNA *per se* had no effect on oligodendrocyte cell apoptosis. In parallel with the experimental data obtained with pharmacological approaches, these results further demonstrated an involvement of $K_V1.3$ in Tat-induced oligodendrocyte injury.

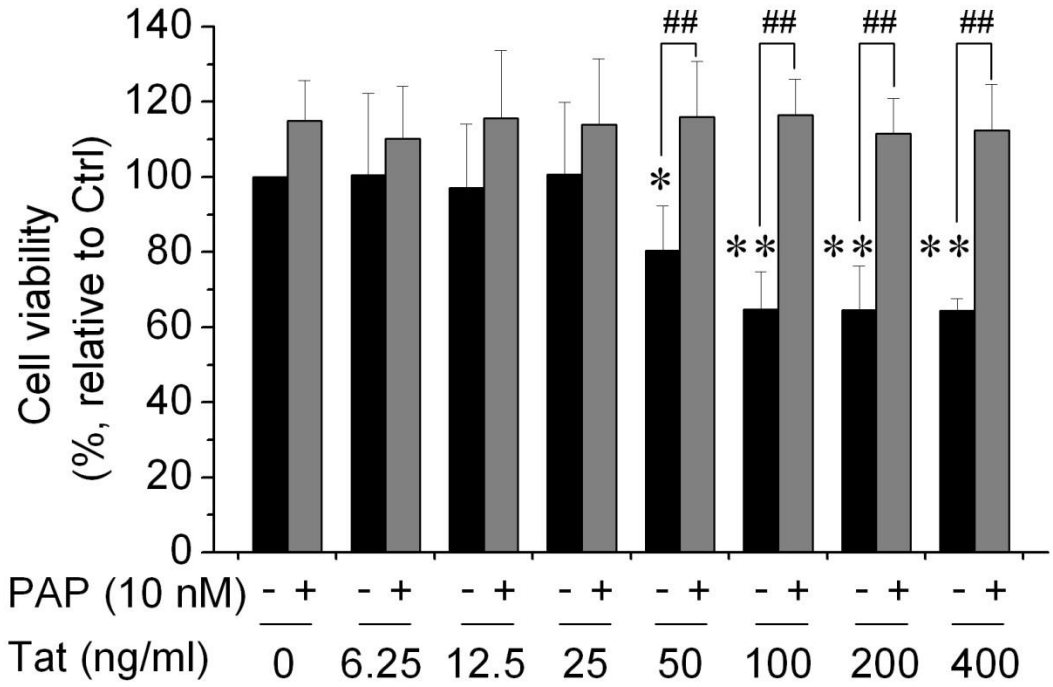

Figure 7. Blockade of K_V1.3 attenuated Tat-induced oligodendrocytes injury. Oligodendrocyte cultures were exposed to Tat for 48 h at different concentrations as indicated with or without pre-addition of 10 nM PAP for 1 h. Tat produced a significant reduction of oligodendrocyte cell viability at concentrations ≥ 50 ng/ml. Tat-mediated reduction of oligodendrocyte cell viability was prevented by addition of a specific K_V1.3 antagonist PAP, suggesting the Tat-mediated reduction of oligodendrocyte cell viability was mediated via K_V1.3. Data presented were from 6 independent experiments. *p < .05 and **p < .01 vs. control; $^{\#\#}p$ < .01 as indicated.

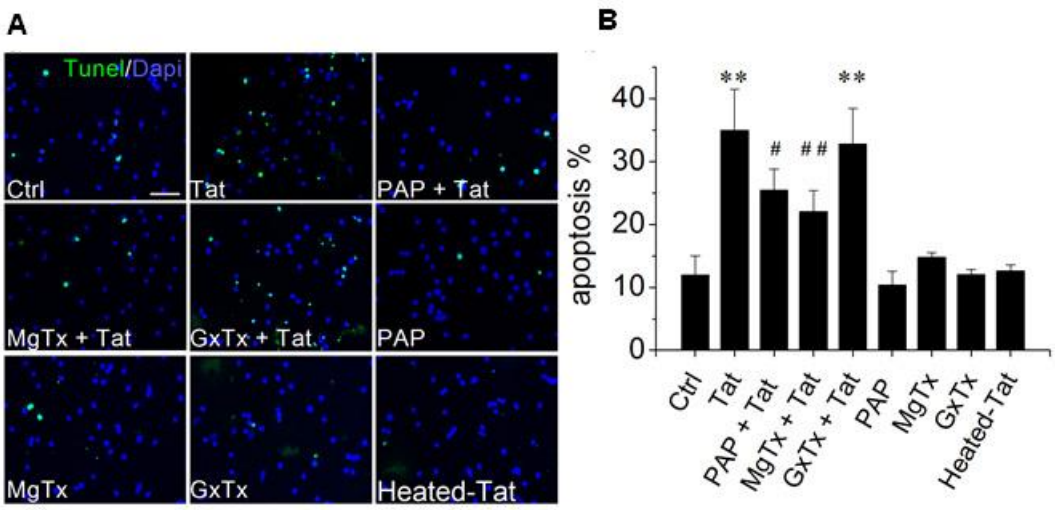

Figure 8. Involvement of $K_V1.3$ in Tat-induced oligodendrocyte apoptosis. Oligodendrocytes were exposed to Tat (50 ng/ml) for 48 h with or without pre-addition (1 h earlier) of PAP (10 mM), MgTx (5 nM), Panel A exhibits Tunel staining (green in color) revealed that Tat induced oligodendrocyte apoptosis (Tat) and the Tat-induced oligodendrocyte apoptosis was attenuated by pre-addition of PAP (PAT + Tat), MgTx (MgTx + Tat) or GxTx (GxTx + Tat) to the cultures. Intact cell nuclei were visualized with Dapi (blue in color). In a subset of cultures, PAP (PAP), MgTx (MgTx), GxTx (GxTx) and heat-inactivated Tat (50 ng/ml, heated-Tat) were tested individually. Panel B shows average percentage of apoptotic cells from five independent experiments. There were nine different experimental treatments in each experiments and 10 randomly selected visual fields were counted for each experimental treatment. As showed in Panel *b*, Tat-induced oligodendrocyte apoptosis was attenuated by either specific $K_V1.3$ antagonist PAP or MgTx, but not by GxTx, a specific antagonist for $K_V2.1$, demonstrating an involvement of $K_V1.3$ in Tat-induced oligodendrocyte apoptosis. ** $p < .01$ vs. control; $^{\#}p < .05$ vs. Tat; $^{\#\#}p < .01$ vs. Tat. Scale bar equals 20 µm.

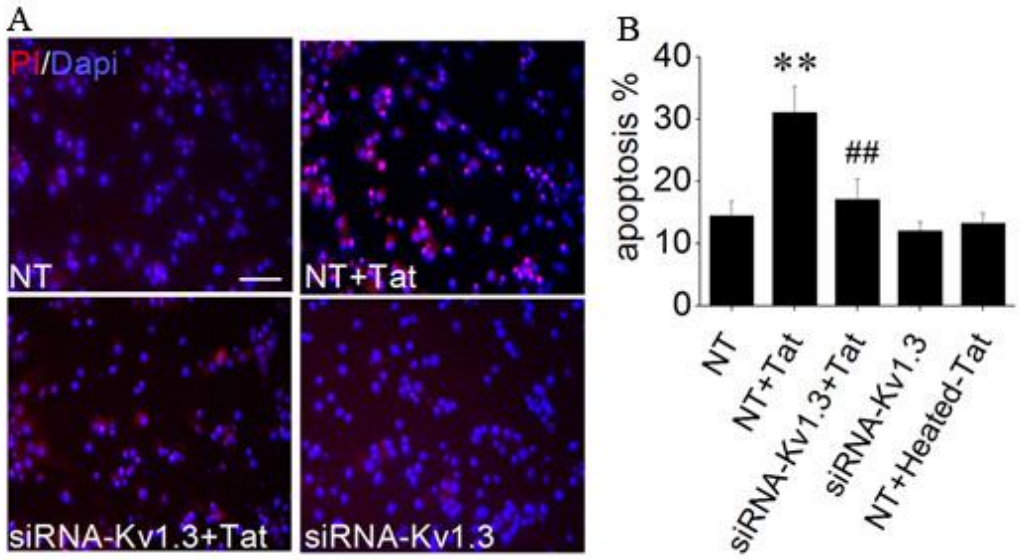

Figure 9. Knockdown of K_V1.3 gene prevented Tat-induced oligodendrocyte apoptosis. Cultured oligodendrocytes were transfected with K_V1.3-siRNA for 72 h to knockdown K_V1.3 gene or with non-targeting siRNA as a control. Following siRNA transfection, 50 ng/ml Tat or heat-inactivated Tat was applied to the transfected cells for another 48 h. Representative PI staining images (Panel A) showed that knockdown of K_V1.3 gene prevented Tat-induced oligodendrocyte apoptosis (siRNA-K_V1.3+Tat). In contrast, non-targeting siRNA (NT) failed to block Tat-induced oligodendrocyte apoptosis (NT + Tat). Non-targeting siRNA (NT) and K_V1.3-siRNA (siRNA-K_V1.3) *per se* had no apparent effect on basal levels of apoptosis. Also, oligodendrocytes transfected with NT and treated with Heat-inactivated Tat (NT + Heated-Tat) had no apparent effect (image not shown). This study was conducted in three independent experiments. Apoptotic cells were counted from 10 randomly selected visual fields in each experiment with different experimental treatments, and then calculated and shown in Panel B that knockdown of K_V1.3 gene prevented Tat-induced oligodendrocyte apoptosis. ** $p < .01$ vs. NT; $^{\#\#}p < .01$ vs. NT + Tat. Scale bar equals 20 μm.

3.3. K_V1.3 blockade prevented oligodendrocyte from Tat-induced MBP reduction and myelin loss.

MBP is an essential myelin structural protein and decreased levels of MBP expression in oligodendrocytes reflect an impaired ability of oligodendrocytes on axonal myelination. Classically, MBP has three isoforms that arise from different transcription start sites and the protein band at 18.5-kDa is considered as the predominant isoform essential for CNS myelin stability [192, 193]. To determine Tat influence on MBP expression, we specifically examined the protein band at 18.5-kDa by Western blot analyses. The same treatments as described in assessing oligodendrocyte cell apoptosis (Fig. 8 and 9) were employed in the experiments. The effectiveness of siRNA-K_V1.3 on knockdown K_V1.3 gene was first evaluated. As shown in Fig. 10A, oligodendrocytes transfected with siRNA-K_V1.3 revealed the K_V1.3 gene silence as evidenced by a significant reduction on the levels of K_V1.3 protein expression when compared with the K_V1.3 protein expression levels in non-targeting siRNA (NT)-treated oligodendrocytes. The involvement of K_V1.3 on Tat-induced alteration on MBP expression was then determined through molecular genetic and pharmacological approaches. As illustrated in Fig. 10C, treatment of oligodendrocytes with Tat significantly decreased the levels of MBP expression compared to the MBP levels detected in non-treated controls ($p < .01$). The Tat-induced decrease of MBP expression was blocked by specific K_V1.3 channel antagonists PAP and MgTx, but not by a K_V2.1 antagonist GxTx, demonstrating activation of K_V1.3 underlies Tat-mediated decrease of oligodendrocyte MBP expression. Such experimental results were duplicated by using siRNA to knockdown of K_V1.3 gene (Fig. 10B). These results showed Tat decreases oligodendrocyte myelination ability via K_V1.3.

Since there were no neurons in oligodendrocyte cell cultures in above experiments, it was difficult to evaluate if Tat decrease of MBP expression reflects HIV-1-associated oligodendrocyte/myelin damage seen in HIV-1-infected individuals. Alternatively, cultured brain slices were utilized as an *ex vivo* oligodendrocyte/myelin injury model to address possible pathophysiological processes in an *in vivo* condition. Coronal brain slice cultures, prepared from young adult rats, were utilized to examine Tat alteration of myelination. Tat was added to slice culture for 72 h and specific $K_V1.3$ antagonists were added 1 h prior to addition of Tat. The treated and untreated slices were then subject to MBP immunostaining to examine myelin integrity and myelination was evaluated by western blot analyses of MBP expression. The brain regions of corpus callosum and striatum were selected for analyses of myelin sheath integrity. The MBP reactivity in the corpus callosum was continuously aligned and exhibited an intact appearance in control (Ctrl) brain slices, whereas the MBP reactivity in the corpus callosum was discontinuous aligned and disorganized in brain slices treated with Tat (Fig. 11A left). In comparison with the clear and intense axonal bundles seen in the striatum of control brain slices, the striatum of Tat-treated brain slices showed impaired axonal bundles (Fig. 11A right). These abnormalities of myelinated nerve fibers and bundles were not observed in the slices treated with Tat combined with $K_V1.3$ antagonists PAP and MgTx, illustrating the blockade of Tat-induced impairments of myelin sheaths in both brain regions by $K_V1.3$ antagonists. In parallel with the morphological changes observed in the corpus callosum and striatum, Tat decreased the levels of MBP protein expression in these two brain regions and the Tat-associated decrease of MBP protein expression was also blocked by specific $K_V1.3$ antagonists (Fig. 11B), further support the notion that Tat induces oligodendrocyte/myelin/white matter injury via $K_V1.3$.

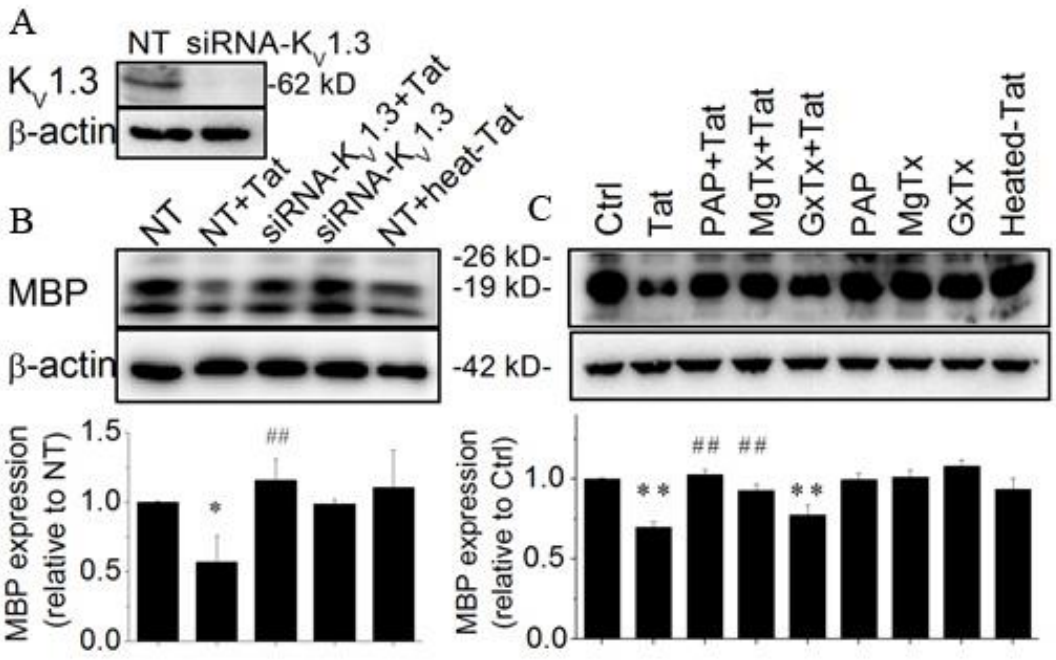

Figure 10. Involvement of K_V1.3 in Tat-induced oligodendrocyte MBP reduction. Cells were treated the same as described in Fig. 8 and 9. Data presented were from three independent experiments. Panel A shows a representative gel demonstrating a successful K_V1.3 protein knockdown as a consequence of K_V1.3 gene silencing. Panel B exhibits representative western blot results showing Tat-induced reduction on MBP expression was blocked by knockdown of K_V1.3 gene (upper). The band densitometric bar graph (lower) revealed a significant Tat reduction of MBP expression and the Tat-associated reduction of MBP expression was abolished by genetic K_V1.3 silence. Panel *c* illustrates Tat reduction of MBP expression was pharmacologically attenuated by specific K_V1.3 antagonists, PAP and MgTx, but not by GxTx, a specific K_V2.1 antagonist, demonstrating that Tat decrease of oligodendrocyte MBP expression via K_V1.3.

*p < .05 vs. ctrl or non-targeting siRNA (NT); ** p < .01 vs. control or NT; $^{\#}p$ < .05 vs. Tat or NT + Tat; $^{\#\#}p$ < .01 vs. Tat or NT + Tat.

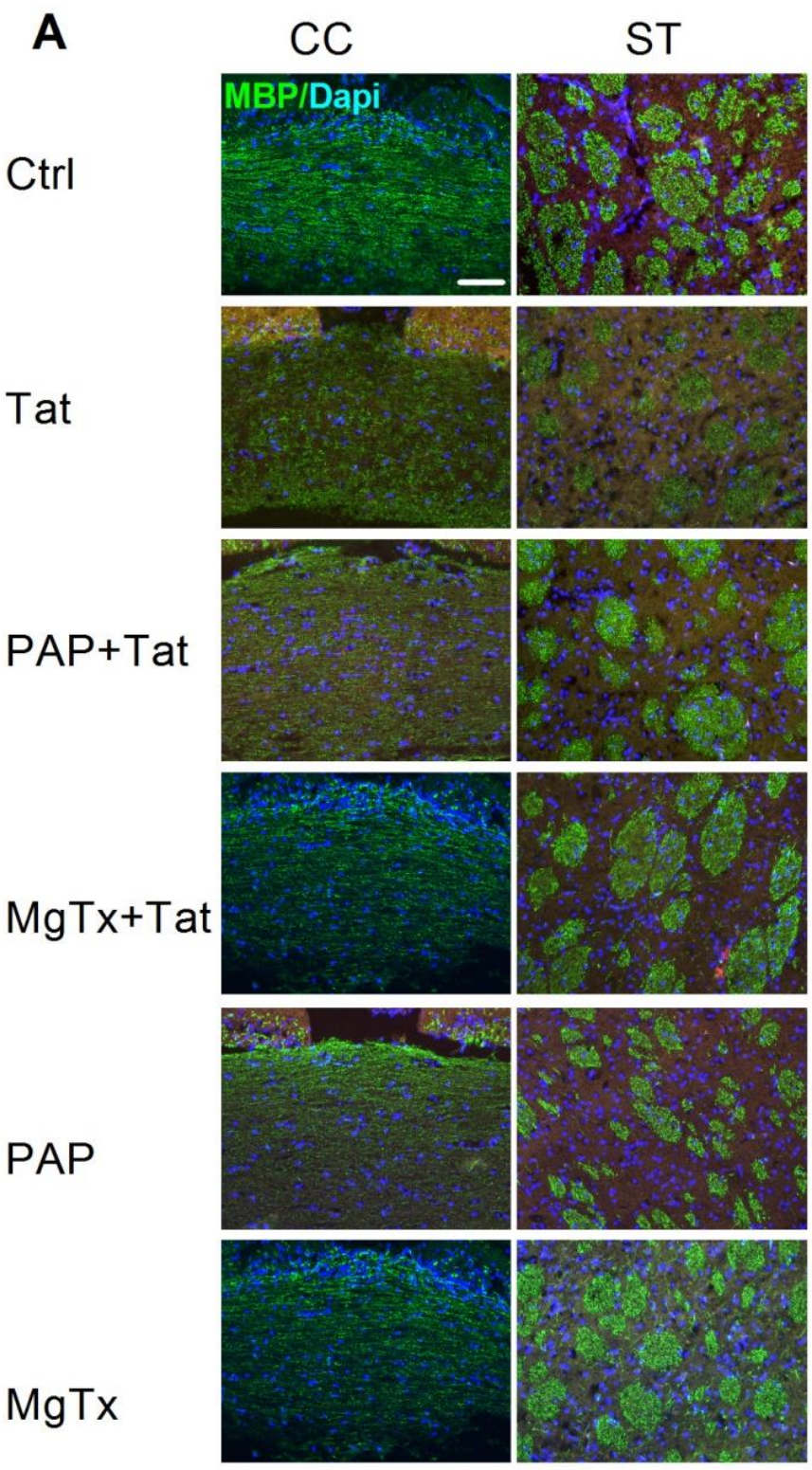
A
CC
ST
MBP/Dapi
Ctrl
Tat
PAP+Tat
MgTx+Tat
PAP
MgTx

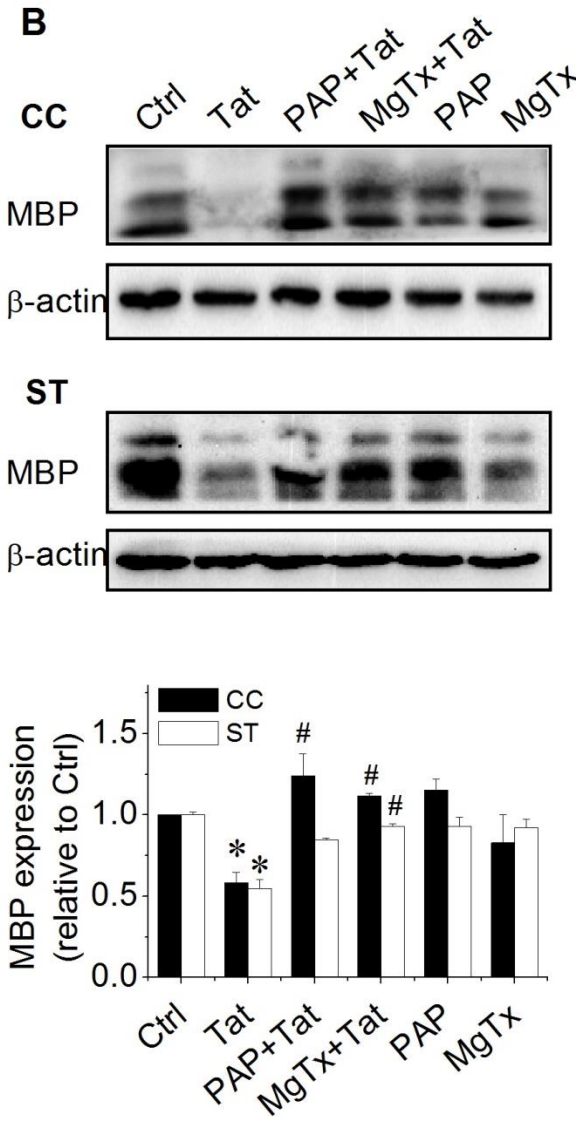

Figure 11. Tat-induced myelin injury in brain slices and its blockage by K_V1.3 antagonists. Cultured brain slices were exposed to 50 ng/ml Tat for 72 h with or without pre-addition (1 h earlier) of 10 nM PAP or 5 nM MgTx. Panel A, representative images of MBP immunofluorescence staining in corpus callosum (CC) and striatum (ST). Intact cell nuclei were visualized with Dapi. Tat impaired the myelin and nerve bundle integrity in the CC and ST. Panel B, western blot analyses of MBP expression in brain tissues of the CC and the ST dissected out from cultured brain slices and lysed in tissue extraction buffer. Tat decreased MBP expression both in the CC (upper) and in the ST (middle).

Band densitometry data are shown in the bar graph (lower). Data are expressed as mean ± S.E.M. after normalized to β-actin shown in each gel. Note that Tat-induced reduction of MBP expression was blocked by PAP and MgTx. Experiments were done in triplicates. Scale bar equals 20 μm *P < .05 vs. ctrl; $^{\#}P$ < .05 vs. Tat.

3.4. Tat interacted with K_V1.3 channel

Having demonstrated the involvement of K_V1.3 in Tat-induced oligodendrocyte/myelin injury, we next sought to examine if Tat interacts directly with K_V1.3 at protein level. For this purpose, we transfected HEK293 cells with pJK/K_V1.3 plasmid, followed by pull-down of GST or GST-HIV-Tat recombinant proteins (GST-Tat) with total HEK293 cell lysates. As anticipated, K_V1.3 protein was successfully over-expressed in HEK293 cells (Fig. 12A, left panel right lane) and, the recombination of GST-Tat was confirmed by western blot (Fig. 12B right panel). K_V1.3 was precipitated by GST-Tat in lysates from HEK293 cells infected with pJK/K_V1.3 (HEK/K_V1.3), but not detected in pJK-infected cells (HEK/pJK, Fig. 12A right panel), suggesting Tat was associated with K_V1.3 in HEK293 cells. The association of Tat and K_V1.3 proteins was also detected in rat brain homogenate by the GST pull-down assay. As showed in Fig. 12B (upper left), K_V1.3 was detectable in precipitated fraction of rat brain with addition of GST-Tat but not in fraction with GST *per se*, suggesting that Tat interacts with K_V1.3 in rat brain tissue as well.

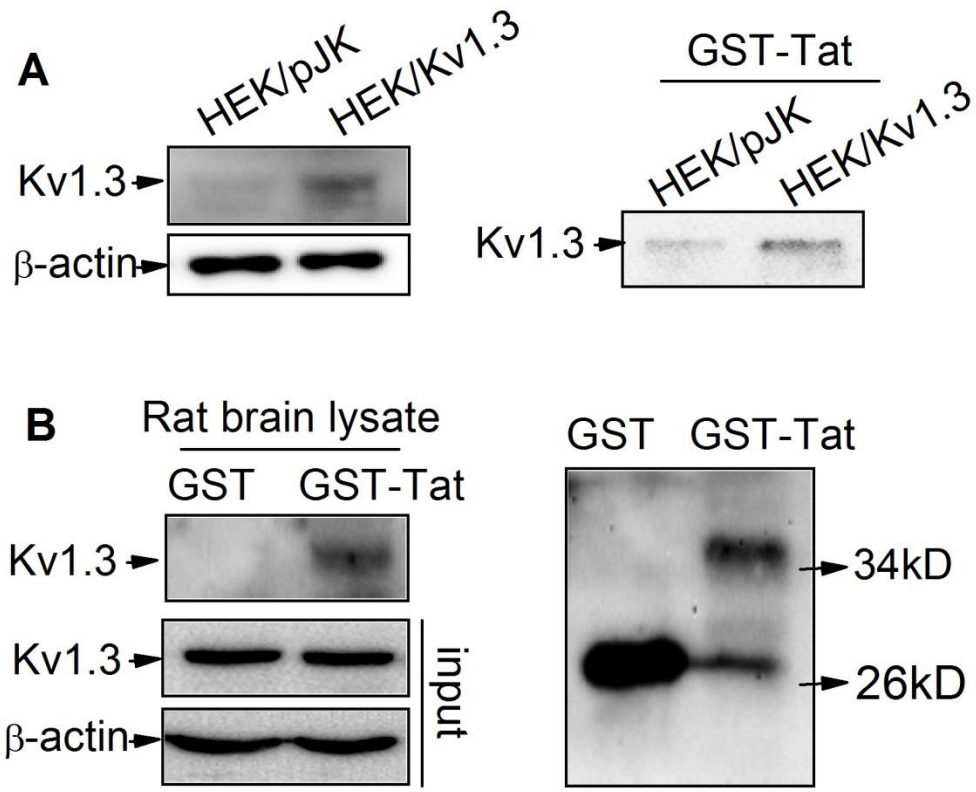

Figure 12. Tat interacted with K_V1.3 protein. GST-Tat recombinant protein was added to pJK-K_V1.3 transfected HEK293 whole cell lysate or rat brain tissue homogenate for protein pull-down assay. Panel A, Tat interacted directly with K_V1.3 expressed in HEK293 cells. Left in panel *a* is representative blot results showing K_V1.3 protein was successfully overexpressed in HEK293 cells transfected with pJK-K_V1.3 (HEK/K_V1.3) plasmids. Right in panel *a* shows pull-down assay demonstrating that Tat can interact with K_V1.3 protein overexpressed in HEK293 cells. Shown in Panel B are the pull-down results illustrating GST-Tat interacts with K_V1.3 protein in rat brain tissue lysates (left). The expression of K_V1.3 in rat brain is showed in the lower left. Right in panel *b* shows the bands of GST (lower bands) in both GST and Tat band (upper band) only in GST-Tat.

3.5. Tat enhances oligodendrocyte $K_V1.3$ current by retarding channel inactivation and downregulation of channel protein phosphorylation

Alterations in the current density of ion channels are generally attribute to three possible factors: changes in channel expression, promotion of channel translocation, or modification of channel kinetic activity. We next investigated the impact of Tat on oligodendrocyte K_V channel kinetics of voltage dependency, which is feasible to cause current change in 2 h. Primary oligodendrocytes were treated with 50 ng/ml Tat for 2 h before recording, and whole cell K^+ currents were recorded before (Tat) and after addition of 5 nM MgTx to the bath solution (MgTx + Tat) for 20 min. Tat did not shift the activation curve of oligodendrocyte K^+ currents ($V_{1/2}$ = 21.52 ± 4.19 mV of control cells and $V_{1/2}$ = 20.93 ± 4.55 mV of Tat-treated cells, $p > .05$), however, the inactivation curve shifted to the right after Tat treatment and, the shift was fully counteracted by MgTx (Fig. 13A). This data suggest $K_V1.3$ is primarily involved in the Tat-induced inactivation shift of oligodendrocyte K^+ currents and, Tat may cause more slowly inactivation of oligodendrocyte $K_V1.3$.

It is known that $K_V1.3$ channel contains several regulatory tyrosine phosphorylation residues at N- and C- terminus, as well as p-loop [194, 195]. Tyrosine kinases phosphorylate $K_V1.3$ at these residues that cause channel inactivation, which is an important mechanism of $K_V1.3$ activity regulation. We confirmed the channel phosphorylation by interaction of $K_V1.3$ and tyrosine kinase p-Src (Fig. 13D), which is similar with previous findings that Src kinase phosphorylates $K_V1.3$ cause current suppression [196, 197]. Combined that Tat affects the channel inactivation, we next determined the possibility that Tat changes the $K_V1.3$ kinetics by disturbing the tyrosine kinase-mediated $K_V1.3$ phosphorylating regulation. Pervanadate (PVD), a universal tyrosine phosphatase inhibitor, was introduced to evaluate whether Tat intervenes

channel phosphorylation. PVD performed to enhance channel phosphorylation thus sustain channel in inactive status. PVD was prepared freshly in prior to use by mixing sodium orthovanadate with H_2O_2 as described previously [179]. The oligodendrocytes were treated with 50 ng/ml Tat for 2 h. Currents were recorded at control and Tat-treated cells before and after application of PVD to bath solution at the working concentration of 200 μM for 10 min. The shift of inactivation curve caused by Tat was neutralized by PVD (Fig. 13B), suggesting that Tat hinder channel inactivation by disturbing tyrosine kinase-mediated channel phosphorylation. To confirm the phosphorylation-mediated inactivation shift is contributory to the current enhancement, the outward K^+ current density was also determined with presence of PVD. Tat increased the total outward K^+ currents in oligodendrocytes as expected and, the increase was counteracted by application of PVD into the bath (Fig. 13C).

So far, we have addressed that the modification of channel kinetic activity is causative to enhanced $K_V1.3$ currents. In addition to the phosphorylating regulation and protein-protein interaction, the potential translocation of $K_V1.3$ channels from cytoplasm to plasma membrane can also induce the $K_V1.3$ current increase in 2 h. We isolated the oligodendrocytes proteins to cytosol- and membrane- sections by membrane protein extraction kit (Biovision Incorporation), then the expression of $K_V1.3$ in each section was evaluated before and after treatment with 50 ng/ml Tat for 2 h. Tat increased the expression of $K_V1.3$ in cytosol section but no significant increase in membrane section (Fig. 14), suggesting translocation is not contributory to detected $K_V1.3$ current enhancement.

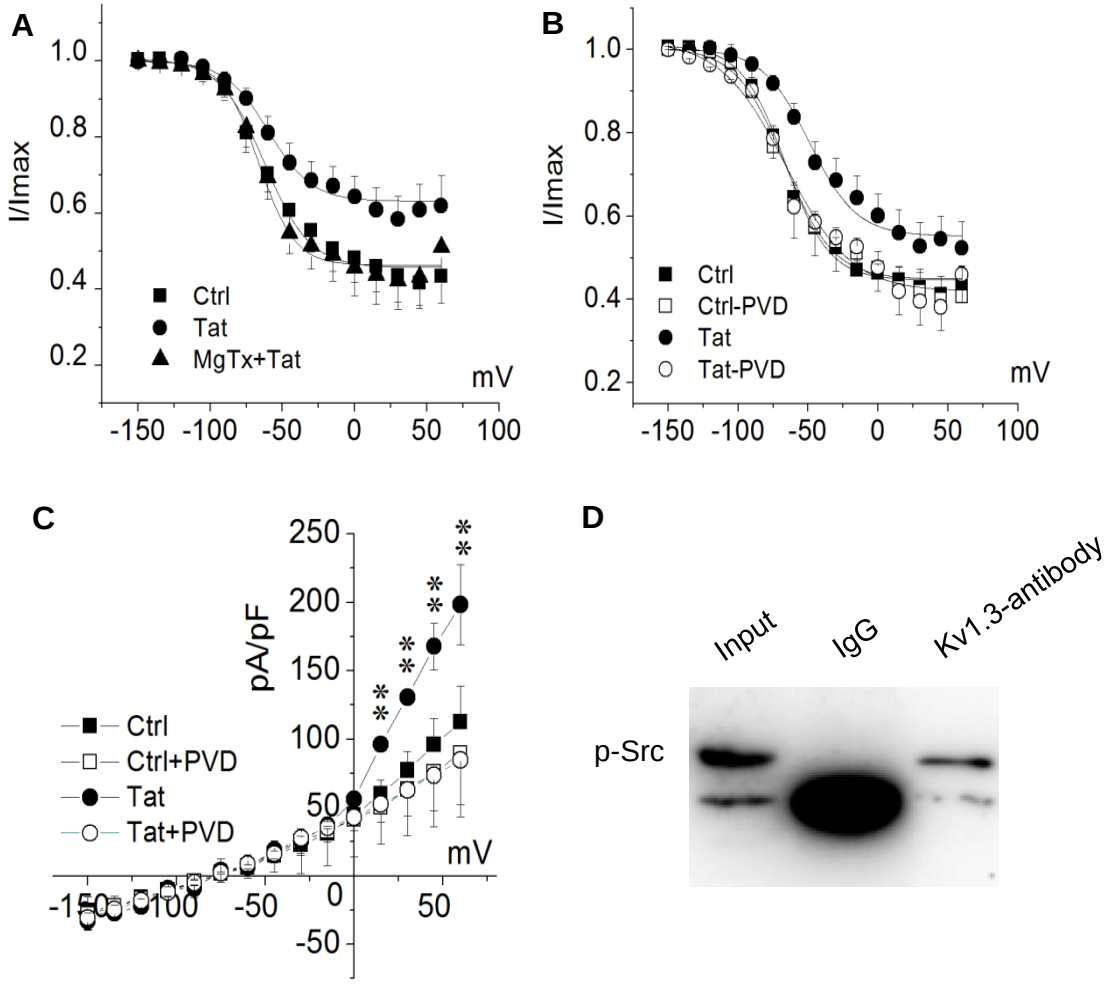

Figure 13. Tat alteration of K_V1.3 channel inactivation and channel phosphorylation regulation. For inactivation analysis, recoded cells were held at -80 mV during voltage-clamping. K^+ channels were pre-activated by voltage steps from the potential -150 mV to 60 mV with 15 mV increments and then tested at the depolarization pulse of 40 mV. Normalized data points were fitted with the Boltzmann equation: $I/I_{max}=1/\{1+\exp[(V-V_{1/2})/k]\}$. Panel A, Fitted inactivation curve of each group as indicated. N = 8 of each group. $V_{1/2}$ of Tat was -57.99 ± 2.23 mV compared with -62.39 ± 1.79 mV in Ctrl; and $V_{1/2}$ was -66.41 ± 2.03 mV with presence of MgTx. Panel B, Fitted

inactivation curves of each group as indicated. n = 6 of each group. $V_{1/2}$ of Tat was -49.06 ± 2.62 mV compare with -66.32 ± 1.46 mV of Ctrl. $V_{1/2}$ of Tat-PVD was -65.01 ± 4.53 mV compare with -66.60 ± 3.78 mV of Ctrl-PVD. Panel C, Mean of I-V curve of peak K^+ current density of n = 6 of each group. ** $p < .01$ vs. Ctrl. Panel D, Representative blot shows the co-immunoprecipitation by application of $K_V1.3$ primary antibody into rat brain homogenate and immunoblotted by p-Src antibody. The expression of p-Src in rat brain is showed in the left. Right lane shows the bands of p-Src pulled down by $K_V1.3$ antibody.

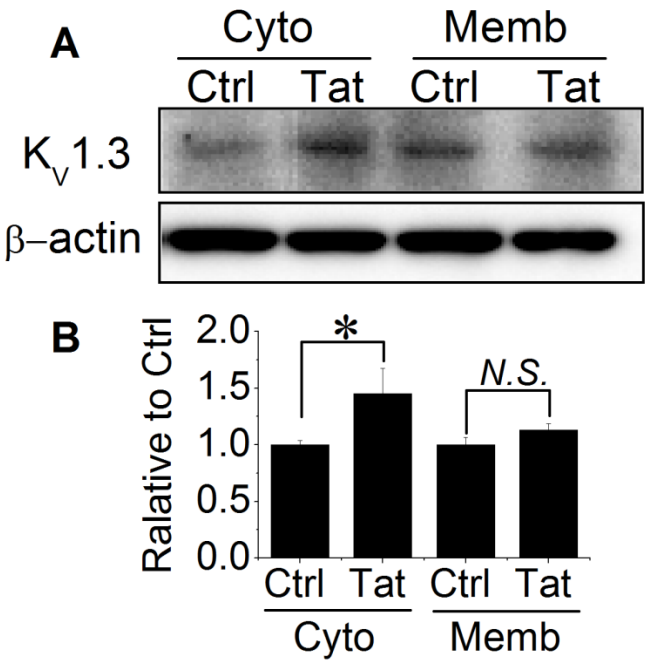

Figure 14. Tat did not promote K_V1.3 translocation in 2 h. Cells were treated with 50 ng/ml Tat for 2 h. Proteins were separated to cytosol (Cyto) and membrane (Memb) fraction. Panel A, representative blot of K_V1.3 immunoreactivities. Panel B, data are normalized to β-actin. Data were obtained from 3 independent experiments. *p < .05, N.S. non-significant.

4. Discussion

It is widely believed that HIV-1 persists in the brain despite of cART. The virus persistent in a latent or restricted manner in monocyte-macrophages, microglia and astrocytes continues to play a significant disease-inciting role. Indeed, HAND remains a subcortical dementia with notable evidence of affected white matter tracts within the corpus callosum, internal capsule and superior longitudinal fasciculus [8, 82, 91]. How HIV-1 brain infection causes white matter damage is not fully understood. In the present study, we investigated the effects of HIV-1 protein Tat on oligodendrocytes, the myelin-forming cells in the CNS. Our results demonstrated that Tat induces oligodendrocyte injury via activation of voltage-gated K^+ channel $K_V1.3$. Such an effect can be blocked by knockdown of $K_V1.3$ gene or by specific $K_V1.3$ antagonists MgTx and PAP, but not by GxTx, a specific K_V 2.1 antagonist, suggesting an involvement of $K_V1.3$ in Tat-induced oligodendrocyte injury. Further studies revealed that Tat interacts with $K_V1.3$ at protein level, resulting in a prolonged channel activation via a decrease of tyrosine phosphorylation of $K_V1.3$ channel. These results, to our knowledge, are the first demonstrations that Tat induces oligodendrocyte injury via $K_V1.3$.

The consensus view regarding HAND pathogenesis has been related to cerebral white matter damage [41, 198]. Many cellular and viral factors are involved in HIV-1-associated brain white matter damage. Amongst them is viral protein Tat. It has been shown that Tat continues to be detectable in the CSF of HIV-infected patients with well-controlled viremia in the cART era [199]. With a broad range of actions on promoting inflammation and producing cytotoxic stress to various types of cells in the CNS [136], Tat might continue playing an important role for HIV-1-associated white matter damage in the cART era. Indeed, Tat has recently been shown to act on oligodendrocytes with a detrimental consequence [9, 12]. In an agreement with the aforementioned findings, our

in vitro studies revealed that Tat had a direct toxic effect on the oligodendrocytes in an oligodendrocyte primary culture system (purity > 85%) (Figs. 7, 8, 9). The detrimental effect of Tat on oligodendrocytes was validated on *ex vivo* studies that treatment of rat brain slices in culture with Tat produced myelin damage and a reduction of MBP expression in corpus callosum and striatum (Fig. 10). Combined with the results of increased apoptosis (Figs. 8 and 9), the reduction of MBP expression may reflect a decrease of oligodendrocyte cell numbers. These results may explain, at least in part, why anti-inflammatory therapies did not achieve a great benefit in HAND patients [200]. However, Tat was found to increase oligodendrocyte cell numbers in the hilus of the dentate gyrus in a study on rats with intrahippocampal injection of Tat [47]. The discrepancy may be caused by potentially inclusion of the population of immature oligodendrocytes in that study [47], since proliferation of oligodendrocyte lineage cells could increase the probability to repair damaged myelin designedly as the response to Tat injection *in vivo*. This notion is supported by an earlier report that mild myelin damage was associated with an increase in oligodendrocyte numbers, but the oligodendrocyte numbers decreased as damage became more severe in HIV-1-infected brains [90, 180]. In conjunction with a previous gross anatomical study on HIV-1-infected brains with demyelination which detected a reduction of corpus callosum volume [8], we posit that Tat induces mature oligodendrocyte injury, resulting in and loss of cerebral cortical white matter. Such a pathological change is concordant with the pattern of white matter damage observed in HAND patients.

Studies have shown that excessive cellular K^+ efflux and/or intracellular K^+ depletion are common characteristics in early apoptosis [84, 201]. $K_V1.3$ is positively associated with apoptosis in different types of cells, including retinal ganglion cell [202], lymphocytes [140, 203], and various cancer cells [1, 27, 174]. In agreement with these

studies, our results showed Tat-induced apoptosis in cultured oligodendrocytes was attenuated either by knockdown $K_V1.3$ gene or by specific $K_V1.3$ antagonists, but not by a $K_V2.1$ antagonist (Fig. 8), suggesting that Tat triggers oligodendrocyte apoptosis by increasing K^+ efflux particularly through $K_V1.3$. Moreover, blockade of $K_V1.3$ rescued Tat-induced MBP reduction (Figs. 10, 11), indicating that $K_V1.3$ is involved in HIV-1-related myelin damage. However, $K_V1.3$ inhibition only partially blocked Tat-induced apoptosis (Fig. 8), implying that Tat may cause oligodendrocyte injury through other mechanisms, such as targeting at glutamate receptors [9]. Myelin impairments may cause further axonal injury related to neurodegeneration in HAND, because myelinated axons exhibit a myelin-dependency during development [201]. Additionally, the increased K^+ efflux from oligodendrocytes in an *in vivo* condition may affect neuronal function through elevating the levels of extracellular K^+, instead of clearing K^+ released from neurons during axonal firings [204, 205]. An earlier study from our laboratory also showed that blockade of $K_V1.3$ or knockdown $K_V1.3$ expression in microglial cells attenuated Tat-induced microglia neurotoxic activity [141]. Taking together, these findings indicate that activation of $K_V1.3$ plays an important role in Tat-associated neurotoxicity.

It has been shown that the activities of several different cloned K_V channels are suppressed after phosphorylation of the channels by both receptor and non-receptor tyrosine kinases [206]. Indeed, there are several tyrosine residues on $K_V1.3$ channel protein and different combinations of phosphorylated tyrosine residues are required for current suppression as consequences of different triggering signals [207-209]. Our GST-pull down assay results showed $K_V1.3$ presence in GST-Tat-precipitated protein complex, indicating a direct interaction between Tat and $K_V1.3$ protein (Fig. 12). Such an interaction may cause an interruption of phosphorylation regulation of $K_V1.3$ channel.

This notion is supported by experimental results that tyrosine phosphatase inhibitor PVD attenuated Tat enhancement of $K_V1.3$ currents and prevented Tat-induced right-shift of $K_V1.3$ channel inactivation curve (Figs. 13B and 13C). Although we did not examine direct phosphorylation of $K_V1.3$ channels due to the paucity of efficient antibody, our available data (Figs. 6 and 13A) indicate that Tat may increase $K_V1.3$ currents by decrease of channel protein tyrosine phosphorylation and prolonged channel in activation state as revealed by a right-shift of inactivation curve (Fig. 13A). However, the tyrosine kinase-associated $K_V1.3$ channel modulation can be influenced by adaptor proteins through direct protein-protein association involving Src homology (SH) domains [195, 210]. As Tat binds to SH3 domains of Grb2 [211], it is also possible that Tat interacts indirectly with $K_V1.3$ via adaptor proteins, of which Grb2 might be a potential candidate. In addition to protein-protein interaction and tyrosine phosphorylation regulation of $K_V1.3$ channel activity, mobilization of cytoplasm $K_V1.3$ channels to plasma membrane could also be possible for underlying mechanism for Tat-induced increase of the $K_V1.3$ current in oligodendrocytes. We separated the oligodendrocyte proteins into cytosol and membrane fractions by membrane protein extraction kit (Biovision Incorporation), then the levels of $K_V1.3$ in each fraction were evaluated. Tat increased the levels of $K_V1.3$ in the cytosol fraction but no significant increase in membrane fraction (Fig. 14), suggesting the translocation of $K_V1.3$ from cytosol to the plasma membrane was not involved in observed Tat-associated increase of $K_V1.3$ current in oligodendrocytes.

It is worth pointing out that the evaluations on oligodendrocyte cell viability/apoptosis and myelin morphology in brain slices were conducted at different time points, 48 h and 72 h, respectively. This is because, at the same concentrations, a longer time was needed to generate significant morphological changes in brain slices than apoptotic

changes seen in primary cell cultures. It is also worth pointing out that, in addition to its toxic effect to mature oligodendrocytes and myelin sheaths, Tat may also induce disturbance of myelin maintenance via $K_V1.3$ channels, such as oligodendrocyte progenitor cells proliferation and differentiation, leading to myelin/white matter abnormalities as seen in the brains of HIV-1-infected patients. As basal activity of K_V channels controls oligodendrocyte proliferation and differentiation [44, 133, 212], the alteration of $K_V1.3$ channel activity by Tat may possibly disturb oligodendrocyte lineage cell proliferation and differentiation, and ultimately myelin maintenance processes. In addition, $K_V1.3$ was shown to play a crucial role in controlling cell cycle activation [133]. This may explain why PAP-treated oligodendrocytes in our studies exhibited higher cell viability (Fig. 7) than the control oligodendrocytes.

In summary, our present studies demonstrated that HIV-1 protein Tat induces oligodendrocyte/myelin injury by enhancing outward K^+ current conducted by a voltage-gated K^+ channel $K_V1.3$ by using specific $K_V1.3$ antagonists and siRNA knockdown of $K_V1.3$ gene. This is the first demonstration that Tat targets at oligodendrocyte $K_V1.3$ channels by direct protein-protein interaction and interruption of channel phosphorylation/de phosphorylation processes. These findings may serve not only to elucidate the mechanisms underlying HIV-1-associated brain white matter damage seen in HIV-1-infected patients in the era of cART, but also to provide a potential target for the development of therapeutic strategies for amelioration of HIV/*Tat*-induced brain myelin/white matter injury.

Chapter 3

Tat impairs oligodendrocyte progenitor cell survival and maturation

Abstract

HIV-1-associated neurocognitive disorder (HAND) is a subcortical disease involving neuronal loss and axonal demyelination. Myelin is deposited by oligodendrocytes through a complex process requiring oligodendrocyte progenitor cell (OPC) proliferation, migration, and maturation. It has been shown that OPC are susceptible to viral proteins such as Tat and that OPC survival and maturation are defective in HAND. Studies also have demonstrated that enhancement of voltage-gated K^+ channels (K_V) are involved in regulation of OPC development. Particularly, suppression of $K_V1.3$ currents is required for OPC maturation. Thus we hypothesized that the HIV-1 protein Tat induces OPC damage and hinders OPC maturation by enhancing outward K^+ current conducted by subtype $K_V1.3$, contributing to HAND pathogenesis. To test this hypothesis, we studied the $K_V1.3$ expression in primary cultured OPCs and, the effect of Tat on OPC apoptosis and maturation. $K_V1.3$ currents and channel expression decreased within development, while incubation of OPC cultures with Tat increased levels of $K_V1.3$ current density and channel expression as revealed by whole-cell patch clamp and RT-PCR. Tat induced OPC apoptosis and decreased the number of mature oligodendrocyte and, these Tat-caused changes were prevented by 5-(4-phenoxybutoxy) psoralen, a specific $K_V1.3$ blocker. Our results suggest that Tat induces OPC apoptosis and maturation deficit through $K_V1.3$, indicating $K_V1.3$ as a potential target for the development of therapeutic strategies for HIV-associated myelin injury.

1. Introduction

Infection with HIV-1 remains a persistent and even growing health problem worldwide. HIV-1 invades the CNS early in the course of infection and provokes progressive cognitive behavioral and neurological impairments, collectively referred to as HIV-1-associated neurocognitive disorder (HAND) [1]. With the advent of combination antiretroviral therapy (cART), the number of severe HAND patients has decreased. However, due to a longer lifespan and drug toxocity, it is becoming apparent that patients suffer from protracted infection may exhibit more subtle forms of mental impairment of which myelin injury is one of the main causes [213]. Brains of HIV-1-infected patients show pathological changes in the corpus callosum, which is associated with a significant decrease in nerve numbers and fiber density, as well as the impaired outer contour and decreased thickness of each single myelin sheath [8]. Because HAND remains highly prevalent and continues to be a significant epidemiological problem, research into the molecular and cellular mechanisms of HIV-induced myelin injury and axonal damage is pressing.

Myelination, formed by oligodendrocytes in the CNS and Schwann cells in the PNS, is achieved by extending oligodendrocyte plasma membrane processes to enclose axons leading to formation of myelin sheath, which is an insulating sheath essential for saltatory propagation of electrical signal along axonal. The process of repairing damaged myelin is remyelination, which is required to maintain the myelin homeostasis and repair damage of myelin injury or loss. Remyelination involves proliferation and survival of oligodendrocyte progenitor cells (OPC), migration of OPCs to the damaged area, and maturation of OPC to mature myelinating oligodendrocytes [214]. In HIV-1 infected brains, mild myelin damage is associated with an increase in oligodendrocyte number, although the number decreases with severe damage [90]. In agreement, the

mRNA level of transcription factor Olig2, a marker with higher expression in OPC and lower expression in mature oligodendrocytes [91], is elevated in the front cortex of HIV-1-infected patients [48]. These results indicate that OPC proliferate to repair damaged myelin sheath in response to HIV infection. Thus, we hypothesize that differentiation of OPCs into post-mitotic oligodendrocyte might be a major check-point for myelin maintenance and repair in HAND.

Although the viral load is minimal in the nervous system, the transcription and release of viral proteins, such as Tat, from early infected cells continues over the course of infection [174]. Tat is a required transcription factor for HIV-1 gene expression. Tat has been linked to progressive development of HAND impairing the integrity of blood brain barrier [203, 215], activating microglia to behave cytotoxic and pro-inflammatory effects [198], and direct toxicity on neuronal cells [216]. Detection of Tat has been demonstrated in both viral-infected and uninfected oligodendrocytes in the brain of AIDS patients may due to its penetrability of plasma membrane [10]. Oligodendrocytes are susceptible to HIV-1 Tat protein involving the activation of Caspase-3 [12]. Because viral protein transcription continues while viral load is well controlled by cART [174, 217], Tat toxicity of oligodendrocyte may contribute to the fact of increased population of milder HAND in cART era.

The K_V channel family is the largest and a rapidly-expanding family of ion channels that are associated with signaling pathways required for cell survival and physiological activities. Accumulating evidence indicate that modulation of K_V channels is a new approach to regulate OPC/oligodendrocyte activity. Generally, K_V expression in oligodendrocyte lineage cells correlates with differentiation stages. Currently, the K_V1 subfamily is mostly studied in oligodendrocyte. $K_V1.3$ [129, 130], $K_V1.5$, $K_V1.6$ [129], and inward rectified K^+ channel 4.1 [131, 132] play crucial roles in regulation of OPC

proliferation and maturation. In particular, K_V1.3 channels play a crucial role in G1/S transition of proliferating OPCs [130, 133]. In addition, Kv1.3 controls cell cycle activation by affecting a component, C5b-9-mediated activation of AKT, thus mediate oligodendrocyte dedifferentiation [133]. However, the role of K_V1.3 in regulation of HIV-induced OPC maturation retardation is not fully understood. The present study demonstrates Tat hinders OPC differentiation and induces OPC apoptosis by increasing K_V1.3 currents, thus interrupting the myelin maintenance and/or remyelination related to HAND pathogenesis.

2. Materials and methods

Information of Tat and animals, experimental procedures of OPC culture, electrophysiology, Western Blotting, immunofluorescence, MTT assay, and Tunel assay are same as described in Chapter 2 Materials and method section, unless otherwise complementarily described below.

2.1. Electrophysiology. The resting membrane potentials were determined by zero-current potential measured shortly after achieving whole-cell recording conformation. The cell capacitances were read under the membrane-test function. Current amplitudes were measured at the peak and at 300 ms for each test potential. These currents correspond to the transient A-type outward K^+ current (I_A) and delayed rectified K^+ current (I_K), respectively.

2.2. RNA extraction. Total RNA isolation was achieved by Trizol reagent (Invitrogen, Carlsbad, CA). Chloroform, isopropyl alcohol and 75% ethanol (in RNase-free water) were all from sigma. RNase-free water was from Promega (Madison, WI).

OPCs were washed twice with sterile cold PBS. Trizol was provided at 1 ml to each well of cultures in 6-well plates. Cells were lysed by passing several times through a pipette. The lysate was collected in freshly-sterilized 1.5-ml tubes and then incubated for 5 min in room temperature. Each tube received addition 0.2 ml of chloroform and then was capped securely. Tubes were shaken vigorously by hand for 15 seconds and incubated in room temperature for 3 min. Samples were centrifuged at 12,000 g for 15 min at 4 °C. The samples were then separated into 3 phases after centrifugation: lower red phase, protein-enriched interphase, and a colorless upper aqueous phase that contained RNA. Approximately 0.5 ml of the upper phase of each sample was carefully transferred into fresh tubes. The same amount of 0.5 ml of isopropyl alcohol was added to each tube to precipitate the RNA. Samples were incubated at room temperature for 10

min. Centrifugation was then performed at 12,000 g for 10 min at 4 °C. The RNA generally formed a gel-like pallet at the bottom of tubes. The supernatant was removed and, 1 ml 75% ethanol was added to each tube to wash the RNA. Samples were preceded to vortex and centrifuged at 7,500 g for 5 min at 4 °C.

The RNA isolation was finally achieved by discarding the supernatant and drying the pallet in room temperature for about 5 min. RNA was dissolved in 12 µl RNase-free water by passing them through a pipette. The amount of 2 µl RNA of each sample was taken for RNA concentration determination. The rest was stored at -80 °C for further reverse transcription. RNA concentration was determined by Nanodrop 2000.

2.3. Reverse transcription-PCR. Reverse transcription was accomplished with a SuperScript III first-strand synthesis kit (Invitrogen). The amount of 2 µg of each RNA sample was taken and balanced the volume of to 8 µl by RNase-free water for every sample, followed by addition of 1 µl oligo-dT primer and 1 µl dNTPs to each sample. The cDNA synthesis mix was prepared in a separate tube by mixing 2 µl of 10 × RT buffer, 4 µl of 25 mM $MgCl_2$, 2 µl of 0.1 M DTT, 1 µl of RnaseOUT, and 1 µl of SuperScript III RT (10 µl total) for each sample. The prepared mix was kept on ice.

The sample (RNA + primer + dNTPs) was projected onto the thermal plate of PCR machine (Eppendorf RealPlex^2). The program was set as 65 °C for 5 min, pause, 50 °C for 50 min, 85 °C for 5 min, pause, 37 °C for 20 min, hold at 4 °C. After reverse transcription program started, the samples were taken out at the first pause and placed on ice for at least 1 min. Prepared cDNA synthesis mix (10 µl) was added to each sample. At the second pause, 1 µl of RNase H was provided for each sample.

Reactions containing cDNA from reverse transcription, unique primer pairs and PCR master mix 2× (Promega) were systematically performed for PCR amplification. Primer sequences were designed according to the rat cDNA: K_V1.3 forward primer, GTA CTT

CGA CCC GCT CCG CAA TGA, reverse primer, GGG CAA GCA AAG AAT CGC ACC AG; GAPDH forward primer, TCA AGA AGG TGG TGA AGC AG, reverse primer, AGG TGG AAG AAT GGG AGT TG. PCR cycles were performed as follows: initial 5 min at 95 °C, then 30 cycles of 95 °C (15 s), 55 °C (30 s), and 72 °C (45 s), followed by 10 min at 72 °C for completion of extension.

2.4. Statistics. All data are expressed as mean ± S.D. unless otherwise indicated. Statistical analyses were performed by student`s *t* test or one-way ANOVA followed by a Fisher`s least-significant difference test for multiple comparisons. The difference between groups was considered significant at $p < .05$.

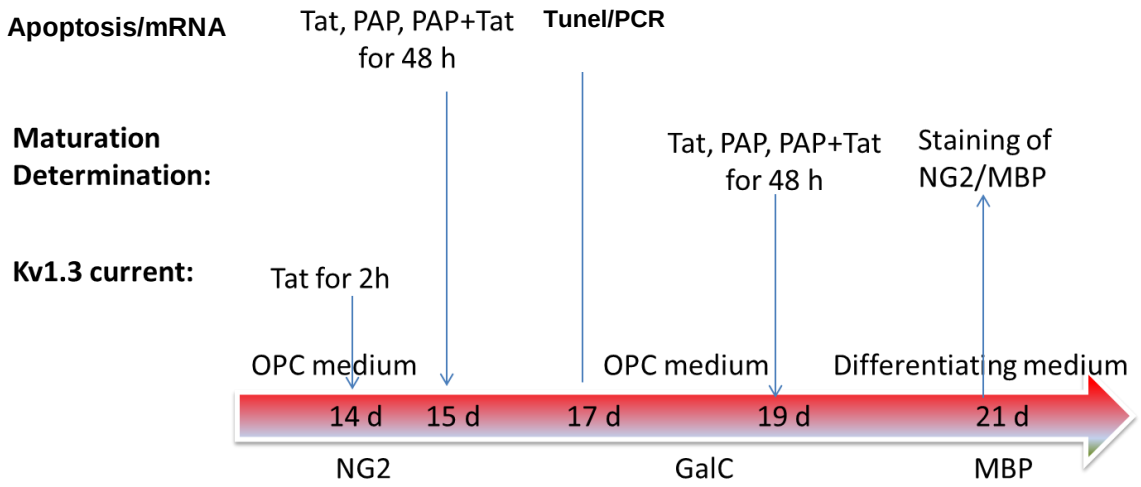

Figure 15. Scheme of experimental treatments.

3. Results

3.1. Developmental changes of OPC/oligodendrocyte resting membrane properties

Whole-cell voltage-clamp studies were performed on cells that had been cultured 12-21 d (2-11 d after isolated from mix glial culture). In order to avoid electrical coupling between adjacent cells, the investigations reported in the present study were confined to cells that extended processes but did not contact with neighbor cells. Table 1 lists resting membrane potential and membrane capacitance that were observed during development in OPC/oligodendrocyte culture. Generally, the resting membrane potential changed toward negative within time during OPC development. However, resting membrane potential of mature MBP^+ oligodendrocytes remained similar compared with late $GalC^+$ OPCs. Membrane capacitances were larger in $GalC^+$ and MBP^+ cells than those in $NG2^+$ OPCs. The membrane capacitances varied from 7.05 pF in a cell had bipolar morphology to 25.40 pF in a cell that developed multiple processes.

3.2. K^+ currents in oligodendrocyte lineage cells at different developmental stages

To investigate the activity of K_V channels in oligodendrocyte lineage cells, whole-cell K^+ currents in OPCs/oligodendrocytes were recorded at different developmental stages. OPCs were recorded at three ages. Early stage of $NG2^+$ OPCs were recorded at 14 d and 17 d ($NG2^+$ 14 d, $NG2^+$ 17 d) respectively. Late stage of $GalC^+$ OPCs were recorded at 19 d ($GalC^+$). MBP^+ cells were recorded at 21 d to represent mature oligodendrocytes (MBP^+). At an early stage of 14 d, $NG2^+$ cells expressed relatively high level of outward K^+ currents. However, the current density of I_A was decreased by 44% as the cells differentiated to MBP^+ oligodendrocytes. In contrast, I_K did not show significant changes during OPC development (Fig. 16).

Table 1 Resting membrane properties of OPCs/oligodendrocytes

Cell marker	Cell age (d)	Resting membrane potential (mV)	Capacitance	n
$NG2^+$	12	-49.89 ± 16.10	12.23 ± 2.01	10
	13	-47.06 ± 11.60	11.34 ± 3.48	10
	14	-54.33 ± 12.10	15.74 ± 4.76	16
	15	-60.02 ± 10.89	13.78 ± 2.80	9
	16	-64.62 ± 5.71	13.92 ± 3.70	9
	17	-65.57 ± 5.92	15.06 ± 3.67	15
$GalC^+$	18	-66.47 ± 3.87	17.44 ± 4.50	21
	19	-67.37 ± 2.24	18.52 ± 6.49	16
MBP^+	21	-65.30 ± 12.56	19.93 ± 5.76	16

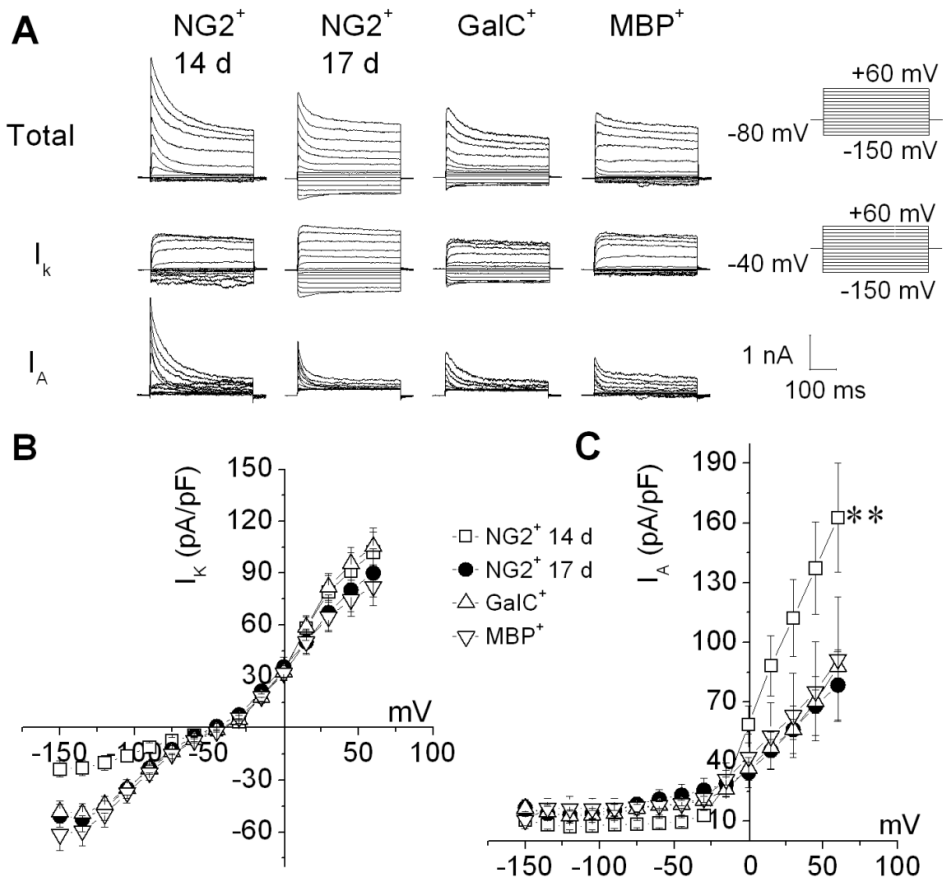

Figure 16. Developmental changes of whole-cell K^+ currents in oligodendrocytes. Panel A, representative current traces recorded during depolarizing and hyperpolarizing pulses are shown in 14 d $NG2^+$ cells ($NG2^+$ 14 d, n = 16), 17 d $NG2^+$ cells ($NG2^+$ 17 d, n = 15), $GalC^+$ cells ($GalC^+$, n = 8), MBP^+ cells (MBP^+, n = 15). To record total currents, cells were held at -80 mV and pulses were applied to various test potentials for 300 ms as shown in the upper voltage-clamp protocol (not proportional to the current traces in duration). I_A was eliminated by holding the membrane potential at -40 mV to record I_K, as shown by the clamp protocol in the second row. I_A was derived by a subtraction of I_K from total K^+ current and mean data are summarized in panel C. Current density-voltage relationship of I_K (B) and I_A (C) in each group. ** $p < .01$ $NG2^+$ 14 d vs. MBP^+ at +60 mV voltage steps.

3.3. Involvement of $K_V1.3$ in Tat-induced K^+ current enhancement

It is known that $K_V1.3$ is expressed at both mRNA and protein levels in OPCs and contributes to the generation of the I_A component [130]. By giving that gradual decrease of outward K^+ currents within maturation, we next determined if $K_V1.3$ is responsible for the observed change in outward K^+ currents. The mRNA expressions of $K_V1.3$ at different developmental stages and the effect of Tat on $K_V1.3$ expression were examined by RT-PCR. At the three tested stages, $K_V1.3$ expression was highest in 14 d $NG2^+$ OPCs and the expression decreased within development. However, application of Tat to OPC culture for 48 h increased $K_V1.3$ expression in OPCs compared with that in same age of OPCs (17 d $NG2^+$ OPCs, Fig. 17). Corresponding results of $K_V1.3$ currents were revealed by electrophysiological studies. The specific $K_V1.3$ blocker, PAP, was used to isolate $K_V1.3$-conducted K^+ currents in OPCs by subtraction (as described in Chapter 2). $K_V1.3$ currents decreased within development in late OPCs compare with the early $NG2^+$ OPCs at 14 d (78.31 ± 16.42 of $NG2^+$ 14 d vs 54.86 ± 12.36 of $GalC^+$ OPC, $p < .05$). Treatment of 50 ng/ml Tat for 2 h increased $K_V1.3$ currents (114.97 ± 22.35) compared with control $NG2^+$ OPCs at 14 d (Fig. 18). These data suggest that $K_V1.3$ is involved in the decrease of total outward K^+ currents during development and Tat increased $K_V1.3$ expression and currents.

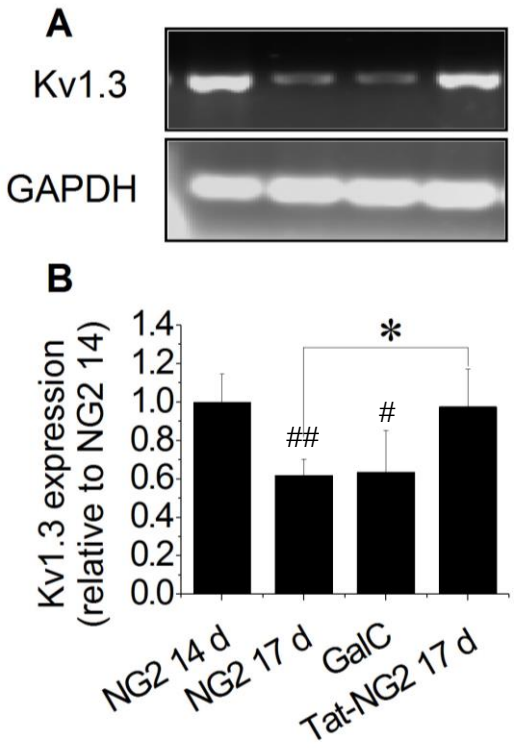

Figure 17. Effect of Tat on OPC K_V1.3 mRNA expression. Cells were collected at different ages as indicated. For Tat-treated OPCs (Tat-NG2 17 d), Tat was applied to culture at 15 d for 48 h and then OPCs was collected at 17 d. Data represent results from three independent experiments. Panel A, representative gel demonstrating mRNA expression of K_V1.3. Band densities were normalized to GAPDH and summarized in panel B. K_V1.3 mRNA expression decreased in NG2 17 d and GalC cells compare with NG2 14d. Tat up-regulated K_V1.3 mRNA expression in NG2 17 d cells. * $p < .05$, # $p < .05$ vs NG2 14 d, ## $p < .01$ vs NG2 14 d.

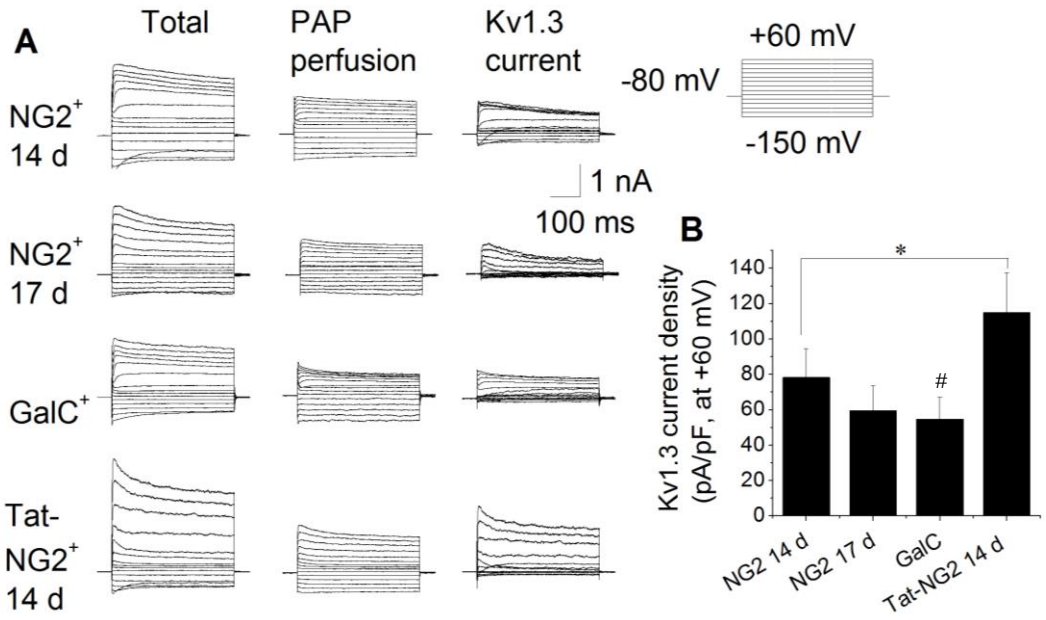

Figure 18. Developmental change of K_V1.3 currents and alteration caused by Tat. Data are shown for OPCs cultured for different days as indicated. Tat was applied to 14 d OPCs for 2 h in prior of recording (Tat-$NG2^+$ 14 d). After recordings were obtained in normal bath solution, 10 nM PAP was perfused into the cell chamber. K_V1.3-excluded currents were recorded at 20 min after perfusion. Isolated K_V1.3 currents were obtained by subtraction of K_V1.3-excluded current from total current. Panel A shows representative current traces. The voltage protocol used to generate K^+ is shown in inset. Panel B summarizes the K_V1.3 current density at +60 mV. n = 6 of each group. * $p < .05$, # $p < .05$ vs NG2 14 d.

3.4. K_V1.3 involved in Tat-induced OPC apoptosis and maturation retardation

Although the typical cells in brain infected by HIV-1 are microglia in the CNS [218], a recent report has shown that Tat decreases OPC cell viability [9]. As previously noted, Tat has been detected in serum and CSF at a concentration between 2-40 ng/ml in HIV patients, however, this concentration could be under-estimated in local tissue [184, 185]. Since Tat cause oligodendrocyte apoptosis through K_V1.3, we sought to determine if Tat cause OPC apoptosis at a similar manner. To explore the effect of Tat on OPC apoptosis and the involvement of K_V1.3 channels, Tat was applied to 15 d OPCs at a dose of 50 ng/ml with (PAP + Tat) or without (Tat) pre-addition of PAP (1 h) for 48 h. Apoptosis was assessed at the OPC age of 17 d by Tunel staining. Exposure of OPCs to 50 ng/ml Tat increased the percentage of apoptotic cells by approximately 2-fold over non-treated control (Ctrl) and such an increase was prevented by PAP (Fig. 19).

As noted in the introduction to Chapter 1, maturation of OPCs to oligodendrocytes is a challenge point for myelin maintenance and remyelination in HAND. Besides Tat-induced OPC toxicity, alterations in OPC maturation is potentially contributory to observed myelin damage in HAND. We examined whether Tat hinders OPC maturation. $GalC^+$ OPCs were treated with 25 ng/ml Tat, which is the dose did not cause OPC apoptosis (Data not shown), while transferring cells into differentiating medium with or without pre-addition of PAP (1 h). After 48 h, the cells in differentiating medium (Ctrl), differentiating medium contained Tat (Tat), and differentiating medium contained PAP and Tat (PAP + Tat) were projected to maturation analysis. The maturation was determined by percentage of MBP^+ cells and $NG2^+$ cells as revealed by immunofluorescence. Tat dramatically decreased the population of MBP^+ cells from 90.91% ± 21.18% (Ctrl) to 44.44% ± 8.92% (Tat), and sustained more cells in $NG2^+$ OPC status (48.15% ± 8.62% of Tat vs 6.06% ± 3.87% of control). Pre-treatment of PAP

partially prevented the MBP^+ cell number decrease, suggesting Tat induce OPC maturation defects through $K_V1.3$.

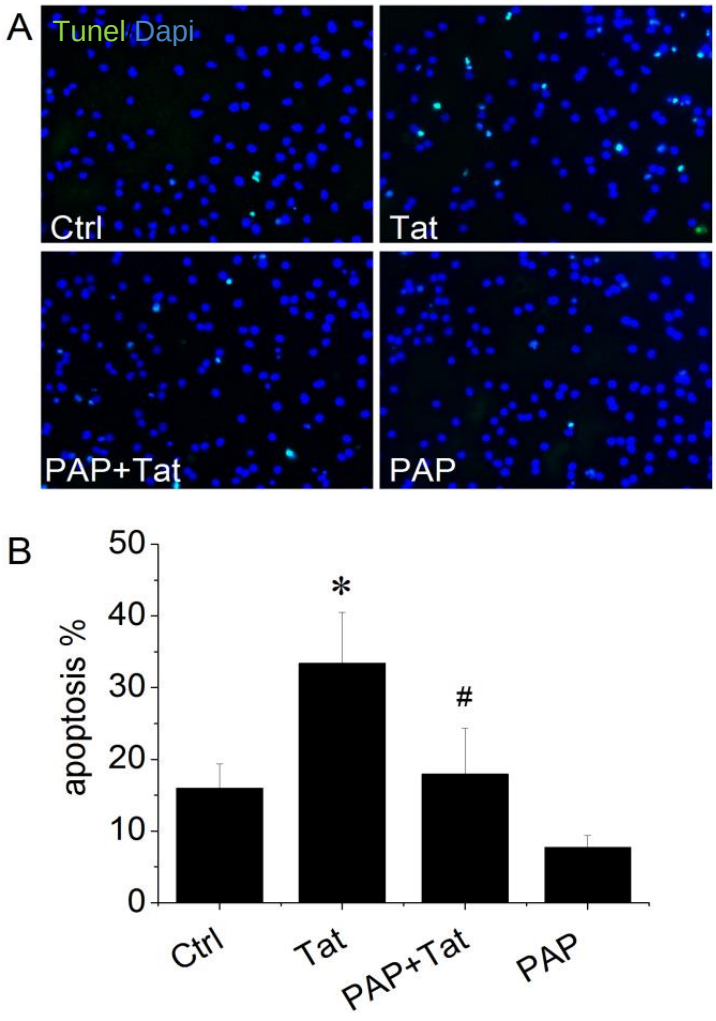

Figure 19. Involvement of $K_V1.3$ in Tat-induced OPC apoptosis. 10 nM PAP was added to the $NG2^+$ OPCs at 15 DIV for 1 h, followed by application of 50 ng/ml Tat (PAP + Tat) for 48 h. In a subset of cultures, 50 ng/ml Tat (Tat) or 10 nM PAP (PAP) alone was added to culture media for 48 h. Panel A shows Tunel staining (green) to identify apoptotic cells. Intact cell nuclei were visualized with Dapi (blue). Mean data are from 10 fields of each treatment from 3 independent experiments. Apoptotic percentage of each group is summarized in panel B. Tat increased OPC apoptosis, which was prevented by pre-addition of PAP. * $p < .05$ vs. control (Ctrl); $^{\#}P < .05$ vs. Tat. magnification was 400 ×.

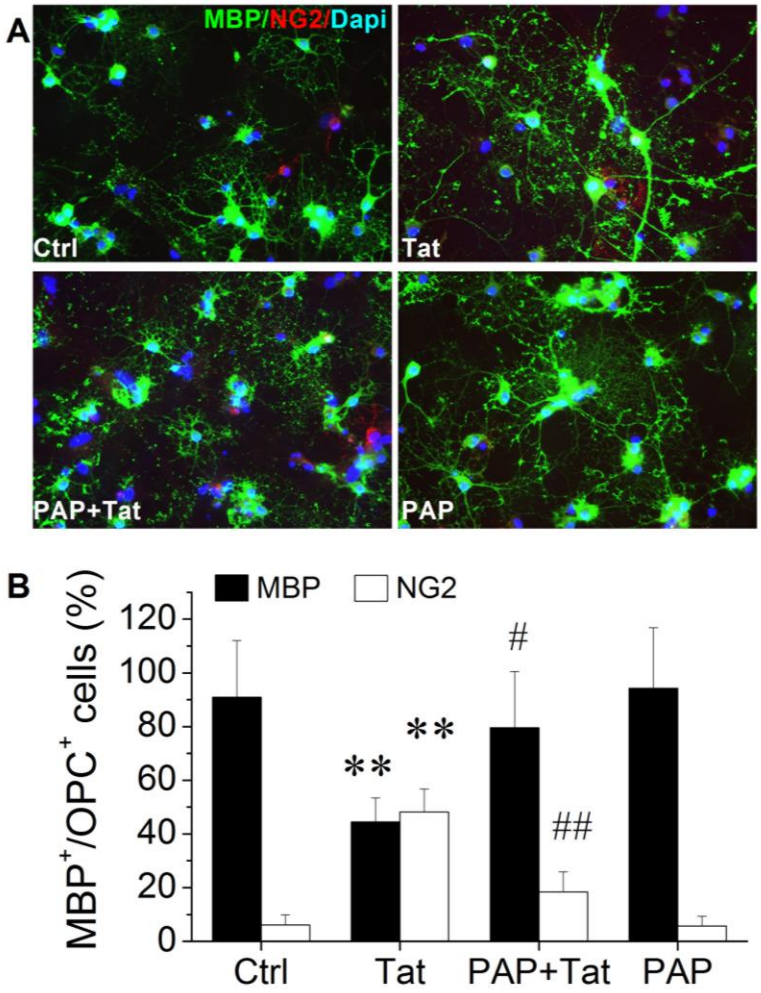

Figure 20. Suppression of $K_V1.3$ prevented Tat-induced maturation retardation. While OPCs being transferred to differentiating medium at 19 DIV, PAP was pre-applied to OPC for 1 h, with (PAP + Tat) or without (PAP) following co-presence of 25 ng/ml Tat for 48 h. In a subset of cultures, cells were in parallel transferred in normal differentiating medium (Ctrl), or differentiating medium contained 25 ng/ml Tat (Tat). Panel A, representative fields show MBP staining (green) an NG2 staining (red) result as a measurement of OPC maturation, with cell nuclei visualized using Dapi stain. 10 visual fields were analyzed for each of three independent experiments. Panel B, Tat induced MBP^+ cell number decrease was prevented by PAP. ** p <.01 vs. control (Ctrl); # p <.05 vs. Tat group; magnification was 400 ×.

4. Discussion

Presently we show that the HIV trans-activator Tat induces OPC injury and hinders OPC maturation using a mechanism involving $K_V1.3$. There are two novel findings: 1) direct induction of OPC apoptosis by HIV Tat, which is independent of the immune system, and 2) $K_V1.3$ channels play an essential role in Tat-induced OPC apoptosis and maturation retardation.

In this study, we described the resting membrane properties of decreased resting membrane potential and capacitance of OPCs as well as the total K^+ currents within development. The developmental I_A declining in OPCs was accompanied with the decrease of $K_V1.3$ mRNA expression (Fig. 17) and decreased $K_V1.3$ currents (Fig. 18). This finding is similar with results previously reported that outward K^+ currents are larger during early stages of development [129, 130, 219, 220]. Moreover, the subtracted current traces shown in Fig 18 imply that $K_V1.3$ is transient-activated, which corresponds to I_A currents. These data suggest the regulation of $K_V1.3$ expression is at least partially responsible for the I_A changes during development (Fig. 17). However, the resting membrane potential becomes more negative within time, indicating that $K_V1.3$ is not a primarily contributory to the maintenance of OPC resting membrane potential. Previous study demonstrated the resting membrane potential did not alter in oligodendrocytes at the age from 1-14 d in primary culture [155]. The discrepancy between this early result and ours is uncertain. However, it may due to the different animal model and culture conditions. Their works were done in $GalC^+$ oligodendrocytes isolated from the lamb brains and cultured in DMEM supplemented with 20% horse serum, whereas ours were isolated from rat brains and cultured in medium as described in Method. In addition, the Na^+ or Ca^{2+} channel inhibitor was not present in recording solutions. There was no Ca^{2+}-like current observed, and Na^+- current was recorded in less than 10% of the whole

recorded cell population. It is possible that the Na^+- current-expressed cells are neural progenitor cells.

Our results show that Tat causes apoptosis in primary culture (Fig. 19), suggesting that Tat perform direct toxicity on OPCs. These findings are consistent with research demonstrating Tat decreases OPC cell viability by targeting at NMDA receptor [9]. The consensus view regarding the pathogenesis of HAND is generated by direct and indirect models as described in Chapter 1 Introduction 1.2., of which are briefly direct toxicity and consequences of inflammatory response caused by neurotoxins secreted from infected macrophages, microglia, or astrocytes. Most studies suggest Tat causes neuronal function deficits predominantly by inducing CNS inflammation (indirect model) in HAND. However, HAND patients given cART with adjunctive “anti-inflammatory” agents do not attain greater benefits compared with those with cART only [221], suggesting inflammation maybe not the primary factor drives HAND pathogenesis in patients on cART. Because Tat transcription continues in these patients with good access with cART, Tat-performed direct toxicity on OPCs provide a potential mechanism for observed myelin damage in cART era [222]. Regarding the concept of increased efflux of K^+ in programmed cell death [84] [223], our recent research has focused attention on the role of K_V channelopathies in HAND pathology. In an earlier publication from our laboratory, we demonstrated that blockade of $K_V1.3$ or knockdown $K_V1.3$ expression in microglial cells eliminated neuronal apoptosis triggered by exposure to supernatant from Tat-containing microglia [141]. We show that Tat exposure leads to an up-regulation of $K_V1.3$ mRNA (Fig. 17) expression and amplification of $K_V1.3$ currents (Fig. 18). Tat-induced apoptosis in cultured OPCs was decreased in the presence of PAP (Fig. 19), suggesting that Tat may trigger OPC apoptosis by amplifying K^+ efflux through $K_V1.3$ (Fig. 18, and 20).

Controversial results have been reported in OPC cell fate in HIV-related pathogenesis. The mRNA levels of transcription factor Olig2, which is expressed to higher levels in OPC and lower levels in mature oligodendrocytes [91], are elevated in the front cortex of HIV patients [48], may due to increased OPC proliferation for repairing damaged myelin sheath in response to HIV infection. However, in another research, Tat exposure reduces the population of $Olig2^+$ OPCs, but progenitor survival is unaffected [85], suggesting the proliferation was interrupted. Overall, as mentioned in Chapter 1, HIV-1 infection or viral protein exposure appears to incline NPC fate toward production of glia/astroglia at the expense of neurons and/or oligodendrocytes [85, 93, 94]. Thus we hypothesized OPC maturation is the key point for myelin maintenance and remyelination in HAND. Studies of genetically altered expression of K_V channels in oligodendrocytes suggest that basal activity of K_V channels directly controls proliferation and differentiation [183, 212]. Immunocytochemical staining of oligodendrocyte lineage cells acutely isolated from tissue slices demonstrated that expression of $K_V1.3$ and $K_V1.5$ subunits was higher in $NG2^+$ and $O4^+$ (late OPC maker) OPCs than in mature $O1^+$ oligodendrocytes. In parallel, the expression of the same subunits within the $NG2^+$, $O4^+$, and $O1^+$ populations had the same pattern as that of cyclin D, suggesting that $K_V1.3$ is developmentally regulated with progression through the oligodendrocyte lineage [130]. Tat exposure decreases the population of MBP^+ cells (Fig. 20) and $K_V1.3$ blockade restrain Tat-induced OPC maturation deficit, suggesting OPC maturation is impaired in HAND and, Tat may act through $K_V1.3$ channel to achieve dysregulation of OPC maturation. It is worth noting that neuronal axons were not present in pure OPC/oligodendrocyte culture; thus, we were not able to detect myelination. Maturation of oligodendrocytes *in vitro* is not equal to successful myelination *in vivo*.

Pathogenesis of myelin injury-related cerebral WM damage in HAND recently attracted attention [41, 224]. HIV-1-associated myelin injury has been attributed to effects of inflammatory response and BBB damage. However, in present study, we show Tat directly target at OPC to cause cell apoptosis and maturation retardation; the presence of PAP mitigates Tat-induced apoptosis and maturation retardation by inhibiting enhancement of $K_V1.3$ currents. Collectively, these findings serve to better understand the myelin damage and repair processes in HAND, and support the role of $K_V1.3$ inhibition as a therapeutic strategy for myelin damage in HIV-1 patients.

Chapter 4

Plasma gelsolin protects HIV-1 gp120-induced neuronal injury via voltage-gated K^+ channel Kv2.1

Abstract

Plasma gelsolin (pGSN), a secreted form of gelsolin, is constitutively expressed throughout the central nervous system (CNS). Neurons, astrocytes and oligodendrocytes are the major sources of pGSN in the CNS. It has been shown that levels of pGSN in cerebrospinal fluid (CSF) are decreased in several neurological conditions including HIV-1-associated neurocognitive disorders (HAND). Although there is no direct evidence that a decreased level of pGSN in CSF is causally related to the pathogenesis of neurological disorders, neural cells, if lacking pGSN, are more vulnerable to cell death. To understand how GSN levels relate to neuronal injury in HAND, we studied the effects of pGSN on HIV-1 gp120-activated outward K^+ currents in primary rat cortical neuronal cultures. Incubation of rat cortical neurons with gp120 enhanced the outward K^+ currents induced by voltage steps and resulted in neuronal apoptosis. Treatment with pGSN suppressed the gp120-induced increase of delayed rectifier current (I_K) and reduced vulnerability to gp120-induced neuronal apoptosis. Application of Guangxitoxin-1E (GxTx), a Kv2.1 specific channel inhibitor, inhibited gp120 enhancement of I_K and associated neuronal apoptosis, similar effects to pGSN. Western blot and PCR analysis revealed gp120 exposure to up-regulate Kv2.1 channel expression, which was also inhibited by treatment with pGSN. Taken together, these results indicate pGSN protects neurons by suppressing gp120 enhancement of I_K through Kv2.1 channels and reduction of pGSN in HIV-1-infected brain may contribute to HIV-1-associated neuropathy.

Keywords: Cortical neurons; Kv channels; HIV-1gp120; Neuronal injury; Plasma gelsolin; Neuroprotection.

1. Introduction

Approximately half of the HIV-1-infected patients develop neurocognitive impairments [225]. With the advent of antiretroviral therapy (ART), the morbidity and mortality resulting from HIV-1 infection has been lessened. However, the incidence of HIV-1-associated neurocognitive disorders (HAND) continues and, due to the longer lifespans of treated patients and ART drug toxicity, the prevalence may actually be increasing [174, 226-228]. Although productive HIV-1 infection of neuronal cells has not been demonstrated, it is well accepted that neurons are affected by HIV-1 through indirect mechanisms [229-231]. These include the release of soluble neurotoxins from HIV-1-infected and immune competent mononuclear phagocytes (perivascular brain macrophage and microglia), leading to neuronal dysfunction and injury [229, 232]. As noted in Chapter 1, such neurotoxins include, but not limited to, proinflammatory cytokines, chemokines, excitatory amino acids, and viral proteins (gp120 and Tat), which can injure or kill neurons [233]. In particular, the envelope protein gp120 has been shown to be lethal to neurons in culture through alterations in signal transduction and excitotoxic influx of Ca^{2+} [234-236]. For these reasons we chose to use gp120 to further investigate the mechanisms underlying HAND pathogenesis in our primary neuronal culture system.

Gelsolin (GSN) is an actin-binding protein best-known for its modulation of cell motility and secretion, is constitutively expressed throughout the CNS and particularly concentrated in neuronal growth cones. This protein exists in two isoforms, cytoplasmic gelsolin (cGSN) and plasma gelsolin (pGSN) [237]. Both isoforms are functionally similar and encoded by a single gene on chromosome 9 [238, 239]. In addition to its widely recognized function as a cytoplasmic regulator of actin organization, accumulating evidence suggests GSN activity prevents neuronal apoptosis in multiple ways [240],

including through the facilitation of voltage-dependent Ca^{2+} channel (VDCC) and NMDA-channel rundown following exposure to excitotoxic stimuli, thereby reducing cytosolic Ca^{2+} overload [241, 242]. Proteomic studies have revealed decreased pGSN levels in CSF of HIV-infected individuals with cognitive disturbance [243]. In addition, altered pGSN levels have been noted in other neurological conditions [244-246], such that pGSN is being considered as a biomarker for certain neurodegenerative disorders [246-248]. In general, GSN has been found neuroprotective and is now being considered as a potential treatment modality in several diseases characterized by neuronal injury [244, 245, 248-251].

K^+ channels necessarily contribute to the process of apoptosis. Regardless of the diverse external and internal stimuli that trigger cell apoptosis, enhanced K^+ efflux has been shown to be an essential mediator of apoptotic cell volume decrease, downstream caspase activation, and DNA fragmentation [84]. In previous experiments, our laboratory has confirmed the association of rat cortical neuron apoptosis and increased K^+ channel currents in models of HAND [143, 144, 252]. While several Kv channel subtypes have been implicated in cortical neuron apoptosis, including Kv2.1 [152], Kv1.1 [253], Kv3.4 [153], Kv4.2, and Kv4.4 [154], the specific subtype involved in HAND pathology and the mechanism underlying its dysfunction remains to be definitively characterized. Collectively, these observations lead us to investigate the protective potential of pGSN against gp120-induced neuronal injury and to determine the function of specific Kv channel subunits in this neuroprotective activity.

2. Experimental Methods

2.1. Materials

HIV-1gp120 IIIB was purchased from Immunodiagnostics, Inc. (Woburn, MA). Aliquots of gp120 were kept as 100 nM stock solution at -80 °C. The stock solution was diluted to desired concentrations with artificial cerebrospinal fluid (ACSF) 2-5 min before test. Gelsolin (recombinant human plasma isoform) was purchased from Cytoskeleton, Inc (Denver, CO). All chemicals, unless otherwise specified, were from Sigma-Aldrich (St. Louis, MO).

2.2. Animals

Pregnant Sprague-Dawley rats were purchased from Charles River Laboratories (Wilmington, MA). Animals were housed at a constant temperature (22°C) and relative humidity (50%) under a regular light-dark cycle (light on at 7 AM and off at 5 PM) with free access to food and water. Animal use procedures were strictly reviewed by the Institutional Animal Care and Use Committee (IACUC) of the University of Nebraska Medical Center (IACUC No. 00-062-07).

2.3. Rat cortical neuron preparation and culture

Neurons were isolated from cortex tissue of E18 fetal Sprague-Dawley rats. Culture dishes or plates were coated with poly-D-lysine (1mg/ml) for 1 h at 37 °C in prior to primary culture. All tools were autoclaved.

Firstly, pregnant rat was anesthetized by isoflurane and, then cut through skin and muscle with a pair of scissors to expose the uterus, intestines, and embryos. Embryos (in amniotic sac) were taken out carefully and placed into 10 cm- petri dish filled with cold HBSS. Embryos were taken from amniotic sac and placed to a fresh petri dish with

cold HBSS. Next, embryos were decapitated with large scissors and the heads were placed in a spate 10 cm-petri dish filled with cold (HBSS).

Microdissecting scissors was used to carefully cut skin and the skull along the midline from neck toward the nose. Brain was then taken out with a spatula and placed to another petri dish contained cold HBSS.

The meninges were removed with forceps under a dissection microscope. Cortex tissue was dissociated by cutting the brain to two hemispheres, followed by removing hippocampus and olfactory bulbs. The tissue was then incubated in 0.25% trypsin and 200 U DNase contained in HBSS at 37 °C for 15 min. FBS was applied to tissue suspension to stop trypsinization and then homogenate was transferred to a 50 ml tube. The contents were pipetted one time to separate any tissue block. The tissue suspension was next collected into a clean 50 ml-tube and centrifuged at 1500 r.p.m for 10 min. The supernatant was removed and 20 ml DMEM was added to suspense the remained cells/tissues by triturating cells/tissue for about 20 times. The remaining tissue suspension was passed through nylon mesh with pore diameter size of 100 µm and 40 µm. Cells were collected by centrifugation at 1500 r.p.m for 10 min.

Isolated cells were then suspended in neurobasal media (Gibco by Life Technologies) supplemented with 2% B27, 1% penicillin/streptomycin, 0.2% FBS, and 0.25 mM L-glutamine (Invitrogen by Life Technologies), and seeded either in 60 mm dishes at 2.5 x 10^6 cells/dish, 0.2 x10^6 cells/well in 12 well plates containing 15 mm diameter coverslips, or in 48-well plates at 0.05 x 10^6 cells/well. Cultures were maintained in supplemented neurobasal media for 8-12 days with half media change every 4 days. The purity of neuronal cells was determined to be >90% (Fig. 21) by staining with microtubule-associated protein-2 antibody (MAP-2: 1:1000, Chemicon International, Inc. Temecula, CA).

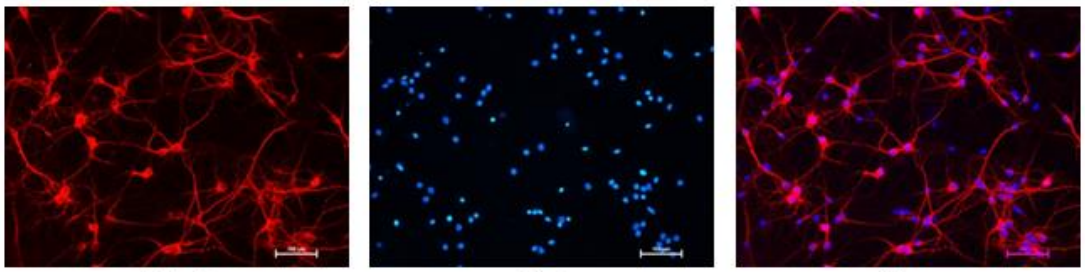

Figure 21. **Purity of cortical neuronal cultures.** View of neurons stained with Map2 (red).Cell nuclei are visualized wih DAPI DNA stain. Neuronal purity >90%.

2.4. MTT assay

Cell viability was assessed by MTT assay. Neurons were cultured in 48-well plates for MTT assay to minimize discrepancies between replicates. The MTT stock solution was prepared in sterile PBS at concentration of 5 mg/ml (10 ×) and store at -20 °C. The working solution was made by diluting the stock MTT solution 10 times with neurobasal media without supplements. Pre-treated cells were exposed to 300 µl of neurobasal media contained 500 µg/ml MTT (Sigma-Aldrich) for 2 h at 37 ºC. The MTT solution was discarded and replaced with 150 µl dimethyl sphingosine (DMSO). Cells were then shaken for 15 min at 200 r.p.m for completed lysis. The dissolved solution was transferred of 100 µl from each well to a 96-well plate and, 96-well plate was eventually placed to a plate reader and tested the optical density at 560 nm.

2.5. Tunel assay

Neuronal apoptosis was evaluated by using a Fluorescein *In Situ* Cell Death Detection Kit (Roche Applied Science, Indianapolis, IN). Briefly, Neurons grown on the poly-D-lysine-coated coverslips were washed twice with PBS and fixed in 4% paraformaldehyde (PFA) for 1 h at room temperature. Then cells were permeabilized by incubation with 0.1% Triton X-100 for 30 min. Cover slips were washed 5 min × 3 times with PBS. Tunel reaction mixture was made by adding 1 part label solution to 50 parts enzyme solution. The reaction mixture was applied onto clean Para film as 30 µl-drops and, cover slips were flipped onto reaction mixture solution spots and incubated for 90 min at 37 °C. After washing, coverslips were mounted in vectashield mounting medium with Dapi stain (Vector Laboratories, Burlingame, CA) and cells were visualized by a fluorescent microscope. Apoptosis was assessed in each of three experiments by examining 10 microscopic fields per experimental group. The percentage of apoptotic

neurons was determined based on Tunel-positive cells normalized to Dapi-stained nuclei in 3 independent experiments.

2.6. Electrophysiology

Whole-cell recordings were made on neurons seeded on glass cover-slips at 9-12 d. Recording electrodes, pulled from borosilicate glass micropipettes (WPI Inc. Sarasota, FL) with a P-97 micropipette puller (Sutter Instruments, Novato, CA), had a resistance of 5.0–8.0 MΩ when filled with intracellular solution contained (in mM): 120 K-gluconate, 10 KCl, 5 NaCl, 1 $CaCl_2$, 2 $MgCl_2$, 11 EGTA, 10 HEPES, 2 Mg-ATP and 1 GTP, adjusted pH to 7.3 with KOH. The extracellular solution was artificial cerebrospinal fluid (ACSF) contained (in mM) 140 NaCl, 5 KCl, 2.5 $CaCl_2$, 10 HEPES and 10 glucose, adjusted pH to 7.4 with NaOH. Tetrodotoxin (TTX, 1μM) and $CdCl_2$ (0.2 mM) were added to the ACSF to block voltage-gated Na^+ and Ca^{2+} channels, respectively. Stock solutions of 4-Aminopyridine (4-AP) and tetraethylammonium (TEA) were prepared in deionized water and diluted to working concentrations (4-AP 5mM, TEA 40mM) with ACSF in order to block A-type transient outward K^+ current (I_A) or delayed rectifier outward K^+ current (I_K). After establishment of the whole-cell patch configuration, the cells were allowed to stabilize for 3-5 min before tests. The recorded cells were held at -80 mV during voltage-clamping. Whole-cell outward K^+ currents were generated by voltage steps from the holding potential -80mV to +80mV in increments of 20mV. Current amplitudes were measured at the initial peak and at 300 ms and current densities (pA/pF) were calculated by dividing the amplitudes by the whole cell capacitance. Junction potential, pipette resistance were corrected and cell capacitance were compensated (~70%). Current signals were filtered at 1 kHz and digitized at 5 kHz using Digidata 1440A digitizer (Molecular Devices). The current and voltage traces were displayed and recorded in a computer using Clampex 8.2 (Molecular Devices).

All experiments were done at room temperature (22-23°C). In prior to recording, the bathing solution was oxygenated (bubbled with 95% O_2 and 5% CO_2) for 30 min. The neuronal cells were identified by their morphology (triangular shaped) and their firing of action potentials in response to a depolarizing current impulse. Data were analyzed by Clampfit 8.2 (Molecular Devices) and graphed using Origin 8.5 (OriginLab, Northampton, MA). For bar graphs illustrating current densities, the instantaneous I_A and steady-state I_K generated by a voltage step from -80mV to +80mV were measured and the current density was then calculated by dividing the current and expressed as pA/pF.

2.7. RT-PCR

The total RNA isolation was completed with Trizol reagent (Invitrogen). Reverse transcription was performed on 1-2 µg of the RNA sample with a SuperScript III first strand synthesis kit (Invitrogen) using the oligo-dT primers.

Pre-treated neurons were washed twice with sterile cold PBS, followed by addition of 1 ml Trizol to each well of culture in 6-well plate. Cells were lysed by passing cells several times through a pipette. The lysate was collected in freshly-sterilized 1.5 ml tubes and then incubated for 5 min in room temperature. Each tube received addition 0.2 ml of chloroform and was capped securely. Tubes were shaken vigorously by hand for 15 seconds, and then incubated in room temperature for 3 min. Samples were centrifuged at 12,000 g for 15 min at 4 °C. Following centrifugation, the samples were then separated into 3 phases: lower red phase, and protein-enriched interphase, and a colorless upper aqueous phase that contained RNA. Approximately 0.5 ml of the upper phase of each sample was carefully transferred into fresh tubes. The same amount of 0.5 ml of isopropyl alcohol was added to each tube to precipitate the RNA. Samples were incubated at room temperature for 10 min. Centrifugation was then performed at 12,000 g for 10 min at 4 °C. The RNA generally formed a gel-like pallet at the bottom of

tubes. The supernatant was removed and, 1 ml 75% ethanol was added to each tube to wash the RNA. Samples were centrifuged at 7,500 g for 5 min at 4 °C. The RNA isolation was finally achieved by discarding the supernatant and drying the pallet in room temperature for about 5 min. RNA was dissolved in 12 µl RNase-free water by passing them through a pipette. The amount of 2 µl RNA of each sample was taken for RNA concentration determination. The rest was stored at -80 °C for further reverse transcription. RNA concentration was determined by Nanodrop 2000.

Reverse transcription was accomplished with a SuperScript III first-strand synthesis kit (Invitrogen). The amount of 2 µg of each RNA sample was taken and balanced the volume of to 8 µl by RNase-free water for every sample, followed by addition of 1 µl oligo-dT primer and 1 µl dNTPs to each sample. The cDNA synthesis mix was prepared in a separate tube by mixing 2 µl of 10 × RT buffer, 4 µl of 25 mM $MgCl_2$, 2 µl of 0.1 M DTT, 1 µl of RnaseOUT, and 1 µl of SuperScript III RT (10 µl total) for each sample. The prepared mix was kept on ice. The samples (RNA + primer + dNTPs) were projected onto the thermal plate of PCR machine (Eppendorf RealPlex^2). The program was set as 65 °C for 5 min, pause, 50 °C for 50 min, 85 °C for 5 min, pause, 37 °C for 20 min, and hold at 4 °C. After reverse transcription program started, the samples were taken out at the first pause and placed on ice for at least 1 min. Prepared cDNA synthesis mix (10 µl) was added to each sample. At the second pause, 1 µl of RNase H was provided for each sample.

The resulting cDNA was next used for PCR amplification. Primer sequences for Kv1.1 were forward GGAGCGCCCCCTACCCGAGAAG, reverse GGTGAATGGTGCCCGTGAAGTCCT, product length 191 base pairs (bp); for Kv2.1, forward TGGAGAAGCCCAACTCATC, reverse CAATGGTGGAGAGGACATG, product length 78bp; for Kv4.2, forward GCCGCAGCGCCTAGTCGTTACC, reverse

TGATAGCCATTGTGAGGGAAAAGAGCA, product length 262 bp; and for GAPDH, forward TCAAGAAGGTGGTGAAGCAG, reverse AGGTGGAAGAATGGGAGTTG, product length 126 bp. PCR cycles were performed as follows: initial 5 min at 95°C, then 30 cycles of 95°C (15 s), 55°C (30 s), and 72°C (45 s), followed by 10 min at 72°C for further extension.

2.8. Immunoblotting

Briefly, pre-treated neurons were washed twice with ice-cold PBS and total proteins were extracted using RIPA (Sigma- Aldrich).

2.8.1. Total protein extraction

The whole cell lysates were prepared in RIPA buffer (BioRad, Hercules, CA) while tissue was lysed in tissue extraction reagent (Invitrogen). In details, following experimental treatments, neurons were washed twice with ice-cold PBS and then PBS was aspirated. RIPA buffer supplemented with protease inhibitor (Sigma) was added (150 µl) to each well of 6-well plate. Cells were detached by scraping the well bottom and gently transferred into a microcentrifuge tube. Lysate was then projected to a freeze-thaw cycle for complete lysis, and then centrifuged at 10,000 r.p.m. for 10 min and supernatant was collected to a fresh tube. Next, 20 µl of each sample was taken out for protein concentration determination. A quarter of the sample volume of 5 × loading buffer was added to protein samples. Protein samples were denatured by boiling water for 7 min, and stored in -20 °C for western blotting.

5 × loading buffer consisted of 0.25% Bromophenol blue, 0.5 M dithiothreitol, 50% glycerol, 10% sodium dodecyl sulfate, and 0.25 M Tris-Cl (pH 6.8).

2.8.2. Protein concentration determination

The BCA protein assay kit (ThermoFisher Scientific, Waltham, MA) was employed to quantify protein concentration. BCA working reagent was prepared by mixing 50 parts of BCA Reagent A with 1 part of BCA reagent B. The needed total volume of working reagent was determined by the following equation: (number of standards + number of unknowns) × (number of replicates) × 100 µl = total volume of working reagent required.

Standards were prepared by diluting 2 mg/ml albumin ampules in working reagent to 200, 100, 50, 25, 12.5 µg/ml. Then 100 µl of each standard was put into a 96-well plate. At separate wells, 100 µl of working reagent only was placed as zero. Next, 10 µl of each unknown samples was diluted to 90 µl working reagent. Every standard and sample was duplicated. After all samples prepared, the plate was incubated in 37 °C for 30 min. The plate was then placed in a plate reader and the absorbance of all the samples were measured with the testing wavelength at 560 nm.

Standard curve was made by plotting the average Blank-corrected measurement for each albumin standard versus its concentration in µg/ml. The standard curve was used to determine the protein concentration of each unknown sample. The volume for 15 µg protein of each sample was calculated and then the denatured samples were projected to Western blotting.

2.8.3. Western blotting

Solutions of 10 × Tris/glycine buffer, 10 × Tris/glycine/SDS buffer, 10% SDS, and 30% Acrylamide/bis solution were all purchased from Bio-Rad. The 10 × TBS (Tris-buffered saline, 1 liter) was prepared by dissolving 24.2 g Tris base, 80 g NaCl in distilled water, and adjust pH to 7.6 with HCl. Washing buffer was prepared by diluting 1 ml 100% Tween-20 to 1 liter 1× TBS (TBST).

Proteins were firstly separated by electrophoresis depending on the molecular weight. In details, 15 μg protein of each sample was loaded onto 10% SDS-polyacrylamide gels. Electrophoresis was run under 70 mV constant voltage and switched to 110 mV when samples enter lower separating gel. Electrophoresis was stopped when the Bromophenol blue reached the bottom edge of SDS-polyacrylamide gel.

After electrophoresis, proteins were transferred from gel to a polyvinylidene difuoride (PVDF) membrane by 100 mV constant voltage in 1 × Tris/glycine/SDS buffer containing 20% methanol for 70 min at 4 °C. The PVDF membrane was then blocked in 5% non-fat milk in TBS for 1 h in room temperature. Following blocking, membranes were incubated at 4 °C overnight in primary antibodies including rabbit polyclonal K_V1.1 (1.500), mouse monoclonal K_V2.1,(1:500) (Abcam Inc. Cambridge, MA), rabbit anti-KV4.2 (1:200, CHENICON International, Inc.), anti-mouse β-actin (1:5,000), or anti-rabbit GAPDH (1:5,000) to detect Kv1.1, Kv2.1, Kv4.2, GAPDH, and β-actin protein. Afterwards, membranes were washed in TBS with 0.2% Tween (TBS-T) and incubated with either HRP-conjugated onto rabbit or anti-mouse secondary antibody (1:10,000, Haacson ImmunoResearch Laboratories, West Grove, PA) for 1 h at room temperature. Finally, membranes were washed and visualized by Pierce ECL Western Blotting Substrate (Thermo Scientific, Rockford, IL). Band densities captured by ImageJ.

2.9. Statistical analyses

All data were expressed as mean ± S.E.M. unless otherwise indicated. Statistical analyses were performed by one-way ANOVA or two-tailed *t* test. The difference between groups was considered significant when $p < .05$.

3. Results

3.1. gp120-induced neuronal toxicity was protected by pGSN

Neuron is not the primary cell type HIV-1 target at in brain [218]. However, viral envelope glycoprotein gp120 has been demonstrated to induce neuronal apoptosis in cell cultures [234, 235]. Further, while pGSN has been shown to be protective against excitotoxic insults [241], it is detected at significantly lower levels in the CSF of HIV-1-infected individuals who exhibit neurocognitive disorder [243, 254]. In light of these findings, we sought to determine the effect of pGSN on gp120-induced neuronal toxicity. First, rat cortical neuronal cultures were prepared and incubated for 24 h with varying concentrations of gp120 (0-1000 pM). Neuronal viability was then assessed by MTT assay and found to diminish significantly at gp120 concentrations above 250 pM (Fig. 23A). Given the nearly 40% loss of viability at concentrations of and greater than 500 pM, the concentration of 500pM was utilized in neurotoxicity experiments. Next, neuronal cultures were treated for 24 h with 500 pM gp120 and different concentrations of pGSN (0-2500 ng/ml). pGSN was found to be significantly protective against gp120-induced toxicity at a concentration of 2.5 µg/ml (Fig. 23B).

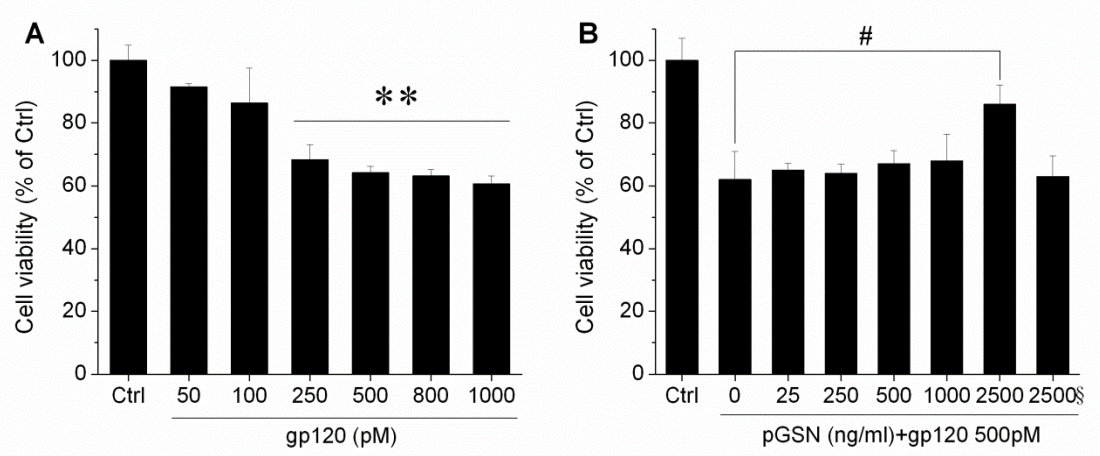

Figure 22.GSN protection of gp120-induced neuronal damage. Panel A, Dose-dependent toxicity of gp120 on cortical neurons. Exposure of neuronal cells to gp120 at and greater than 500 pM resulted in maximal reduction in cell viability. Panel B, neurons were treated with different concentrations of GSN or with 500 pM gp120 for 24 h. pGSN protected neurons from gp120-induced damage at 2.5 µg/ml. Heat (boiled) inactivated pGSN (indicated by a symbol §, the same as in other figures of Chapter 4) failed to produce protective effect. Data represent means ± S.E.M. from at least 5 independent experiments and expressed as % of control. * $p < .05$ vs. control, ** $p < .01$ vs. control; $^{\#}$ $p < .05$ vs. gp120 (0 GSN).

3.2. pGSN attenuation of gp120 increase of outward K^+ current

It has been shown that activation of neuronal Kv channels is involved in neuronal dysfunction and apoptosis [139, 255]. In HIV-1 infection, secreted cellular and viral products can increase Kv channel activity, leading to neuronal dysfunction and cognitive deficits [145]. Specifically, previous experiments in our laboratory have demonstrated gp120 can induce apoptosis by enhancing 4-AP-sensitive I_A current via PKC signaling [143]. Given the prominent role of Kv channels in mediating neuronal damage, coupled with the protective effects of pGSN against gp120-induced neurotoxicity observed here, we further sought to determine if the protection provided by pGSN occurs via alterations in Kv channel activity. First, rat cortical neuron cultures were prepared and treated with gp120 at concentrations of 50 pM or 100 pM for 24 h. Whole-cell outward K^+ currents were then recorded. As shown in Figure 23A, gp120 produced an increase of outward K^+ currents. Further analyses revealed that gp120 significantly ($p < .01$) increased both instantaneous and steady-state outward K^+ currents at a concentration of 100 pM (Fig. 23B). Next, we examined effects of pGSN on its blockade of gp120 increase of neuronal outward K^+ currents. Neuronal cultures were treated for 24 h with either 100 pM gp120 alone or with gp120 (100 pM) and different concentrations of pGSN (0, 5, 50, 500 ng/ml). As expected, gp120 enhanced both instantaneous and steady-state outward K^+ currents (Fig. 24). Treatment with pGSN reduced gp120-associated increase of outward K^+ currents, with a significant ($p < .01$) reduction of the steady-state outward K^+ current at a concentration of 500 ng/ml (Fig. 24B). Application of pGSN alone at concentrations of 5, 50 and 500 ng/ml (data not shown) or heat-inactivated pGSN (500 ng/ml, Fig. 24B) had no significant effects on gp120 increase of outward K^+ currents. These results indicate that pGSN inhibits gp120 enhancement of neuronal steady-state outward K^+ currents.

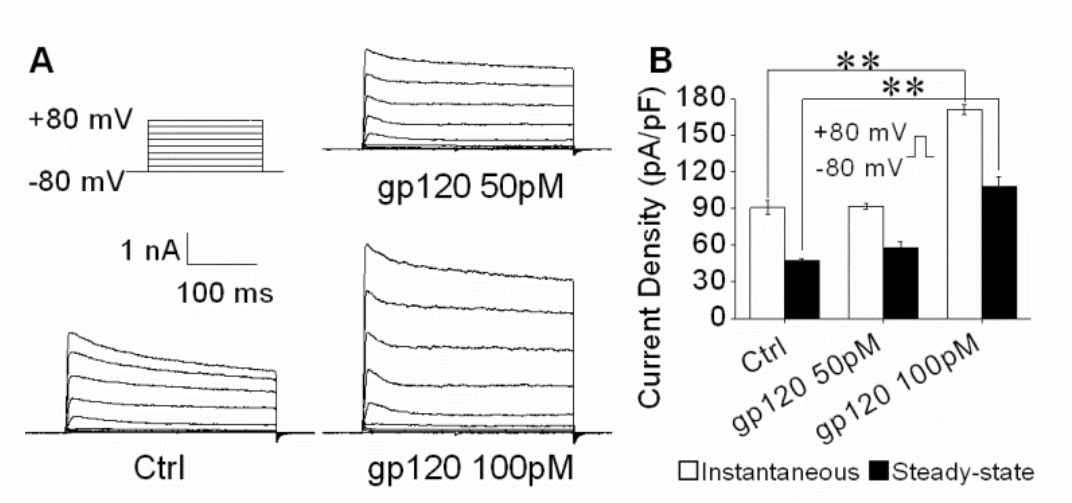

Figure 23. Gp120 increase of outward K^+ currents. Cultures were treated without or with 50 pM or 100 pM gp120 respectively for 24 h. Panel A, representative current traces evoked by voltage protocol (upper left, not proportional to the current traces in duration) from three different neurons treated without (Ctrl) or with 50 pM, 100 pM gp120 respectively for 24 h. Note gp120 at 100 pM increased outward K^+ currents. Current amplification was measured at the peak for instantaneous current and at 300 ms for steady-state current. Panel B, instantaneous and steady-state current densities measured at +80 mV from groups of neurons treated without (Ctrl, n = 15) or with 50 pM gp120 (n = 13), 100 pM gp120 (n = 18). Note that gp120 increased both instantaneous and steady-state outward K^+ currents at 100 pM. ** $p < 0.01$ vs. control.

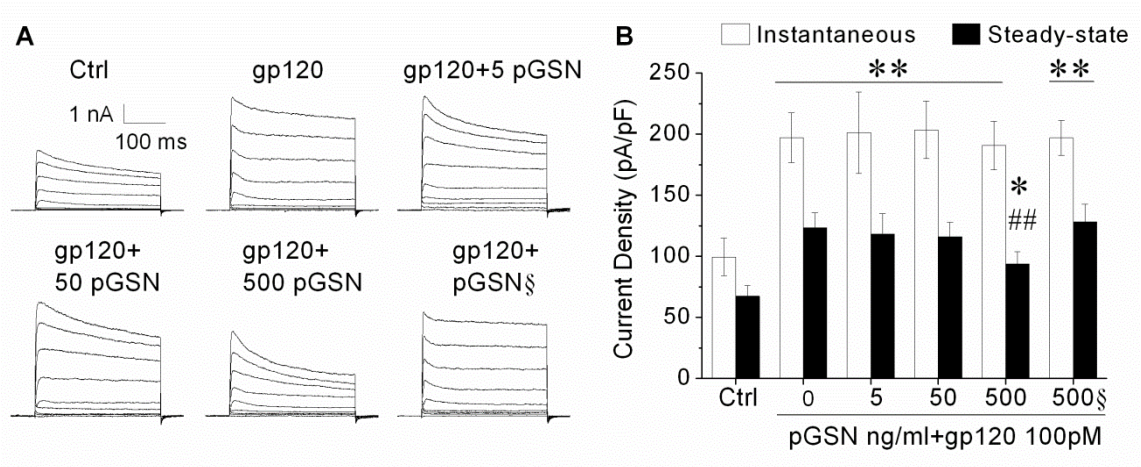

Figure 24. pGSN decrease of gp120 enhancement of neuronal outward K^+ currents. Panel A, representative current traces recorded from6 different neurons treated with gp120 (100 pM) alone, or gp120 (100 pM) and different concentrations of pGSN (5, 50, 500, 500§), or untreated control. Whole-cell currents were generated by voltage steps from the holding potential of −80 mV to +80 mV in increments of 20 mV. Both instantaneous and steady-state outward K^+ currents were measured and current densities were calculated and displayed in Panel B. pGSN only inhibited gp120-induced steady-state K^+ current. In contrast, heat denatured pGSN lose such an inhibitory ability. * $p < .05$ vs. control, ** $p < .01$ vs. control; ## $p < .01$ vs. gp120 alone.

3.3. Gp120 enhancement of TEA-sensitive I_K was inhibited by pGSN.

Two components of outward K^+ currents recorded TEA-sensitive I_K and 4-AP-sensitive I_A were recorded in neurons. Previous studies indicate certain outward K^+ currents may be more involved in apoptosis [223]. In order to determine the specific outward K^+ currents enhanced by exposure to gp120 and attenuated by treatment with pGSN, whole-cell recordings were repeated in the presence of 4-AP (5 mM) or TEA (40 mM). As seen in Figure 25, gp120 (100 pM) augmented both 4-AP-sensitive I_A and TEA-sensitive I_K (Fig. 25A), while only TEA-sensitive I_K was suppressed with GSN treatment (Figs. 25A and 25C). Application of pGSN (500 ng/ml) alone did not affect the outward K^+ current amplitude or current density of either type.

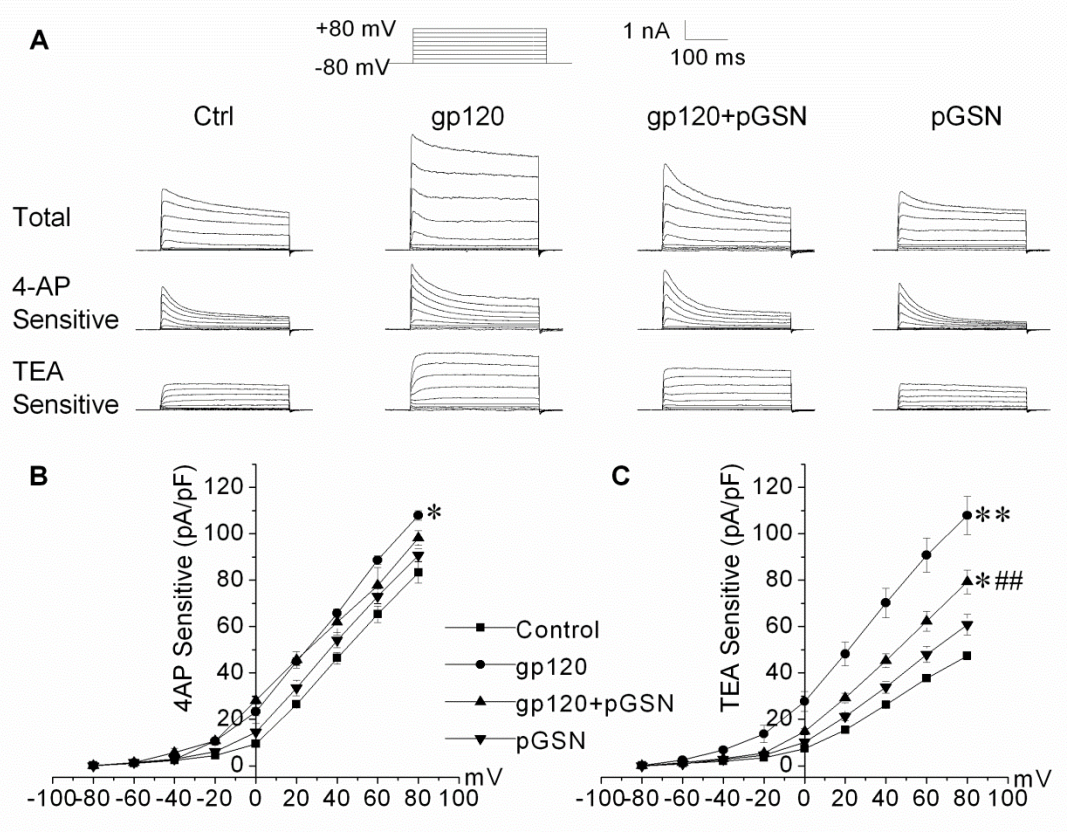

Figure 25. pGSN inhibited gp120 enhancement of TEA-sensitive I_K, but not 4-AP-sensitive I_A. Panel A shows representative total (upper), 4-AP-sensitive (middle) and TEA-sensitive (lower) outward K^+ currents recorded from neurons treated with gp120 (100 pM), gp120 (100 pM) + pGSN (500 ng/ml), pGSN (500 ng/ml) or untreated controls (Ctrl). Panel B and C are current density-voltage relationships, illustrating GSN inhibition of TEA-sensitive I_K. pGSN alone did not affect either the 4-AP- or TEA-sensitive outward K^+ currents ($P < .05$). For each type of outward K^+ currents, 25 neurons were recorded in each treatment group. * $p < .05$ vs. control, ** $p < .01$ vs. control; ## $p < .01$ vs. gp120 group.

3.4. Involvement of Kv2.1 in pGSN attenuation of gp120-induced I_K enhancement

The predominant subtypes of Kv channels reported that involve in neuronal injury and apoptosis are Kv1 [253, 256], Kv4 [257], and Kv2 [152]. In neurons, Kv1.1 and Kv4.2 are the principal components of I_A, while Kv2.1 is responsible for I_K [258]. Given our immediate findings, we postulated Kv2.1 channels to be the predominant mediator of the neuroprotection provided by pGSN. To test this hypothesis, we utilized the Kv2.1-specific inhibitor, Guangxitoxin (GxTx) [259, 260]. Control, gp120, and gp120 + pGSN groups were again prepared as described above. During the recordings, I_K was isolated by the addition of 4-AP (5 mM) to the bath solution and its Kv2.1 contribution suppressed by application of GxTx (50 nM). The addition of GxTx to the control group suppressed nearly 40% of the I_K component (Fig. 26B), demonstrating the contribution of Kv2.1 channels to the delayed outward K^+ current in these neurons. More importantly, the previously observed enhancements in I_K induced by exposure to gp120 were absent in the presence of GxTx, indicating the increase was comprised of current through Kv2.1 channels (Fig. 26). Lastly, the gp120-enhanced I_K attenuated by co-incubation with GSN was not further inhibited by the addition of GxTx, allowing us to infer that both may affect I_K via modulation of Kv2.1 channel activity.

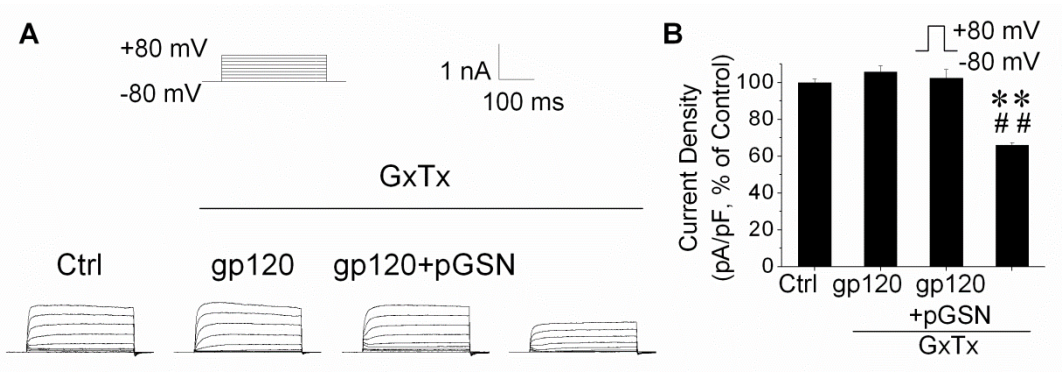

Figure. 26. Involvement of Kv2.1 in pGSN inhibition of gp120 enhancement of TEA-sensitive I_K. Cultures were treated for 24 h with 100 pM gp120, 500 ng/ml pGSN or gp120 and pGSN. Panel A, representative TEA sensitive currents recorded from neurons with treatments indicated. TEA sensitive I_K was recorded in the presence of 4-AP (5 mM) alone or 4-AP and GxTx (50 nM). Note that GxTx, a specific Kv2.1 channel blocker, abolished gp120 enhancement of the TEA sensitive I_K. Panel B, a summary bar graph of current densities (n = 25) showing GxTx inhibition of gp120 increase of TEA sensitive K^+ currents generated by a voltage step from −80 to +80 mV and GxTx *per se* decreased TEA sensitive K^+ currents. ** $p < .01$ vs. control; ## $p < .01$ vs. gp120 group.

3.5. Gp120-induced TEA sensitive I_K inactivation curve shift was blocked by pGSN

The causative factors resultant in alterations of the current amplitudes of ion channels are potentially: regulation of channel expression, promotion of channel translocation, or modification of channel activation. To further determine the mechanism of gp120 enhancement of I_K and its inhibition by pGSN, we next investigated the impact of gp120 and pGSN on Kv channel activation and inactivation properties. Rat cortical neuron cultures were first prepared for whole-cell recordings as described previously. I_K current was then isolated for recording by the addition of 4-AP to the bath solution. To characterize the steady-state inactivation behavior of I_K, 400 ms pre-conditioning pulses were applied to step the membrane potential from -120 mV to +40 mV in 10 mV increments, followed by a 200 ms testing at +40 mV. I-V curves were then plotted and fit using the Boltzmann equation ($I/I_{max}=1/\{1+\exp[(V-V1/2)/k]\}$) to yield the inactivation curve (Fig. 27A, 27B). Similarly, the activation curve was generated by applying 400 ms depolarizing pulses to step the membrane potential from 120 to +40 mV in 20 mV increments and fitting the I-V data using the Boltzmann equation ($G/G_{max}=1-1/\{1+\exp[(V-V1/2)]/k\}$ (Fig. 27A, 27B). Having established the I_K inactivation and activation tendencies under control conditions, cells were then perfused for 10 min with either gp120 (200 pM) or gp120 (200 pM) + pGSN (1000 ng/ml) and recorded using the identical protocol. Exposure to gp120 resulted in a significant right-ward shift of the steady-state I_K inactivation curve and a slight left-ward shift of the activation curve, reflecting a greater open channel probability at a given voltage. Further, the gp120-induced depolarizing shift in the inactivation curve was counteracted by pGSN co-perfusion (Fig. 27B, 27C).

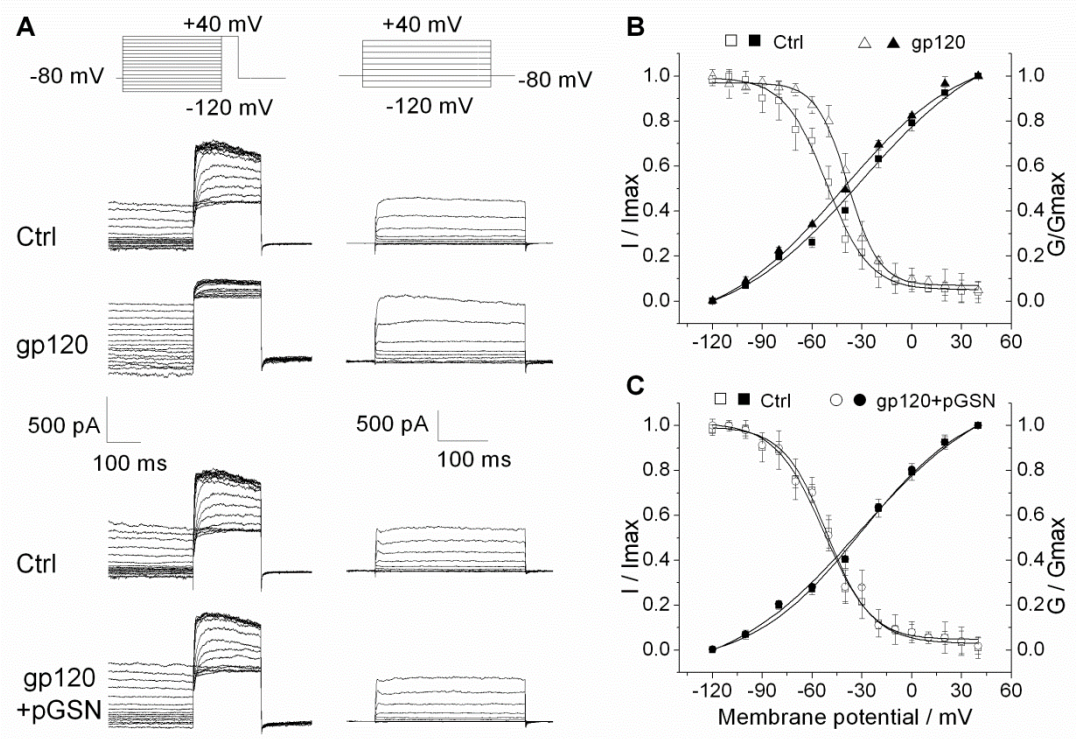

Figure 27. pGSN blockage of gp120-mediated outward K^+ current inactivation shift. Panel A, the original current traces before and after the perfusion of 200 pM gp120 or 200 pM gp120 and 1 μg/ml GSN showed as above, and currents of treatment induced after recording 10 min in the same cell as control. Normalized data points were fitted with the Boltzmann equation: $I/I_{max}=1/\{1+\exp[(V-V_{1/2})/k]\}$ and $G/G_{max}=1-1/\{1+\exp[(V-V_{1/2})]/k\}$. Each point represents the mean ± S.E.M., n = 5. Panel B, for inactivation, in the presence of gp120, $V_{1/2}$ was -38.51 mV compared with -51.64 mV in Control (Ctrl); and $V_{1/2}$ was -52.61 mV for gp120 + GSN compared with -51.14 mV for Control. Panel C, for activation, $V_{1/2}$ values for TEA sensitive currents were -41.93 mV in gp120 and -30.59 in Control; and -31.13 mV in Gp120 + GSN group compared with -30.32 mV in Control group. Thus, gp120 caused depolarizing shifts of the steady-state inactivation of TEA sensitive currents and GSN can inhibit the right shift.

3.6. pGSN inhibition of gp120-caused Kv2.1 protein expression up-regulation

To further characterize the mechanism of gp120-enhanced I_K and its reduction by GSN, we next examined alterations in Kv channel expression related to exposure to gp120 and pGSN. Rat cortical neurons were first incubated for 24 h with gp120 (500 pM), pGSN (2500 ng/ml), or gp120 and pGSN combined. The mRNA and protein levels of the Kv channels responsible for outward K^+ current in neurons, Kv1.1, Kv2.1, and Kv4.2, were then assessed by RT-PCR and Western blot. As expected, application of pGSN alone did not affect Kv channel mRNA expression. In comparison to control, exposure to gp120 increased the mRNA expression of all three channel subtypes, with Kv1.1 mRNA expression reaching statistical significance (Fig. 28A). Consistent with our electrophysiological findings, co-incubation with pGSN attenuated gp120-enhanced expression of Kv2.1 channel mRNA, but did not affect the elevated expression of Kv1.1 and Kv4.2 mRNA (Fig. 28A). Similarly, channel protein levels were unaffected by the application of pGSN alone, but were significantly increased for all three Kv channel subtypes in the gp120 exposed group (Fig. 28B). Again in agreement with our electrophysiological studies, co-incubation with pGSN was found to prevent gp120-induced elevations in Kv2.1 protein level, without inhibiting similar increases in the amount Kv1.1 and Kv4.2 protein (Fig. 28B).

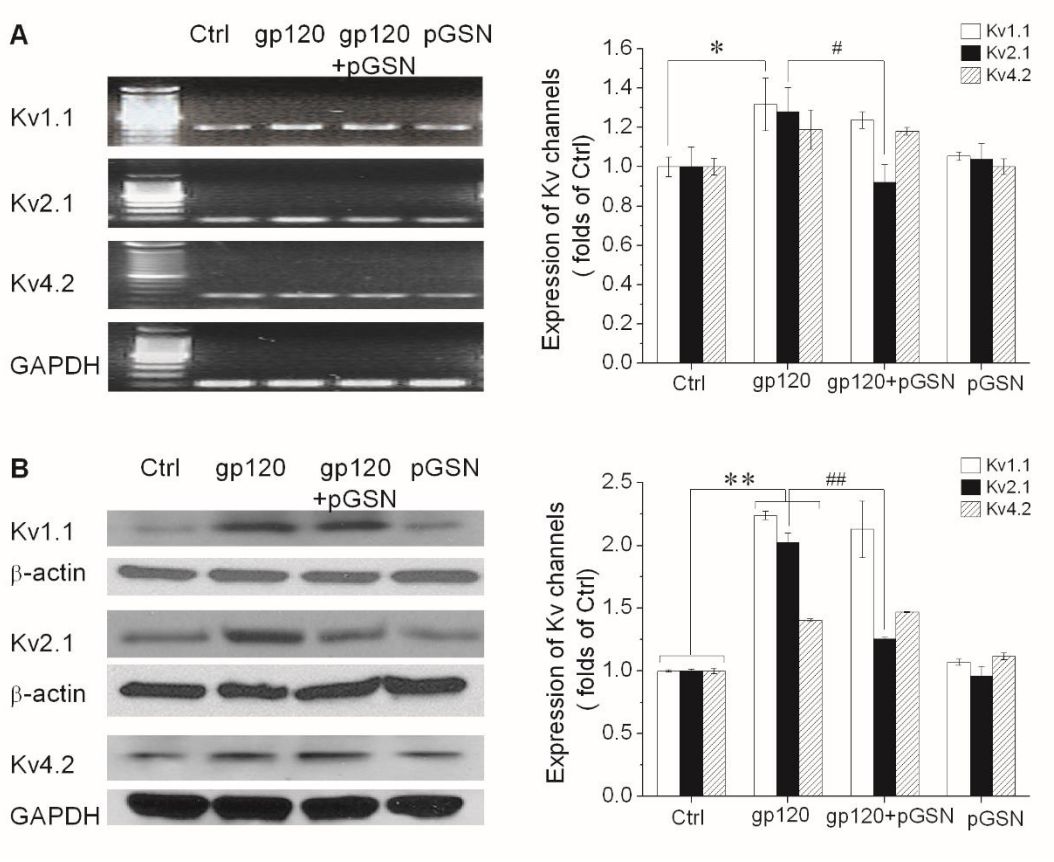

Figure 28. pGSN inhibition of gp120-induced Kv2.1 channel expression. Neuronal cultures were treated with 500 pM gp120 with or without 2.5 µg/ml pGSN for 24 h. Band density was analyzed by Image J and normalized by internal control. Data represents means ± S.E.M. from 3 independent experiments. Panel A, gp120 increased the levels of Kv1.1 mRNA expression ($p < .05$). Although increased levels of Kv2.1 and Kv4.2 mRNA expression did not reach the statistical significance ($p < .05$ compare to control), the expression levels of Kv2.1 mRNA was down-regulated by pGSN compared to gp120 group ($p < .05$). Panel B, gp120 significantly increased the levels of Kv1.1, Kv2.1 and Kv4.2 channel protein expression ($p < .01$). pGSN significantly reduced only Kv2.1 channel protein expression ($p < .01$). pGSN alone did not alter the expression levels of Kv channels. * $p < .05$ vs. control; ** $p < .01$ vs. control; # $p < .05$ vs. gp120 group; ## $p < .01$ vs. gp120 group.

3.7. pGSN protected neurons from gp120-induced damage via Kv2.1

By giving that pGSN mitigates gp120-induced neuronal viability decrease, prevents gp120-indued alterations in I_K inactivation properties and Kv2.1 channel expression, we then determined the involvement of Kv2.1 in gp120-associated neuronal apoptosis to establish the neuroprotective activity of pGSN in gp120-associated neuronal injury by Kv2.1. We performed studies on neuronal apoptosis and viability using gp120, pGSN, and the Kv2.1-specific inhibitor GxTx. First, rat cortical neuron cultures were incubated for 24 h with gp120 (500 pM), pGSN (2500 ng/ml), GxTx (12.5 or 25 nM), gp120 + pGSN, or gp120 + GxTx. Neuronal apoptosis was then assessed by Tunel stain and neuronal viability by MTT assay. In comparison to control, neuronal viability was reduced by 33% in cultures incubated with gp120 (500 pM), while co-incubation treatment with pGSN (2500 ng/ml), GxTx (12.5 nM), or GxTx (25 nM) restored neuronal viability to 88.5%, 79.0%, and 83.0%, respectively (Fig. 28A). Similarly, exposure to gp120 resulted in a 5-fold increase in neuronal apoptosis, which was attenuated by GSN and GxTx in a dose-dependent manner (Fig. 28B).

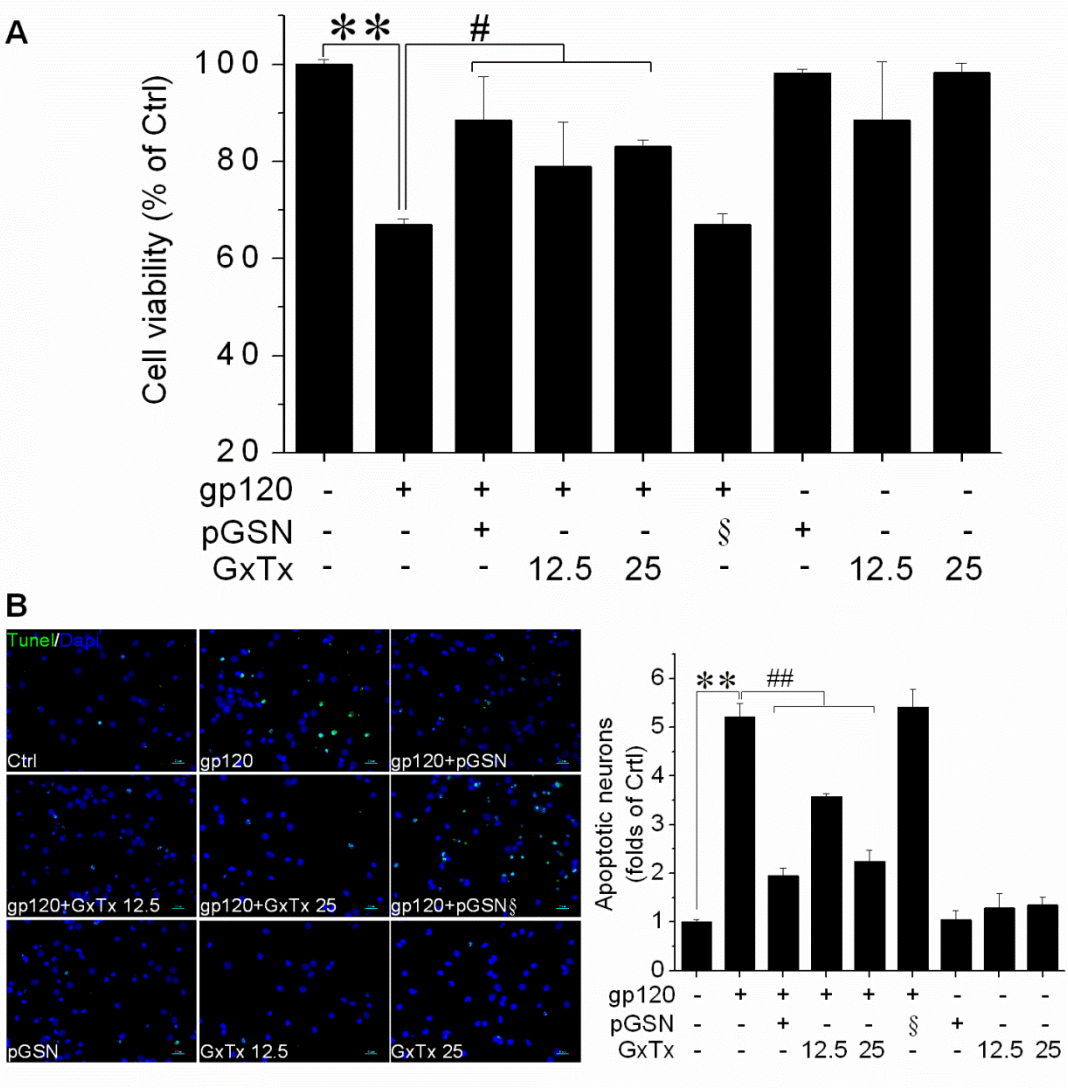
A
**
#
Cell viability (% of Ctrl)
100
80
60
40
20
gp120 - + + + + + - - -
pGSN - - + - - § + - -
GxTx - - - 12.5 25 - - 12.5 25
B
Tunel/Dapi
Ctrl
gp120
gp120+pGSN
gp120+GxTx 12.5
gp120+GxTx 25
gp120+pGSN§
pGSN
GxTx 12.5
GxTx 25
Apoptotic neurons (folds of Crtl)
**
##
6
5
4
3
2
1
0
gp120 - + + + + + - - -
pGSN - - + - - § + - -
GxTx - - - 12.5 25 - - 12.5 25

Figure 29. pGSN attenuated gp120-induced neuronal damage via Kv2.1. Neurons were exposed to gp120 (500 pM), pGSN (2.5 μg/ml), gp120 (500 pM) and pGSN (2.5 μg/ml), or heat inactivated pGSN (2.5 μg/ml) in the presence or absence co-incubated GxTx (12.5 or 25 nM) for 24 h. Panel A, cell viability determined by MTT assay exhibited that gp120 exposure reduced cell viability ($p < .01$ compare to Control), which was attenuated by GSN or GxTx. Heat-inactivated pGSN (§) showed no protective effect. pGSN or GxTx alone did not alter cell viability. Panel B, Left panel shows Tunel staining results as a measure of apoptosis, with cell nuclei visualized using Dapi stain. 10 visual fields were analyzed for each of three independent experiments. Gp120 induced neuronal apoptosis that was attenuated by either pGSN or GxTx. These data suggest that pGSN protects against gp120-induced neuronal damage via Kv2.1. ** $p < .01$ vs. control; # $p < .05$ vs. gp120 group; ## $p < .01$ vs. gp120 group. Scale bars denote 50 μm.

4. Discussion

In the present study, we showed that the HIV-1 envelope protein gp120 induced cortical neuron dysfunction and apoptosis via Kv2.1. There are two novel findings: first, pGSN performs neuroprotection in gp120-induced neuronal impairments; second, Kv2.1 is involved in gp120-mediated neurotoxicity and pGSN protection.

The main proposed mechanisms of HIV-infection and HAND are toxic substances released from infected macrophages and microglia, including viral products such as gp120, causing neuronal dysfunction and apoptosis [261-264]. Given the requirement for K^+ efflux in processes of programmed cell death [84], our recent research has focused on the role of Kv channelopathies in HAND pathology [143, 144, 252, 265]. Based on research demonstrating the protective effect of GSN against Ca^{2+}-mediated excitotoxicity [241, 242], combined with proteomic studies indicating the level of pGSN is decreased in the CSF of HIV-infected individuals with cognitive impairment [243], here we delve into the connection between gp120, pGSN, and Kv channels. Presently we show two novel findings: first, the induction of neuronal injury by HIV-1 envelope protein gp120 entails enhanced I_K through Kv2.1 channels, and second, pGSN provides neuroprotection against gp120 by preventing the modification of channel expression and inactivation properties underlying I_K enhancement.

Previous research into the pathways of HAND neuropathogenesis has focused primarily on infected and/or activated mononuclear phagocyte releasing neurotoxins including, but not limited to, arachidonic acid, platelet-activation factor, free radicals, glutamate, quinolinate, cysteine, cytokines, amines and viral proteins (Tat and gp120). Although neurons do not express CD4 receptor, a principal receptor for HIV-1 entry into host cells, they do express the chemokine and HIV-1 infection co-receptors CXCR4 and CCR5. Along with NMDA receptors, these receptors can be pathologically activated by

aforementioned neurotoxins and viral products such as gp120, leading to alterations in signal transduction, excitotoxic influx of Ca^{2+}, neuronal dysfunction, and eventual apoptosis [234-236]. While the process of apoptosis is now generally accepted to involve excess K^+ efflux regardless of cell type or initiating stimuli [84, 223], reports of Kv channel contribution to gp120-related neuronal damage are rare. In a previous publication, our data suggested gp120 may induce caspase-3 dependent neuronal apoptosis by enhancing I_A via CXCR4-PKC signaling [143]. Results from the present experiment indicate gp120 exposure also leads to amplification of an I_K current (Fig. 25), which was found to be susceptible to Kv2.1-specific inhibition (Fig. 26), by provoking a depolarizing shift in I_K channel inactivation properties (Fig. 27) and an upregulation of Kv2.1 channel expression (Fig. 28). Furthermore, the significance of this increased Kv2.1 channel activity was demonstrated by MTT assay and Tunel staining assessments of neuronal health, which established that gp120-induced neuronal damage could be alleviated by Kv2.1-specific inhibition (Fig. 28). These findings are consistent with research on hippocampal neurons demonstrating upregulation of Kv2.1 to be essential to the induction of apoptosis under conditions of excess glutamate, the natural ligand of NMDAR [256]. In a similar experiment, glutamate was found to act through NMDAR to induce dephosphorylation of Kv2.1 channels and thereby alter channel function [266]. While HIV-1 infection of the CNS is associated with excess glutamate release and impaired uptake [267], gp120 is also known to trigger NMDAR-mediated neuronal death and thus may initiate similar apoptotic cascades [267, 268].

Neuron loss is a common feature observed in many neurodegenerative diseases. In order to better understand the cellular milieu in which this occurs and identify practical diagnostic markers, proteomic studies of CSF and plasma have been undertaken for numerous conditions including HAND. Proteomic analysis revealed that pGSN was

diminished in the CNS across varied conditions characterized by neuronal injury or dysfunction, including Alzheimer's disease [245], multiple sclerosis [244], and epilepsy [246]. In HAND, pGSN is decreased in the CSF [243] and elevated in plasma [254]. Given the increased permeability of the blood brain barrier associated with HIV-1 infection, the depletion of pGSN in the CSF may have significance for neuronal health and function, while the plasma abundance could be used as a diagnostic indicator [247]. It is important to note however, there are two isoforms of GSN, pGSN and cGSN, which may have different roles and be present in different concentrations [269]. HIV-infected macrophage have been found to secrete pGSN [270], which has been shown to be involved in further recruitment of macrophage to sites of injury [271] and is present in high concentration in the macrophage nodules of rhesus monkeys with SIV encephalitis [270]. While this might imply high CNS pGSN levels may be detrimental, several studies support the use of pGSN as a neuroprotective agent, for example in the treatment of Alzheimer's disease [245], multiple sclerosis [250], and stroke [249, 251, 272]. Interestingly, in a primary cortical neuron model of ischemic neuronal injury, the enhanced expression of cGSN using the histone deacetylation inhibitor trichostatin A was found to provide neuroprotection [251], perhaps indicating a means for targeting the different isoforms for treatment. The mechanisms for these effects of GSN have yet to be definitively characterized.

GSN is known to be regulated by micromolar Ca^{2+}, among other factors, in its function of modulating filament disassembly of the actin cytoskeleton [273] as part of ion channel regulation, intracellular signaling, and apoptotic processes [274]. With regard to cell death, the presence of pGSN mitigates common features such as mitochondrial dysfunction, loss of membrane potential, and cytochrome C release [240]. Perhaps relevant here, however, is evidence that pGSN may reduce the cytosolic Ca^{2+} overload

resulting from exposure to excitotoxic stimuli by facilitating voltage-dependent Ca^{2+} channel (VDCC) and NMDA receptor channel rundown, while primary hippocampal neurons cultured from GSN-null mice and exposed to glutamate exhibited decreased actin filament depolymerization, increased Ca^{2+} influx, and amplified currents through VDCC and NMDA receptor channels [241, 242]. In one report, GSN even directly inhibited an HIV-1 viral protein Vpr from activating VDCC, thereby decreasing Ca^{2+} influx and reducing apoptosis [275]. Despite what is known the altered concentration of pGSN in HAND and its anti-apoptotic effects, no research has been yet undertaken to explore the link between gp120-related neuronal damage, apoptotic Kv channel activity, and pGSN. While GSN has been found to oppose gp120-mediated actin remodeling [276], here we sought to determine concretely if pGSN might provide neuroprotective activity against gp120 exposure and to make clear the pathways involved. In addition, one report found the addition of GSN actually increased K^+ channel activity in human syncytiotrophoblasts [277]. In contrast, our results show that pGSN does indeed lessen apoptosis in cortical neurons exposed to gp120 (Fig. 22) by suppressing the gp120-associated upregulation of Kv2.1 expression (Fig. 28) and depolarizing shift of I_K inactivation properties (Fig. 27), thereby inhibiting gp120-enhanced I_K (Figs. 24 and 25) through Kv2.1 channels (Fig. 26), ultimately resulting in a reduction of gp120-induced Kv2.1-dependent apoptosis (Fig. 28). Considered with research conducted elsewhere and previously described, a tentative global picture emerges of the relationship between HIV-1 gp120 exposure, apoptotic K^+ efflux through Kv2.1 channels, and the protective role of pGSN in suppressing gp120-mediated enhancement of apoptotic Kv2.1 currents.

Although the present study demonstrates that pGSN protects gp120-induced neuronal injury via inhibition of gp120 enhancement of Kv2.1 expression and Kv2.1 current in rat cortical neuronal cultures, the exact mechanism underlying pGSN-

mediated protection is not yet clear, nor is the site(s) of action – intracellular and/or extracellular? A previous study from our laboratory showed gp120 interacts with intracellular signaling, resulting in an enhancement of outward K^+ currents and consequent neuronal injury [143]. In another study carried out on Jurkat T cells, GSN was found to block the interaction between viral protein and voltage-gated ion channel. These results suggest that pGSN may inhibit the interaction between gp120 and Kv2.1 leading to its neuroprotection. Another possibility is pGSN blocks the interaction between gp120 and Kv2.1 channel as viral proteins were found to interact with ion channels [275]. In addition, pGSN may protect neurons through inhibition of gp120-mediated activation of caspases since gp120 has been shown to induce neuronal injury via activation of caspases [278, 279] and GSN has been reported to, in complex with phosphatidylinositol 4, 5-biphosphate, inhibit caspase activity and retard apoptotic progression [280]. As to the site of pGSN action, it appears that pGSN acts extracellularly since pGSN inhibited gp120-induced shift of outward K^+ current inactivation curve shortly after brief bath perfusion of pGSN (Fig. 27). Nevertheless, further studies are definitely needed to unravel the mechanisms of pGSN-mediated neuroprotection and the site(s) of action.

It is worth pointing out that the effective concentrations for gp120 and GSN were different in studies measuring cell viability and K^+ current, with higher concentrations for studying cell viability. This is because, in the same time window, higher concentrations were needed to produce changes in cell viability in comparison with the concentrations used to generate alterations of membrane ionic currents conducted by ion channels. Importantly, it is difficult to form gigaohm seal and record whole-cell current from injured cells. For these reasons, different concentrations of gp120 and GSN were employed in the present study.

In summarizing the present experiment, several principal findings bear mention. First, exposure to gp120 causes neuronal injury by amplifying neuronal I_K current via modification of Kv2.1 channel expression and activation. Second, the presence of pGSN mitigates gp120-induced apoptosis by inhibiting gp120-related enhancements of Kv2.1 channel activity. Collectively, these experimental results serve to further define the link between HAND pathogenesis and Kv channelopathies [265], while at the same time supporting a potentially neuroprotective role for pGSN in the treatment of HAND and other neurodegenerative diseases.

This is a peer-reviewed article published in Molecular and Cellular Neuroscience. Volume 57, November 2013, Pages 73–82.

Chapter 5

Summary and prospect

Milder forms of HAND remain prevalent in the era of cART. Given that HIV-1 proteins and toxic factors released from infected cells persist in brain while viral load is well controlled in blood, there are remaining uncertain mechanisms of viral protein neurotoxicity and increasing interests in myelin sheath loss and WM damage in neuroHIV brain. Presently we show six novel findings: 1) HIV-1 Tat increases $K_V1.3$ currents in oligodendrocytes by interacting with $K_V1.3$ channel and interrupting channel phosphorylating regulation; 2) Continuous increased K^+ efflux through $K_V1.3$ leads to OPC and oligodendrocyte apoptosis and loss of cell viability; 3) Tat exposure decreases MBP expression in highly purified primary rat oligodendrocyte cultures and, disturbs myelin structures in corpus callosum and stratum of cultured brain slices; 4) Tat treatment hinders OPC maturation in primary OPC culture; 5) In primary neuronal culture, the induction of neuronal injury by HIV-1 envelope protein gp120 entails enhanced I_K through Kv2.1 channels; 6) pGSN provides neuroprotection against gp120 by preventing the modification of channel expression and inactivation properties underlying I_K enhancement. Collectively, these experimental results serve to further define the link between HAND pathogenesis and K_V channelopathies, while at the same time supporting a protective role of $K_V1.3$ blockade for OPC/oligodendrocytes protection and neuroprotective role of pGSN in the treatment of HAND and other demyelination/neurodegenerative disease.

The axon damage and myelin injury are still challenging in therapeutic strategy of HAND. The ways on the regulation of oligodendrocyte lineage cell development are well-established including the extracellular pathways, cell to cell contact, and intracellular pathways. The strategies for promoting axonal remyelination have been introduced especially in those demyelinating disease like multiple sclerosis, of which K_V channel is an attractive target. It is anticipated that those strategies for promoting axonal

remyelination in other neurodegenerative disorders can be applied for HIV-1-associated oligodendrocyte/myelin injury; thought studies are needed to elucidate the underlying mechanisms for HIV-1-associated brain WM damage. However, further studies on understanding the mechanisms underlying HIV-1-associated oligodendrocyte/myelin injury may be hampered by the following potential difficulties. First, oligodendrocytes share many common extracellular signals and intracellular signaling pathways with neurons, the proposed “inside-out” and “outside-in” mechanisms are indistinguishable [65]. Second, the pro-proliferation signals for OPC are generally anti-differentiation. This will be a significant challenge to specify the certain time window to access proper remyelination *in vivo*. Overall, enhancing remyelination will be an important therapeutic strategy for HAND and other neurodegenerative disorders in the future [175].

Reference

1. Antinori, A., et al., *Updated research nosology for HIV-associated neurocognitive disorders.* Neurology, 2007. **69**(18): p. 1789-99.
2. Tozzi, V., et al., *Persistence of neuropsychologic deficits despite long-term highly active antiretroviral therapy in patients with HIV-related neurocognitive impairment: prevalence and risk factors.* J Acquir Immune Defic Syndr, 2007. **45**(2): p. 174-82.
3. Heaton, R.K., et al., *HIV-associated neurocognitive disorders before and during the era of combination antiretroviral therapy: differences in rates, nature, and predictors.* Journal of neurovirology, 2011. **17**(1): p. 3-16.
4. Li, R., et al., *White matter damage and effects of nadir CD4+ count on patients with asymptomatic HIV associated dementia complex–A DTI study.* Radiology of Infectious Diseases, 2014. **1**(1): p. 11-16.
5. Wang, B., et al., *Gray and white matter alterations in early HIV-infected patients: Combined voxel-based morphometry and tract-based spatial statistics.* J Magn Reson Imaging, 2015.
6. Correa, D.G., et al., *Diffusion tensor MR imaging of white matter integrity in HIV-positive patients with planning deficit.* Neuroradiology, 2015. **57**(5): p. 475-82.
7. Stubbe-Drger, B., et al., *Early microstructural white matter changes in patients with HIV: a diffusion tensor imaging study.* BMC Neurol, 2012. **12**: p. 23.
8. Wohlschlaeger, J., et al., *White matter changes in HIV-1 infected brains: a combined gross anatomical and ultrastructural morphometric investigation of the corpus callosum.* Clin Neurol Neurosurg, 2009. **111**(5): p. 422-9.
9. Zou, S., et al., *Oligodendrocytes Are Targets of HIV-1 Tat: NMDA and AMPA Receptor-Mediated Effects on Survival and Development.* J Neurosci, 2015. **35**(32): p. 11384-98.
10. Del Valle, L., et al., *Detection of HIV-1 Tat and JCV capsid protein, VP1, in AIDS brain with progressive multifocal leukoencephalopathy.* J Neurovirol, 2000. **6**(3): p. 221-8.
11. Bellizzi, A., et al., *Human polyomavirus JC reactivation and pathogenetic mechanisms of progressive multifocal leukoencephalopathy and cancer in the era of monoclonal antibody therapies.* J Neurovirol, 2012. **18**(1): p. 1-11.
12. Hauser, K.F., et al., *HIV-1 Tat and morphine have interactive effects on oligodendrocyte survival and morphology.* Glia, 2009. **57**(2): p. 194-206.
13. Boska, M.D., et al., *Associations between brain microstructures, metabolites, and cognitive deficits during chronic HIV-1 infection of humanized mice.* Molecular neurodegeneration, 2014. **9**(1): p. 1-18.
14. Kimura-Kuroda, J., K. Nagashima, and K. Yasui, *Inhibition of myelin formation by HIV-1 gp120 in rat cerebral cortex culture.* Arch Virol, 1994. **137**(1-2): p. 81-99.
15. Bernardo, A., C. Agresti, and G. Levi, *HIV-gp120 affects the functional activity of oligodendrocytes and their susceptibility to complement.* J Neurosci Res, 1997. **50**(6): p. 946-57.
16. Nukuzuma, S., et al., *Exogenous human immunodeficiency virus-1 protein, Tat, enhances replication of JC virus efficiently in neuroblastoma cell lines.* J Med Virol, 2012. **84**(4): p. 555-61.
17. Radja, F., et al., *Oligodendrocyte-specific expression of human immunodeficiency virus type 1 Nef in transgenic mice leads to vacuolar myelopathy and alters oligodendrocyte phenotype in vitro.* J Virol, 2003. **77**(21): p. 11745-53.

18. Crews, L., et al., *Molecular pathology of neuro-AIDS (CNS-HIV).* Int J Mol Sci, 2009. **10**(3): p. 1045-63.
19. *Nomenclature and research case definitions for neurologic manifestations of human immunodeficiency virus-type 1 (HIV-1) infection. Report of a Working Group of the American Academy of Neurology AIDS Task Force.* Neurology, 1991. **41**(6): p. 778-85.
20. Cherner, M., et al., *Neuropathologic confirmation of definitional criteria for human immunodeficiency virus-associated neurocognitive disorders.* J Neurovirol, 2007. **13**(1): p. 23-8.
21. Cohen, M.A. and J.M. Gorman, *Comprehensive textbook of AIDS psychiatry*. 2007: Oxford University Press.
22. Singh, D., et al., *Normative scores for a brief neuropsychological battery for the detection of HIV-associated neurocognitive disorder (HAND) among South Africans.* BMC Res Notes, 2010. **3**: p. 28.
23. Lipton, S.A., *Neuronal injury associated with HIV-1: approaches to treatment.* Annu Rev Pharmacol Toxicol, 1998. **38**: p. 159-77.
24. Lindl, K.A., et al., *HIV-associated neurocognitive disorder: pathogenesis and therapeutic opportunities.* J Neuroimmune Pharmacol, 2010. **5**(3): p. 294-309.
25. Gonzalez-Scarano, F. and J. Martin-Garcia, *The neuropathogenesis of AIDS.* Nat Rev Immunol, 2005. **5**(1): p. 69-81.
26. Gelman, B.B., *Neuropathology of HAND With Suppressive Antiretroviral Therapy: Encephalitis and Neurodegeneration Reconsidered.* Curr HIV/AIDS Rep, 2015. **12**(2): p. 272-9.
27. Bagashev, A. and B.E. Sawaya, *Roles and functions of HIV-1 Tat protein in the CNS: an overview.* Virol J, 2013. **10**: p. 358.
28. Zhang, J., et al., *HIV-1 gp120-induced axonal injury detected by accumulation of beta-amyloid precursor protein in adult rat corpus callosum.* J Neuroimmune Pharmacol, 2011. **6**(4): p. 650-7.
29. Alizadeh, A., S.M. Dyck, and S. Karimi-Abdolrezaee, *Myelin damage and repair in pathologic CNS: challenges and prospects.* Front Mol Neurosci, 2015. **8**: p. 35.
30. Barnabe-Heider, F., et al., *Origin of new glial cells in intact and injured adult spinal cord.* Cell Stem Cell, 2010. **7**(4): p. 470-82.
31. Payne, S.C., et al., *Early proliferation does not prevent the loss of oligodendrocyte progenitor cells during the chronic phase of secondary degeneration in a CNS white matter tract.* PLoS One, 2013. **8**(6): p. e65710.
32. Lau, L.W., et al., *Chondroitin sulfate proteoglycans in demyelinated lesions impair remyelination.* Ann Neurol, 2012. **72**(3): p. 419-32.
33. Mi, S., et al., *LINGO-1 is a component of the Nogo-66 receptor/p75 signaling complex.* Nat Neurosci, 2004. **7**(3): p. 221-8.
34. Mi, S., et al., *LINGO-1 negatively regulates myelination by oligodendrocytes.* Nat Neurosci, 2005. **8**(6): p. 745-51.
35. Bongarzone, E.R., et al., *Platelet-derived growth factor and basic fibroblast growth factor regulate cell proliferation and the expression of notch-1 receptor in a new oligodendrocyte cell line.* J Neurosci Res, 2000. **62**(3): p. 319-28.
36. Kim, H., et al., *Notch-regulated oligodendrocyte specification from radial glia in the spinal cord of zebrafish embryos.* Dev Dyn, 2008. **237**(8): p. 2081-9.
37. Shimizu, T., et al., *Wnt signaling controls the timing of oligodendrocyte development in the spinal cord.* Dev Biol, 2005. **282**(2): p. 397-410.
38. Bhat, N.R., P. Zhang, and S.B. Mohanty, *p38 MAP kinase regulation of oligodendrocyte differentiation with CREB as a potential target.* Neurochem Res, 2007. **32**(2): p. 293-302.

39. Chew, L.J., et al., *Mechanisms of regulation of oligodendrocyte development by p38 mitogen-activated protein kinase.* J Neurosci, 2010. **30**(33): p. 11011-27.
40. Flores, A.I., et al., *Constitutively active Akt induces enhanced myelination in the CNS.* J Neurosci, 2008. **28**(28): p. 7174-83.
41. Gongvatana, A., et al., *White matter tract injury and cognitive impairment in human immunodeficiency virus-infected individuals.* J Neurovirol, 2009. **15**(2): p. 187-95.
42. Uban, K.A., et al., *White matter microstructure among youth with perinatally acquired HIV is associated with disease severity.* AIDS, 2015. **29**(9): p. 1035-44.
43. Leite, S.C., et al., *Diffusion tensor MRI evaluation of the corona radiata, cingulate gyri, and corpus callosum in HIV patients.* J Magn Reson Imaging, 2013. **38**(6): p. 1488-93.
44. Xuan, A., et al., *Initial study of magnetic resonance diffusion tensor imaging in brain white matter of early AIDS patients.* Chin Med J (Engl), 2013. **126**(14): p. 2720-4.
45. Boska, M.D., et al., *Associations between brain microstructures, metabolites, and cognitive deficits during chronic HIV-1 infection of humanized mice.* Mol Neurodegener, 2014. **9**: p. 58.
46. Lackner, P., et al., *Antibodies to myelin oligodendrocyte glycoprotein in HIV-1 associated neurocognitive disorder: a cross-sectional cohort study.* J Neuroinflammation, 2010. **7**: p. 79.
47. Fitting, S., et al., *Dose-dependent long-term effects of Tat in the rat hippocampal formation: a design-based stereological study.* Hippocampus, 2010. **20**(4): p. 469-80.
48. Levine, A.J., et al., *Systems analysis of human brain gene expression: mechanisms for HIV-associated neurocognitive impairment and common pathways with Alzheimer's disease.* BMC Med Genomics, 2013. **6**: p. 4.
49. Berger, J.R., et al., *PML diagnostic criteria: consensus statement from the AAN Neuroinfectious Disease Section.* Neurology, 2013. **80**(15): p. 1430-8.
50. Del Valle, L. and S. Pina-Oviedo, *HIV disorders of the brain: pathology and pathogenesis.* Front Biosci, 2006. **11**: p. 718-32.
51. Sacktor, N., *The epidemiology of human immunodeficiency virus-associated neurological disease in the era of highly active antiretroviral therapy.* J Neurovirol, 2002. **8 Suppl 2**: p. 115-21.
52. Crossley, K.M., et al., *Recurrence of progressive multifocal leukoencephalopathy despite immune recovery in two HIV seropositive individuals.* J Neurovirol, 2016. **22**(4): p. 541-545.
53. Mascarello, M., et al., *Progressive multifocal leukoencephalopathy in an HIV patient receiving successful long-term HAART.* J Neurovirol, 2011. **17**(2): p. 196-9.
54. Gates, T.M. and L.A. Cysique, *The Chronicity of HIV Infection Should Drive the Research Strategy of NeuroHIV Treatment Studies: A Critical Review.* CNS Drugs, 2016. **30**(1): p. 53-69.
55. Sharpless, N., et al., *The restricted nature of HIV-1 tropism for cultured neural cells.* Virology, 1992. **191**(2): p. 813-25.
56. Takahashi, K., et al., *Localization of HIV-1 in human brain using polymerase chain reaction/in situ hybridization and immunocytochemistry.* Ann Neurol, 1996. **39**(6): p. 705-11.
57. Albright, A.V., et al., *HIV-1 infection of cultured human adult oligodendrocytes.* Virology, 1996. **217**(1): p. 211-9.

58. Albright, A., et al., *HIV-1 infection of a CD4-negative primary cell type: The oligodendrocyte.* Perspectives in Drug Discovery and Design, 1996. **5**(1): p. 43-50.
59. Patel, J.R., et al., *CXCR4 promotes differentiation of oligodendrocyte progenitors and remyelination.* Proc Natl Acad Sci U S A, 2010. **107**(24): p. 11062-7.
60. Stettner, M.R., et al., *SMAD proteins of oligodendroglial cells regulate transcription of JC virus early and late genes coordinately with the Tat protein of human immunodeficiency virus type 1.* J Gen Virol, 2009. **90**(Pt 8): p. 2005-14.
61. Wright, C.A., J.A. Nance, and E.M. Johnson, *Effects of Tat proteins and Tat mutants of different human immunodeficiency virus type 1 clades on glial JC virus early and late gene transcription.* J Gen Virol, 2013. **94**(Pt 3): p. 514-23.
62. Cinque, P., et al., *The good and evil of HAART in HIV-related progressive multifocal leukoencephalopathy.* J Neurovirol, 2001. **7**(4): p. 358-63.
63. Martin-Blondel, G., et al., *In situ evidence of JC virus control by CD8+ T cells in PML-IRIS during HIV infection.* Neurology, 2013. **81**(11): p. 964-70.
64. Codazzi, F., et al., *HIV-1 gp120 glycoprotein induces [Ca2+]i responses not only in type-2 but also type-1 astrocytes and oligodendrocytes of the rat cerebellum.* Eur J Neurosci, 1995. **7**(6): p. 1333-41.
65. Tsunoda, I. and R.S. Fujinami, *Inside-Out versus Outside-In models for virus induced demyelination: axonal damage triggering demyelination.* Springer Semin Immunopathol, 2002. **24**(2): p. 105-25.
66. Langford, T.D., et al., *Severe, demyelinating leukoencephalopathy in AIDS patients on antiretroviral therapy.* AIDS, 2002. **16**(7): p. 1019-29.
67. Smith, T.W., et al., *Human immunodeficiency virus (HIV) leukoencephalopathy and the microcirculation.* J Neuropathol Exp Neurol, 1990. **49**(4): p. 357-70.
68. Miller, F., et al., *Blood-brain barrier and retroviral infections.* Virulence, 2012. **3**(2): p. 222-9.
69. Strazza, M., et al., *Breaking down the barrier: the effects of HIV-1 on the blood-brain barrier.* Brain Res, 2011. **1399**: p. 96-115.
70. Louboutin, J.P. and D.S. Strayer, *Blood-brain barrier abnormalities caused by HIV-1 gp120: mechanistic and therapeutic implications.* ScientificWorldJournal, 2012. **2012**: p. 482575.
71. Titulaer, M.J. and J. Dalmau, *Antibodies to NMDA receptor, blood-brain barrier disruption and schizophrenia: a theory with unproven links.* Mol Psychiatry, 2014. **19**(10): p. 1054.
72. Avison, M., et al. *Viremia in the presence of blood-brain barrier compromise increases severity of HIV-associated neurocognitive impairment*. in *ANNALS OF NEUROLOGY*. 2003: WILEY-LISS DIV JOHN WILEY & SONS INC, 605 THIRD AVE, NEW YORK, NY 10158-0012 USA.
73. Gray, F., et al., *Acute, relapsing brain oedema with diffuse blood-brain barrier alteration and axonal damage in the acquired immunodeficiency syndrome.* Neuropathol Appl Neurobiol, 1998. **24**(3): p. 209-16.
74. Relucio, J., et al., *Laminin regulates postnatal oligodendrocyte production by promoting oligodendrocyte progenitor survival in the subventricular zone.* Glia, 2012. **60**(10): p. 1451-67.
75. Chintawar, S., et al., *Blood-brain barrier promotes differentiation of human fetal neural precursor cells.* Stem Cells, 2009. **27**(4): p. 838-46.
76. Plane, J.M., et al., *Intact and injured endothelial cells differentially modulate postnatal murine forebrain neural stem cells.* Neurobiol Dis, 2010. **37**(1): p. 218-27.

77. Juliet, P.A., et al., *Toxic effect of blood components on perinatal rat subventricular zone cells and oligodendrocyte precursor cell proliferation, differentiation and migration in culture.* J Neurochem, 2009. **109**(5): p. 1285-99.
78. Navikas, V., et al., *Increased mRNA expression of IL-6, IL-10, TNF-alpha, and perforin in blood mononuclear cells in human HIV infection.* J Acquir Immune Defic Syndr Hum Retrovirol, 1995. **9**(5): p. 484-9.
79. Antel, J.P., et al., *Oligodendrocyte lysis by CD4+ T cells independent of tumor necrosis factor.* Ann Neurol, 1994. **35**(3): p. 341-8.
80. Guo, H., et al., *HIV-1 infection induces interleukin-1beta production via TLR8 protein-dependent and NLRP3 inflammasome mechanisms in human monocytes.* J Biol Chem, 2014. **289**(31): p. 21716-26.
81. Takahashi, J.L., et al., *Interleukin-1beta promotes oligodendrocyte death through glutamate excitotoxicity.* Ann Neurol, 2003. **53**(5): p. 588-95.
82. Amaral, J.D., et al., *The role of p53 in apoptosis.* Discov Med, 2010. **9**(45): p. 145-52.
83. Jayadev, S., et al., *The glial response to CNS HIV infection includes p53 activation and increased expression of p53 target genes.* J Neuroimmune Pharmacol, 2007. **2**(4): p. 359-70.
84. Remillard, C.V. and J.X. Yuan, *Activation of K+ channels: an essential pathway in programmed cell death.* Am J Physiol Lung Cell Mol Physiol, 2004. **286**(1): p. L49-67.
85. Hahn, Y.K., et al., *HIV-1 alters neural and glial progenitor cell dynamics in the central nervous system: coordinated response to opiates during maturation.* Glia, 2012. **60**(12): p. 1871-87.
86. Buch, S.K., et al., *Glial-restricted precursors: patterns of expression of opioid receptors and relationship to human immunodeficiency virus-1 Tat and morphine susceptibility in vitro.* Neuroscience, 2007. **146**(4): p. 1546-54.
87. Chatterjee, D., et al., *Microglia play a major role in direct viral-induced demyelination.* Clin Dev Immunol, 2013. **2013**: p. 510396.
88. Marker, D.F., et al., *LRRK2 kinase inhibition prevents pathological microglial phagocytosis in response to HIV-1 Tat protein.* J Neuroinflammation, 2012. **9**: p. 261.
89. Tremblay, M.E., et al., *Ultrastructure of microglia-synapse interactions in the HIV-1 Tat-injected murine central nervous system.* Commun Integr Biol, 2013. **6**(6): p. e27670.
90. Esiri, M.M., C.S. Morris, and P.R. Millard, *Fate of oligodendrocytes in HIV-1 infection.* AIDS, 1991. **5**(9): p. 1081-8.
91. Bradl, M. and H. Lassmann, *Oligodendrocytes: biology and pathology.* Acta Neuropathol, 2010. **119**(1): p. 37-53.
92. Mishra, M., et al., *Human immunodeficiency virus type 1 Tat modulates proliferation and differentiation of human neural precursor cells: implication in NeuroAIDS.* J Neurovirol, 2010. **16**(5): p. 355-67.
93. Hahn, Y.K., et al., *beta-Chemokine production by neural and glial progenitor cells is enhanced by HIV-1 Tat: effects on microglial migration.* J Neurochem, 2010. **114**(1): p. 97-109.
94. Peng, H., et al., *HIV-1-infected and immune-activated macrophages induce astrocytic differentiation of human cortical neural progenitor cells via the STAT3 pathway.* PLoS One, 2011. **6**(5): p. e19439.
95. Mitew, S., et al., *Mechanisms regulating the development of oligodendrocytes and central nervous system myelin.* Neuroscience, 2014. **276**: p. 29-47.

96. Tanaka, T. and S. Yoshida, *Mechanisms of remyelination: recent insight from experimental models.* Biomol Concepts, 2014. **5**(4): p. 289-98.
97. Wu, J.Q., et al., *Differential regulation of cytotoxicity pathway discriminating between HIV, HCV mono-and co-infection identified by transcriptome profiling of PBMCs.* Virology journal, 2015. **12**(1): p. 1-16.
98. Weiser, K., et al., *HIV's Nef Interacts with β-Catenin of the Wnt Signaling Pathway in HEK293 Cells.* PLoS One, 2013. **8**(10): p. e77865.
99. Richards, M.H., et al., *Dynamic interaction between astrocytes and infiltrating PBMCs in context of neuroAIDS.* Glia, 2015. **63**(3): p. 441-451.
100. Zhang, Y., et al., *Notch1 signaling plays a role in regulating precursor differentiation during CNS remyelination.* Proc Natl Acad Sci U S A, 2009. **106**(45): p. 19162-7.
101. Curry, C.L., et al., *Gamma secretase inhibitor blocks Notch activation and induces apoptosis in Kaposi's sarcoma tumor cells.* Oncogene, 2005. **24**(42): p. 6333-44.
102. Liu, Y., et al., *CD44 expression identifies astrocyte-restricted precursor cells.* Dev Biol, 2004. **276**(1): p. 31-46.
103. Tuohy, T.M., et al., *CD44 overexpression by oligodendrocytes: a novel mouse model of inflammation-independent demyelination and dysmyelination.* Glia, 2004. **47**(4): p. 335-45.
104. Suyama, M., et al., *Reactivation from latency displays HIV particle budding at plasma membrane, accompanying CD44 upregulation and recruitment.* Retrovirology, 2009. **6**: p. 63.
105. Chao, C., et al., *A comparative study of molecular characteristics of diffuse large B-cell lymphoma from patients with and without human immunodeficiency virus infection.* Clin Cancer Res, 2015. **21**(6): p. 1429-37.
106. Fields, J., et al., *Role of neurotrophic factor alterations in the neurodegenerative process in HIV associated neurocognitive disorders.* J Neuroimmune Pharmacol, 2014. **9**(2): p. 102-16.
107. Peferoen, L., et al., *Oligodendrocyte-microglia cross-talk in the central nervous system.* Immunology, 2014. **141**(3): p. 302-13.
108. Jiang, Y., et al., *PDGF-B Can sustain self-renewal and tumorigenicity of experimental glioma-derived cancer-initiating cells by preventing oligodendrocyte differentiation.* Neoplasia, 2011. **13**(6): p. 492-503.
109. Erlandsson, A., et al., *Autocrine/paracrine platelet-derived growth factor regulates proliferation of neural progenitor cells.* Cancer Res, 2006. **66**(16): p. 8042-8.
110. Luo, F., et al., *Cyclin-dependent kinase 5 mediates adult OPC maturation and myelin repair through modulation of akt and gsk-3β signaling.* The Journal of Neuroscience, 2014. **34**(31): p. 10415-10429.
111. Azim, K. and A.M. Butt, *GSK3beta negatively regulates oligodendrocyte differentiation and myelination in vivo.* Glia, 2011. **59**(4): p. 540-53.
112. Chao, J., et al., *Platelet-derived growth factor-BB restores HIV Tat -mediated impairment of neurogenesis: role of GSK-3beta/beta-catenin.* J Neuroimmune Pharmacol, 2014. **9**(2): p. 259-68.
113. Frederick, T.J., et al., *Synergistic induction of cyclin D1 in oligodendrocyte progenitor cells by IGF-I and FGF-2 requires differential stimulation of multiple signaling pathways.* Glia, 2007. **55**(10): p. 1011-22.
114. Ascherl, G., et al., *Serum concentrations of fibroblast growth factor 2 are increased in HIV type 1-infected patients and inversely related to survival probability.* AIDS Res Hum Retroviruses, 2001. **17**(11): p. 1035-9.

115. Albrecht, D., et al., *Trophic factors in cerebrospinal fluid and spinal cord of patients with tropical spastic paraparesis, HIV, and Creutzfeldt-Jakob disease.* AIDS Res Hum Retroviruses, 2006. **22**(3): p. 248-54.
116. Sui, Z., et al., *Human immunodeficiency virus-encoded Tat activates glycogen synthase kinase-3beta to antagonize nuclear factor-kappaB survival pathway in neurons.* Eur J Neurosci, 2006. **23**(10): p. 2623-34.
117. Maggirwar, S.B., et al., *HIV-1 Tat-mediated activation of glycogen synthase kinase-3beta contributes to Tat-mediated neurotoxicity.* J Neurochem, 1999. **73**(2): p. 578-86.
118. Lannuzel, A., et al., *Human immunodeficiency virus type 1 and its coat protein gp120 induce apoptosis and activate JNK and ERK mitogen-activated protein kinases in human neurons.* Ann Neurol, 1997. **42**(6): p. 847-56.
119. Lundgaard, I., et al., *Neuregulin and BDNF induce a switch to NMDA receptor-dependent myelination by oligodendrocytes.* PLoS Biol, 2013. **11**(12): p. e1001743.
120. Cavaliere, F., et al., *NMDA modulates oligodendrocyte differentiation of subventricular zone cells through PKC activation.* Frontiers in cellular neuroscience, 2013. **7**.
121. Zeitler, M., et al., *HIV-Tat Forms Phosphoinositide Dependent Membrane Pores Implicated in Unconventional Protein Secretion.* J Biol Chem, 2015.
122. Fulmer, C.G., et al., *Astrocyte-derived BDNF supports myelin protein synthesis after cuprizone-induced demyelination.* J Neurosci, 2014. **34**(24): p. 8186-96.
123. Tsiperson, V., et al., *Brain-derived neurotrophic factor deficiency restricts proliferation of oligodendrocyte progenitors following cuprizone-induced demyelination.* ASN Neuro, 2015. **7**(1).
124. Ramos-Cejudo, J., et al., *Brain-derived neurotrophic factor administration mediated oligodendrocyte differentiation and myelin formation in subcortical ischemic stroke.* Stroke, 2015. **46**(1): p. 221-8.
125. Vondran, M.W., et al., *BDNF+/- mice exhibit deficits in oligodendrocyte lineage cells of the basal forebrain.* Glia, 2010. **58**(7): p. 848-56.
126. Bachis, A., et al., *Human immunodeficiency virus type 1 alters brain-derived neurotrophic factor processing in neurons.* J Neurosci, 2012. **32**(28): p. 9477-84.
127. Xiao, H., et al., *A cofactor, TIP30, specifically enhances HIV-1 Tat-activated transcription.* Proc Natl Acad Sci U S A, 1998. **95**(5): p. 2146-51.
128. Yang, W., et al., *TIP30 inhibits oligodendrocyte precursor cell differentiation via cytoplasmic sequestration of Olig1.* Glia, 2015. **63**(4): p. 684-698.
129. Attali, B., et al., *Characterization of delayed rectifier Kv channels in oligodendrocytes and progenitor cells.* J Neurosci, 1997. **17**(21): p. 8234-45.
130. Chittajallu, R., et al., *Regulation of Kv1 subunit expression in oligodendrocyte progenitor cells and their role in G1/S phase progression of the cell cycle.* Proc Natl Acad Sci U S A, 2002. **99**(4): p. 2350-5.
131. Kalsi, A.S., et al., *Kir4.1 expression by astrocytes and oligodendrocytes in CNS white matter: a developmental study in the rat optic nerve.* J Anat, 2004. **204**(6): p. 475-85.
132. Neusch, C., et al., *Kir4.1 potassium channel subunit is crucial for oligodendrocyte development and in vivo myelination.* J Neurosci, 2001. **21**(15): p. 5429-38.
133. Tegla, C.A., et al., *C5b-9-activated, K(v)1.3 channels mediate oligodendrocyte cell cycle activation and dedifferentiation.* Exp Mol Pathol, 2011. **91**(1): p. 335-45.
134. Cheli, V.T., et al., *Voltage-gated Ca2+ entry promotes oligodendrocyte progenitor cell maturation and myelination in vitro.* Exp Neurol, 2015. **265**: p. 69-83.

135. Jensen, B.K., et al., *Altered Oligodendrocyte Maturation and Myelin Maintenance: The Role of Antiretrovirals in HIV-Associated Neurocognitive Disorders.* J Neuropathol Exp Neurol, 2015. **74**(11): p. 1093-118.
136. French, H.M., et al., *Oxidative stress disrupts oligodendrocyte maturation.* J Neurosci Res, 2009. **87**(14): p. 3076-87.
137. Hoare, J., et al., *White matter micro-structural changes in ART-naive and ART-treated children and adolescents infected with HIV in South Africa.* AIDS, 2015. **29**(14): p. 1793-801.
138. Borjabad, A., et al., *Significant effects of antiretroviral therapy on global gene expression in brain tissues of patients with HIV-1-associated neurocognitive disorders.* PLoS Pathog, 2011. **7**(9): p. e1002213.
139. Yu, S.P., et al., *Mediation of neuronal apoptosis by enhancement of outward potassium current.* Science, 1997. **278**(5335): p. 114-7.
140. Visentin, S., M. Renzi, and G. Levi, *Altered outward-rectifying K(+) current reveals microglial activation induced by HIV-1 Tat protein.* Glia, 2001. **33**(3): p. 181-90.
141. Liu, J., et al., *HIV-1 Tat protein increases microglial outward K(+) current and resultant neurotoxic activity.* PLoS One, 2013. **8**(5): p. e64904.
142. Madsen, L.S., P. Christophersen, and S.P. Olesen, *Blockade of Ca2+-activated K+ channels in T cells: an option for the treatment of multiple sclerosis?* Eur J Immunol, 2005. **35**(4): p. 1023-6.
143. Chen, L., et al., *HIV-1gp120 induces neuronal apoptosis through enhancement of 4-aminopyridine-senstive outward K+ currents.* PLoS One, 2011. **6**(10): p. e25994.
144. Hu, D., J. Liu, and H. Xiong, *Enhancement of neuronal outward delayed rectifier K+ current by human monocyte-derived macrophages.* Glia, 2009. **57**(14): p. 1492-500.
145. Keblesh, J., D. Hu, and H. Xiong, *Voltage-gated potassium channels in human immunodeficiency virus type-1 (HIV-1)-associated neurocognitive disorders.* J Neuroimmune Pharmacol, 2009. **4**(1): p. 60-70.
146. Hille, B., *Ionic Channels of Excitable Membrane*. 1984, Sunderland, Massachusetts: Sinauer Associates.
147. Black, J.A., S.G. Waxman, and K.J. Smith, *Remyelination of dorsal column axons by endogenous Schwann cells restores the normal pattern of Nav1.6 and Kv1.2 at nodes of Ranvier.* Brain, 2006. **129**(Pt 5): p. 1319-29.
148. Lai, H.C. and L.Y. Jan, *The distribution and targeting of neuronal voltage-gated ion channels.* Nat Rev Neurosci, 2006. **7**(7): p. 548-62.
149. Gu, C. and Y. Gu, *Clustering and activity tuning of Kv1 channels in myelinated hippocampal axons.* J Biol Chem, 2011. **286**(29): p. 25835-47.
150. Jukkola, P.I., et al., *K+ channel alterations in the progression of experimental autoimmune encephalomyelitis.* Neurobiol Dis, 2012. **47**(2): p. 280-93.
151. David, G., et al., *Electrical and morphological factors influencing the depolarizing after-potential in rat and lizard myelinated axons.* J Physiol, 1995. **489 (Pt 1)**: p. 141-57.
152. Pal, S., et al., *Mediation of neuronal apoptosis by Kv2.1-encoded potassium channels.* J Neurosci, 2003. **23**(12): p. 4798-802.
153. Pannaccione, A., et al., *Up-regulation and increased activity of KV3.4 channels and their accessory subunit MinK-related peptide 2 induced by amyloid peptide are involved in apoptotic neuronal death.* Mol Pharmacol, 2007. **72**(3): p. 665-73.

154. Pieri, M., et al., *SP protects cerebellar granule cells against beta-amyloid-induced apoptosis by down-regulation and reduced activity of Kv4 potassium channels.* Neuropharmacology, 2010. **58**(1): p. 268-76.
155. Soliven, B., et al., *Voltage-gated potassium currents in cultured ovine oligodendrocytes.* J Neurosci, 1988. **8**(6): p. 2131-41.
156. Sontheimer, H., et al., *Channel expression correlates with differentiation stage during the development of oligodendrocytes from their precursor cells in culture.* Neuron, 1989. **2**(2): p. 1135-45.
157. Peretz, A., et al., *Hypomyelination and increased activity of voltage-gated K(+) channels in mice lacking protein tyrosine phosphatase epsilon.* EMBO J, 2000. **19**(15): p. 4036-45.
158. Dai, X., P. Qu, and C.F. Dreyfus, *Neuronal signals regulate neurotrophin expression in oligodendrocytes of the basal forebrain.* Glia, 2001. **34**(3): p. 234-9.
159. Walz, W., *Role of astrocytes in the clearance of excess extracellular potassium.* Neurochem Int, 2000. **36**(4-5): p. 291-300.
160. D'Ambrosio, R., et al., *Impaired K(+) homeostasis and altered electrophysiological properties of post-traumatic hippocampal glia.* J Neurosci, 1999. **19**(18): p. 8152-62.
161. Kucheryavykh, Y.V., et al., *Downregulation of Kir4.1 inward rectifying potassium channel subunits by RNAi impairs potassium transfer and glutamate uptake by cultured cortical astrocytes.* Glia, 2007. **55**(3): p. 274-81.
162. Takumi, T., et al., *A novel ATP-dependent inward rectifier potassium channel expressed predominantly in glial cells.* J Biol Chem, 1995. **270**(27): p. 16339-46.
163. Ton, H. and H. Xiong, *Astrocyte Dysfunctions and HIV-1 Neurotoxicity.* J AIDS Clin Res, 2013. **4**(11): p. 255.
164. Maragakis, N.J. and J.D. Rothstein, *Mechanisms of Disease: astrocytes in neurodegenerative disease.* Nat Clin Pract Neurol, 2006. **2**(12): p. 679-89.
165. Benarroch, E.E., *Microglia: Multiple roles in surveillance, circuit shaping, and response to injury.* Neurology, 2013. **81**(12): p. 1079-88.
166. Dickson, D.W., et al., *Macrophages and microglia in HIV-related CNS neuropathology.* Res Publ Assoc Res Nerv Ment Dis, 1994. **72**: p. 99-118.
167. Pan, G. and M. Shipston. *The expression & function of potassium channels in mouse N9 microglia*. in *Proceedings of The Physiological Society*. 2012: The Physiological Society.
168. Rangaraju, S., et al., *Potassium channel Kv1.3 is highly expressed by microglia in human Alzheimer's disease.* J Alzheimers Dis, 2015. **44**(3): p. 797-808.
169. Lam, D. and L.C. Schlichter, *Expression and contributions of the Kir2. 1 inward-rectifier K+ channel to proliferation, migration and chemotaxis of microglia in unstimulated and anti-inflammatory states.* Frontiers in cellular neuroscience, 2015. **9**: p. 185.
170. Liu, J., et al., *Involvement of Kv1.3 and p38 MAPK signaling in HIV-1 glycoprotein 120-induced microglia neurotoxicity.* Cell Death Dis, 2012. **3**: p. e254.
171. Nutile-McMenemy, N., A. Elfenbein, and J.A. Deleo, *Minocycline decreases in vitro microglial motility, beta1-integrin, and Kv1.3 channel expression.* J Neurochem, 2007. **103**(5): p. 2035-46.
172. Ferreira, R. and L.C. Schlichter, *Selective activation of KCa3.1 and CRAC channels by P2Y2 receptors promotes Ca(2+) signaling, store refilling and migration of rat microglial cells.* PLoS One, 2013. **8**(4): p. e62345.
173. D'Alessandro, G., et al., *KCa3.1 channels are involved in the infiltrative behavior of glioblastoma in vivo.* Cell Death Dis, 2013. **4**: p. e773.

174. Heaton, R.K., et al., *HIV-associated neurocognitive disorders persist in the era of potent antiretroviral therapy: CHARTER Study.* Neurology, 2010. **75**(23): p. 2087-96.
175. Liu, H., et al., *Oligodendrocyte Injury and Pathogenesis of HIV-1-Associated Neurocognitive Disorders.* Brain Sci, 2016. **6**(3).
176. Ferns, R.B., et al., *Hepatitis C virus quasispecies and pseudotype analysis from acute infection to chronicity in HIV-1 co-infected individuals.* Virology, 2016. **492**: p. 213-224.
177. Gandhi, N.S., et al., *Comparison of scales to evaluate the progression of HIV-associated neurocognitive disorder.* HIV Ther, 2010. **4**(3): p. 371-379.
178. Ranka, J.L. and C.J. Chapparo, *Assessment of productivity performance in men with HIV Associated Neurocognitive Disorder (HAND).* Work, 2010. **36**(2): p. 193-206.
179. Fantus, I.G., et al., *Pervanadate [peroxide(s) of vanadate] mimics insulin action in rat adipocytes via activation of the insulin receptor tyrosine kinase.* Biochemistry, 1989. **28**(22): p. 8864-71.
180. Esiri, M.M. and C.S. Morris, *Cellular basis of HIV infection of the CNS and the AIDS dementia complex: oligodendrocyte.* J NeuroAIDS, 1996. **1**(1): p. 133-60.
181. Hoare, J., et al., *Clinical associations of white matter damage in cART-treated HIV-positive children in South Africa.* J Neurovirol, 2015. **21**(2): p. 120-8.
182. Rumbaugh, J.A. and W. Tyor, *HIV-associated neurocognitive disorders: Five new things.* Neurol Clin Pract, 2015. **5**(3): p. 224-231.
183. Schmidt, K., et al., *Heterogeneous expression of voltage-gated potassium channels of the shaker family (Kv1) in oligodendrocyte progenitors.* Brain Res, 1999. **843**(1-2): p. 145-60.
184. Xiao, H., et al., *Selective CXCR4 antagonism by Tat: implications for in vivo expansion of coreceptor use by HIV-1.* Proc Natl Acad Sci U S A, 2000. **97**(21): p. 11466-71.
185. Johnson, T.P., et al., *Induction of IL-17 and nonclassical T-cell activation by HIV-Tat protein.* Proc Natl Acad Sci U S A, 2013. **110**(33): p. 13588-93.
186. Chen, Y., et al., *Isolation and culture of rat and mouse oligodendrocyte precursor cells.* Nat Protoc, 2007. **2**(5): p. 1044-51.
187. Baumann, N. and D. Pham-Dinh, *Biology of oligodendrocyte and myelin in the mammalian central nervous system.* Physiol Rev, 2001. **81**(2): p. 871-927.
188. Stoppini, L., P.A. Buchs, and D. Muller, *A simple method for organotypic cultures of nervous tissue.* J Neurosci Methods, 1991. **37**(2): p. 173-82.
189. Szabo, I., et al., *A novel potassium channel in lymphocyte mitochondria.* J Biol Chem, 2005. **280**(13): p. 12790-8.
190. Schmitz, A., et al., *Design of PAP-1, a selective small molecule Kv1.3 blocker, for the suppression of effector memory T cells in autoimmune diseases.* Mol Pharmacol, 2005. **68**(5): p. 1254-70.
191. Xu, C.J., *Comment on "chondroitin sulfate proteoglycans in demyelinated lesions impair remyelination".* Ann Neurol, 2013. **73**(2): p. 316.
192. Vassall, K.A., et al., *The effects of threonine phosphorylation on the stability and dynamics of the central molecular switch region of 18.5-kDa myelin basic protein.* PLoS One, 2013. **8**(7): p. e68175.
193. Smith, G.S., et al., *Classic 18.5- and 21.5-kDa myelin basic protein isoforms associate with cytoskeletal and SH3-domain proteins in the immortalized N19-oligodendroglial cell line stimulated by phorbol ester and IGF-1.* Neurochem Res, 2012. **37**(6): p. 1277-95.

194. Fadool, D.A. and I.B. Levitan, *Modulation of olfactory bulb neuron potassium current by tyrosine phosphorylation.* J Neurosci, 1998. **18**(16): p. 6126-37.
195. Colley, B.S., et al., *Brain-derived neurotrophic factor modulation of Kv1.3 channel is disregulated by adaptor proteins Grb10 and nShc.* BMC Neurosci, 2009. **10**: p. 8.
196. Cayabyab, F.S., et al., *Suppression of the rat microglia Kv1.3 current by src-family tyrosine kinases and oxygen/glucose deprivation.* Eur J Neurosci, 2000. **12**(6): p. 1949-60.
197. Cook, K.K. and D.A. Fadool, *Two adaptor proteins differentially modulate the phosphorylation and biophysics of Kv1.3 ion channel by SRC kinase.* J Biol Chem, 2002. **277**(15): p. 13268-80.
198. Minghetti, L., et al., *Multiple actions of the human immunodeficiency virus type-1 Tat protein on microglial cell functions.* Neurochem Res, 2004. **29**(5): p. 965-78.
199. Nael, A., et al., *CD4-Positive T-Cell Primary Central Nervous System Lymphoma in an HIV Positive Patient.* Am J Clin Pathol, 2016. **145**(2): p. 258-65.
200. Henderson, L.J., et al., *Human immunodeficiency virus type 1 (HIV-1) transactivator of transcription through its intact core and cysteine-rich domains inhibits Wnt/beta-catenin signaling in astrocytes: relevance to HIV neuropathogenesis.* J Neurosci, 2012. **32**(46): p. 16306-13.
201. Nakaoke, R. and W.A. Banks, *In vitro methods in the study of viral and prion permeability across the blood-brain barrier.* Cell Mol Neurobiol, 2005. **25**(1): p. 171-80.
202. Koeberle, P.D., Y. Wang, and L.C. Schlichter, *Kv1.1 and Kv1.3 channels contribute to the degeneration of retinal ganglion cells after optic nerve transection in vivo.* Cell Death Differ, 2010. **17**(1): p. 134-44.
203. Banks, W.A., S.M. Robinson, and A. Nath, *Permeability of the blood-brain barrier to HIV-1 Tat.* Exp Neurol, 2005. **193**(1): p. 218-27.
204. Gipson, K. and A. Bordey, *Analysis of the K+ current profile of mature rat oligodendrocytes in situ.* J Membr Biol, 2002. **189**(3): p. 201-12.
205. Menichella, D.M., et al., *Genetic and physiological evidence that oligodendrocyte gap junctions contribute to spatial buffering of potassium released during neuronal activity.* J Neurosci, 2006. **26**(43): p. 10984-91.
206. Fadool, D.A., *Tyrosine phosphorylation downregulates a potassium current in rat olfactory bulb neurons and a cloned Kv1.3 channel.* Ann N Y Acad Sci, 1998. **855**: p. 529-32.
207. Valencia-Cruz, G., et al., *K(bg) and Kv1.3 channels mediate potassium efflux in the early phase of apoptosis in Jurkat T lymphocytes.* Am J Physiol Cell Physiol, 2009. **297**(6): p. C1544-53.
208. Bock, J., et al., *Actinomycin D-induced apoptosis involves the potassium channel Kv1.3.* Biochem Biophys Res Commun, 2002. **295**(2): p. 526-31.
209. Brevet, M., et al., *Expression of K+ channels in normal and cancerous human breast.* Histol Histopathol, 2008. **23**(8): p. 965-72.
210. Abdul, M. and N. Hoosein, *Reduced Kv1.3 potassium channel expression in human prostate cancer.* J Membr Biol, 2006. **214**(2): p. 99-102.
211. Brevet, M., et al., *Deregulation of 2 potassium channels in pancreas adenocarcinomas: implication of KV1.3 gene promoter methylation.* Pancreas, 2009. **38**(6): p. 649-54.
212. Vautier, F., et al., *Shaker-type potassium channel subunits differentially control oligodendrocyte progenitor proliferation.* Glia, 2004. **48**(4): p. 337-45.
213. Carmeli, C., et al., *Demyelination in mild cognitive impairment suggests progression path to Alzheimer's disease.* PLoS One, 2013. **8**(8): p. e72759.

214. Chang, A., et al., *Premyelinating oligodendrocytes in chronic lesions of multiple sclerosis.* N Engl J Med, 2002. **346**(3): p. 165-73.
215. Gandhi, N., et al., *Interactive role of human immunodeficiency virus type 1 (HIV-1) clade-specific Tat protein and cocaine in blood-brain barrier dysfunction: implications for HIV-1-associated neurocognitive disorder.* J Neurovirol, 2010. **16**(4): p. 294-305.
216. Chang, J.R., et al., *HIV-1 Tat protein promotes neuronal dysfunction through disruption of microRNAs.* J Biol Chem, 2011. **286**(47): p. 41125-34.
217. Pasternak, A.O., V.V. Lukashov, and B. Berkhout, *Cell-associated HIV RNA: a dynamic biomarker of viral persistence.* Retrovirology, 2013. **10**(1): p. 1.
218. Anderson, E., et al., *HIV-1-associated dementia: a metabolic encephalopathy perpetrated by virus-infected and immune-competent mononuclear phagocytes.* J Acquir Immune Defic Syndr, 2002. **31 Suppl 2**: p. S43-54.
219. Chvatal, A., et al., *Changes in glial K+ currents with decreased extracellular volume in developing rat white matter.* J Neurosci Res, 1997. **49**(1): p. 98-106.
220. Soliven, B., et al., *Expression and modulation of K+ currents in oligodendrocytes: possible role in myelinogenesis.* Dev Neurosci, 1989. **11**(2): p. 118-31.
221. Tan, I.L. and J.C. McArthur, *HIV-associated neurological disorders: a guide to pharmacotherapy.* CNS Drugs, 2012. **26**(2): p. 123-34.
222. Everall, I.P., L.A. Hansen, and E. Masliah, *The shifting patterns of HIV encephalitis neuropathology.* Neurotox Res, 2005. **8**(1-2): p. 51-61.
223. Yu, S.P., *Regulation and critical role of potassium homeostasis in apoptosis.* Prog Neurobiol, 2003. **70**(4): p. 363-86.
224. Raja, F., et al., *Cerebral white matter damage in HIV infection demonstrated using beta-amyloid precursor protein immunoreactivity.* Acta Neuropathol, 1997. **93**(2): p. 184-9.
225. Gannon, P., M.Z. Khan, and D.L. Kolson, *Current understanding of HIV-associated neurocognitive disorders pathogenesis.* Curr Opin Neurol, 2011. **24**(3): p. 275-83.
226. Mothobi, N.Z. and B.J. Brew, *Neurocognitive dysfunction in the highly active antiretroviral therapy era.* Curr Opin Infect Dis, 2012. **25**(1): p. 4-9.
227. Kranick, S.M. and A. Nath, *Neurologic complications of HIV-1 infection and its treatment in the era of antiretroviral therapy.* Continuum (Minneap Minn), 2012. **18**(6 Infectious Disease): p. 1319-37.
228. McArthur, J. and B. Smith, *Neurologic Complications and Considerations in HIV-Infected Persons.* Curr Infect Dis Rep, 2013. **15**(1): p. 61-6.
229. Kaul, M. and S.A. Lipton, *Mechanisms of neuronal injury and death in HIV-1 associated dementia.* Curr HIV Res, 2006. **4**(3): p. 307-18.
230. Nath, A. and J. Geiger, *Neurobiological aspects of human immunodeficiency virus infection: neurotoxic mechanisms.* Prog Neurobiol, 1998. **54**(1): p. 19-33.
231. Xiong, H., et al., *HIV-1 infected mononuclear phagocyte secretory products affect neuronal physiology leading to cellular demise: relevance for HIV-1-associated dementia.* J Neurovirol, 2000. **6 Suppl 1**: p. S14-23.
232. Gendelman, H.E., et al., *The Neuropathogenesis of HIV-1-Dementia: APanel Discussion*, in *The neurology of AIDS*, H.E. Gendelman, et al., Editors. 1998, Chapman and Hall: New York. p. 1-10.
233. Mattson, M.P., N.J. Haughey, and A. Nath, *Cell death in HIV dementia.* Cell Death Differ, 2005. **12 Suppl 1**: p. 893-904.
234. Meucci, O. and R.J. Miller, *gp120-induced neurotoxicity in hippocampal pyramidal neuron cultures: protective action of TGF-beta1.* J Neurosci, 1996. **16**(13): p. 4080-8.

235. Muller, W.E., et al., *gp120 of HIV-1 induces apoptosis in rat cortical cell cultures: prevention by memantine.* Eur J Pharmacol, 1992. **226**(3): p. 209-14.
236. Catani, M.V., et al., *gp120 induces cell death in human neuroblastoma cells through the CXCR4 and CCR5 chemokine receptors.* J Neurochem, 2000. **74**(6): p. 2373-9.
237. Yin, H.L., et al., *Structure and biosynthesis of cytoplasmic and secreted variants of gelsolin.* J Biol Chem, 1984. **259**(8): p. 5271-6.
238. Kwiatkowski, D.J., et al., *Plasma and cytoplasmic gelsolins are encoded by a single gene and contain a duplicated actin-binding domain.* Nature, 1986. **323**(6087): p. 455-8.
239. Kwiatkowski, D.J., et al., *Localization of gelsolin proximal to ABL on chromosome 9.* Am J Hum Genet, 1988. **42**(4): p. 565-72.
240. Harms, C., et al., *Neuronal gelsolin prevents apoptosis by enhancing actin depolymerization.* Mol Cell Neurosci, 2004. **25**(1): p. 69-82.
241. Furukawa, K., et al., *The actin-severing protein gelsolin modulates calcium channel and NMDA receptor activities and vulnerability to excitotoxicity in hippocampal neurons.* J Neurosci, 1997. **17**(21): p. 8178-86.
242. Endres, M., et al., *Neuroprotective effects of gelsolin during murine stroke.* J Clin Invest, 1999. **103**(3): p. 347-54.
243. Rozek, W., et al., *Cerebrospinal fluid proteomic profiling of HIV-1-infected patients with cognitive impairment.* J Proteome Res, 2007. **6**(11): p. 4189-99.
244. Kulakowska, A., et al., *Gelsolin concentration in cerebrospinal fluid from patients with multiple sclerosis and other neurological disorders.* Eur J Neurol, 2008. **15**(6): p. 584-8.
245. Carro, E., *Gelsolin as therapeutic target in Alzheimer's disease.* Expert Opin Ther Targets, 2010. **14**(6): p. 585-92.
246. Peng, X., et al., *Gelsolin in cerebrospinal fluid as a potential biomarker of epilepsy.* Neurochem Res, 2011. **36**(12): p. 2250-8.
247. Haverland, N., et al., *Immunoreactivity of anti-gelsolin antibodies: implications for biomarker validation.* J Transl Med, 2010. **8**: p. 137.
248. Bucki, R., et al., *Plasma gelsolin: function, prognostic value, and potential therapeutic use.* Curr Protein Pept Sci, 2008. **9**(6): p. 541-51.
249. Le, H.T., et al., *The protective effects of plasma gelsolin on stroke outcome in rats.* Exp Transl Stroke Med, 2011. **3**(1): p. 13.
250. Kulakowska, A., et al., *Hypogelsolinemia, a disorder of the extracellular actin scavenger system, in patients with multiple sclerosis.* BMC Neurol, 2010. **10**: p. 107.
251. Meisel, A., et al., *Inhibition of histone deacetylation protects wild-type but not gelsolin-deficient neurons from oxygen/glucose deprivation.* J Neurochem, 2006. **98**(4): p. 1019-31.
252. Keblesh, J.P., et al., *4-Aminopyridine improves spatial memory in a murine model of HIV-1 encephalitis.* J Neuroimmune Pharmacol, 2009. **4**(3): p. 317-27.
253. Hu, C.L., et al., *Kv 1.1 is associated with neuronal apoptosis and modulated by protein kinase C in the rat cerebellar granule cell.* J Neurochem, 2008. **106**(3): p. 1125-37.
254. Wiederin, J., et al., *Biomarkers of HIV-1 associated dementia: proteomic investigation of sera.* Proteome Sci, 2009. **7**: p. 8.
255. Pal, S.K., et al., *Apoptotic surface delivery of K+ channels.* Cell Death Differ, 2006. **13**(4): p. 661-7.

256. Shen, Q.J., et al., *Contribution of Kv channel subunits to glutamate-induced apoptosis in cultured rat hippocampal neurons.* J Neurosci Res, 2009. **87**(14): p. 3153-60.
257. Lei, Z., et al., *Downregulation of Kv4.2 channels mediated by NR2B-containing NMDA receptors in cultured hippocampal neurons.* Neuroscience, 2010. **165**(2): p. 350-62.
258. Murakoshi, H. and J.S. Trimmer, *Identification of the Kv2.1 K+ channel as a major component of the delayed rectifier K+ current in rat hippocampal neurons.* J Neurosci, 1999. **19**(5): p. 1728-35.
259. Lee, S., et al., *Solution structure of GxTX-1E, a high-affinity tarantula toxin interacting with voltage sensors in Kv2.1 potassium channels.* Biochemistry, 2010. **49**(25): p. 5134-42.
260. Herrington, J., *Gating modifier peptides as probes of pancreatic beta-cell physiology.* Toxicon, 2007. **49**(2): p. 231-8.
261. Nath, A., et al., *Synergistic neurotoxicity by human immunodeficiency virus proteins Tat and gp120: protection by memantine.* Ann Neurol, 2000. **47**(2): p. 186-94.
262. Kaul, M., G.A. Garden, and S.A. Lipton, *Pathways to neuronal injury and apoptosis in HIV-associated dementia.* Nature, 2001. **410**(6831): p. 988-94.
263. Kaul, M. and S.A. Lipton, *Mechanisms of neuroimmunity and neurodegeneration associated with HIV-1 infection and AIDS.* J Neuroimmune Pharmacol, 2006. **1**(2): p. 138-51.
264. Lipton, S.A. and H.E. Gendelman, *Dementia associated with the acquired immunodeficiency syndrome.* N. Engl. J. Med., 1995. **332**: p. 934-940.
265. Gelman, B.B., et al., *Acquired neuronal channelopathies in HIV-associated dementia.* J Neuroimmunol, 2004. **157**(1-2): p. 111-9.
266. Misonou, H., et al., *Regulation of ion channel localization and phosphorylation by neuronal activity.* Nat Neurosci, 2004. **7**(7): p. 711-8.
267. Potter, M.C., et al., *Targeting the Glutamatergic System for the Treatment of HIV-Associated Neurocognitive Disorders.* J Neuroimmune Pharmacol, 2013. **8**(3): p. 594-607.
268. Wu, P., et al., *Direct cytotoxicity of HIV-1 envelope protein gp120 on human NT neurons.* Neuroreport, 1996. **7**(5): p. 1045-9.
269. Pottiez, G., N. Haverland, and P. Ciborowski, *Mass spectrometric characterization of gelsolin isoforms.* Rapid Commun Mass Spectrom, 2010. **24**(17): p. 2620-4.
270. Jagadish, T., et al., *Plasma gelsolin accumulates in macrophage nodules in brains of simian immunodeficiency virus infected rhesus macaques.* J Neurovirol, 2012. **18**(2): p. 113-9.
271. Goncalves, A.F., et al., *Gelsolin is required for macrophage recruitment during remyelination of the peripheral nervous system.* Glia, 2010. **58**(6): p. 706-15.
272. Zhang, Q.H., et al., *Treatment with gelsolin reduces brain inflammation and apoptotic signaling in mice following thermal injury.* J Neuroinflammation, 2011. **8**: p. 118.
273. Schafer, D.A. and J.A. Cooper, *Control of actin assembly at filament ends.* Annu Rev Cell Dev Biol, 1995. **11**: p. 497-518.
274. Kwiatkowski, D.J., *Functions of gelsolin: motility, signaling, apoptosis, cancer.* Curr Opin Cell Biol, 1999. **11**(1): p. 103-8.
275. Qiao, H. and J.R. McMillan, *Gelsolin segment 5 inhibits HIV-induced T-cell apoptosis via Vpr-binding to VDAC.* FEBS Lett, 2007. **581**(3): p. 535-40.

276. Garcia-Exposito, L., et al., *Gelsolin activity controls efficient early HIV-1 infection.* Retrovirology, 2013. **10**: p. 39.
277. Montalbetti, N., et al., *Cytoskeletal regulation of calcium-permeable cation channels in the human syncytiotrophoblast: role of gelsolin.* J Physiol, 2005. **566**(Pt 2): p. 309-25.
278. Louboutin, J.P., et al., *Gene delivery of antioxidant enzymes inhibits human immunodeficiency virus type 1 gp120-induced expression of caspases.* Neuroscience, 2012. **214**: p. 68-77.
279. Tun, C., et al., *Activation of the extrinsic caspase pathway in cultured cortical neurons requires p53-mediated down-regulation of the X-linked inhibitor of apoptosis protein to induce apoptosis.* J Neurochem, 2007. **102**(4): p. 1206-19.
280. Azuma, T., et al., *Gelsolin in complex with phosphatidylinositol 4,5-bisphosphate inhibits caspase-3 and -9 to retard apoptotic progression.* J Biol Chem, 2000. **275**(6): p. 3761-6.